NASA Contractor Report 159159

HIGH TEMPERATURE UF_6 RF PLASMA EXPERIMENTS APPLICABLE TO URANIUM PLASMA CORE REACTORS

Ward C. Roman

UNITED TECHNOLOGIES RESEARCH CENTER
East Hartford, Connecticut 06108

NASA Contract NAS1-14329
October 1979

National Aeronautics and Space Administration

Langley Research Center
Hampton Virginia 23665

TABLE OF CONTENTS

SUMMARY

An experimental and analytical investigation was conducted using the United Technologies Research Center (UTRC) 1.2 MW rf induction heater facility to aid in developing the technology necessary for designing a self-critical fissioning uranium plasma core reactor (PCR). Pure, high temperature uranium hexafluoride (UF_6) was injected into an argon fluid-mechanically-confined, steady-state, rf-heated plasma while employing different exhaust systems and diagnostic techniques to simulate and investigate some potential characteristics of uranium plasma core nuclear reactors.

The objectives of this follow-on research were: (1) to continue the development of techniques and equipment for fluid mechanical confinement of rf-heated uranium plasmas with a high density of uranium vapor within the plasma while simultaneously minimizing deposition of uranium and uranium compounds on the test chamber peripheral wall, endwall surfaces, and primary exhaust ducts; (2) continue to develop and test materials and handling techniques suitable for use with high-temperature, high-pressure, gaseous UF_6; and (3) to continue development of complementary diagnostic instrumentation and measurement techniques to characterize the uranium plasma, effluent exhaust gases, and residue deposited on the test chamber and exhaust system components. In preparation for near-term interfacing of the UF_6 rf-heated plasma experiments with downstream separator/reprocessing systems, emphasis was also placed on development of a primary exhaust system capable of transporting the UF_6 effluent exhaust gas to the downstream traps with minimum uranium compound wall deposition.

The test configuration used in the majority of tests employed a water-cooled, fused-silica cylindrical test chamber. The test chamber peripheral wall was 5.7-cm-ID by 10-cm-long. The radial inflow vortex was driven by injectors located on one endwall. In addition to a centerline exhaust thru-flow duct, an axial bypass annulus was located near the periphery. This test chamber flow configuration was designed to operate at pressures up to 20 atm and rf discharge power levels up to approximately 100 kW. The pure UF_6 was supplied to the endwall on-axis injector from a heated canister system capable of supplying the gaseous UF_6 at temperatures up to 450 K and pressures up to 20 atm.

The different exhaust systems employed in the tests included: provision for varying the temperature of the individual endwalls and primary exhaust duct sections, and the use of a porous exhaust duct assembly incorporating a diluent bleed radial flow injection. These schemes were used to aid in reducing the wall coatings due to uranium compound deposition.

Diagnostic measurements included exhaust gas sampling using both off- and on-line IR spectrophotometric absorption and Time-of-Flight (T.O.F.) mass spectrometer techniques. In selected tests, a residue analysis was conducted on the material deposited on the various key components of the test chamber and exhaust system.

Supporting studies included: continued development of uranium compound reference standards using six different complementary diagnostic techniques for use in post-test characterization of the residue; continued research on the corrosion/contamination aspects of hot, pressurized UF_6; and a heat and mass transfer analysis of swirling hot flow within a porous duct with bleed flow augmentation.

The overall test results have demonstrated the feasibility of employing on-line diagnostic techniques to measure the concentration of UF_6 at different locations in the exhaust system. Results of hot flow tests with pure UF_6 injection indicated that the quantity and composition of the residue deposited on the surfaces of the different components of the test chamber and exhaust system were affected by the component surface temperature and the contamination levels of oxygen and water in the test gases. Operating the test components at a high temperature and using appropriate traps and getters on the inlet gas systems resulted in a significant reduction in the residue coatings; similar reductions were also achieved using flow augmentation in the primary exhaust duct system. In selected tests employing a porous Monel interstage exhaust duct assembly with argon transpiration flow, the absolute level of uranium compound residue found on the exhaust duct surface in post-test analysis was reduced three (3) orders of magnitude (to typically hundreds of microgram range equivalent to approximately 3 $\mu g/cm^2$ of exposed surface) compared to prior tests under comparable test conditions. This level of coating approached the detectability limit of the available measurement techniques. There are several reasons for trying to prevent deposition of fuel/fission products on the exhaust duct of an actual device. These include: cooling problems associated with the fuel deposition hot spots and associated structural problems: undesirable localized regions of high dose rate radiation; and requirement to remove fuel/fission products to selected reprocessing components downstream of the actual cavity where efficient reprocessing can occur.

The results obtained from long run times indicate about 13 percent of the total UF_6 injected into the rf plasma test chamber was deposited out on the components upstream of the main cold trap system. Less than 0.1 percent was deposited within the confines of the rf plasma test chamber; approximately 0.6 percent was deposited within the axial bypass exhaust duct. The residue was determined to consist primarily of UF_4 and UO_2F_2.

These results indicate the option now exists for future tests wherein a very large fraction of the total UF_6 injected into the test chamber ($\approx$ 99.9 percent) can be made available for recovery/regeneration back to UF_6 using an exhaust trap system with minimal uranium compound losses to the walls of the test chamber, axial bypass duct, and primary exhaust duct system. Simultaneous with this can be the on-line measurement of the UF_6 concentration within different sections of the exhaust system using an improved T.O.F. mass spectrometer system of the type employed in the UF_6 rf plasma tests.

RESULTS AND CONCLUSIONS

RF plasma tests with pure UF_6 injection using the UTRC 1.2 MW induction heater system, different exhaust systems, and various diagnostic techniques yielded the following results.

1. Results from tests conducted over test times of up to about eleven minutes and using selected configurations and flow techniques indicated that less than 0.1 percent of the total UF_6 initially injected into the rf plasma test chamber was deposited on the test chamber itself; approximately 0.6 percent was deposited within the axial bypass exhaust duct. Of the total UF_6 injected, 43 g, about 13 percent was deposited out on the components upstream of the main cold trap system where future UF_6 regeneration schemes can be applied to eliminate the wall coating. The remainder reached the cold trap system where efficient reprocessing can be accomplished.

2. Employing independent cooling control of the different components of the test chamber and exhaust system has aided in significantly reducing the residue coatings (e.g., early test results indicated typically several hundred milligrams of primarily UO_2F_2 and UF_4 was uniformly deposited on the endwall surfaces -- 8 mg/cm^2 of endwall area). By operating the endwalls at as high a temperature as possible (≤ 800 K), subject to heat transfer limitations, the residue coating was reduced to levels of nominally 1-10 mg (0.04-0.4 mg/cm^2). Similarly, by throttling down the water cooling supplied to the interstage exhaust duct system, comparable reductions in residue wall coating were achieved.

3. Incorporation of filter traps and getters on the gas inlet systems to eliminate the O_2 and H_2O impurities has aided in reducing the formation of the oxides of uranium and also contributed in reducing the magnitude of residue deposition on the test components.

4 Use of different flow augmentation schemes immediately upstream of the interstage exhaust duct resulted in an approximate order of magnitude reduction in the residue wall coating.

5. Tests employing a porous (≈ 5 μm-dia nominal pore size) Monel exhaust duct system demonstrated the feasibility of employing radial transpiration injection of argon gas as a means for significantly reducing the post-test uranium compound wall coating. In several controlled tests, the quantity of residue was reduced by a factor of approximately 3000 compared to earlier test results not employing the porous exhaust duct scheme. The hundreds of microgram levels achieved (equivalent to approximately 3 $\mu g/cm^2$ of exposed surface) approached the detectability limit of the available measurement techniques; the maximum UF_6 mass thru-put employed in these tests was 43 g.

6. The continued development of complementary diagnostic instrumentation and measurement techniques to characterize the effluent exhaust gases resulted in the demonstration of two techniques applicable for use in future exhaust gas sampling measurements. One scheme is optical, involving the use of an IR spectrophotometer and absorption cell; the other scheme employed a modified commercially available T.O.F. mass spectrometer/sampling probe system. The feasibility of using either system in an off- or on-line mode of operation was demonstrated and the test results obtained using both systems under similar test conditions were in reasonable agreement. Based on several inherent advantages, the T.O.F. system is recommended over the IR absorption scheme. Two of the key advantages are: the ability to rapidly scan over a wide spectral range to provide analysis of both major and minor species; and, provide quantitative data on the radial UF_6 concentration distribution within different sections of the exhaust system.

7. Test results obtained using the IR spectrophotometer absorption and gas sampling system indicated no trace of UF_6 was detected in the axial bypass exhaust duct system in any of the tests. The T.O.F. mass spectrometer and gas sampling system indicated low concentrations (< 500 ppm*) of UF_6 were present on the centerline of the axial bypass exhaust duct system. This is encouraging from the standpoint of minimizing the complexity of the exhaust gas collection and reprocessing systems required in future closed-loop PCR systems; it is also significant because it provides a quantitative measure of the uranium confinement characteristics of the vortex flow employed in the plasma test chamber.

8. Various complementary diagnostic techniques were employed for identifying and quantifying the small amounts of uranium compound residue deposited onto the different components of the test chamber and exhaust duct system. These techniques included use of the electron microscope, scanning electron microprobe, IR spectrophotometer, x-ray diffractometer, ion scattering spectrometer, and secondary ion mass spectrometer. The residue, which was uniformly deposited (not plated) on the walls of the exhaust system was determined to be primarily UF_4 and UO_2F_2.

9. An initial heat and mass transfer analysis of swirling flow within a porous duct with bleed flow augmentation was completed. Within the range of flow conditions of interest the results indicate the diffusion of the uranium compounds toward the wall can be counterbalanced by the radial transpiration injection of the bleed gas through the porous wall. This was also demonstrated in the experimental results.

10. Throughout this research effort, valuable data were also accumulated on the corrosion aspects of hot, pressurized UF_6 in a regime where very little published information is available. Included was an extended compilation of uranium compound reference standards for use in future post-test residue compound identification. The majority of these standards included the U-O-F compounds.

*Lower detectability limit of existing gas sampling system and T.O.F. mass spectrometer.

INTRODUCTION

Uranium nuclear reactors which employ gaseous fissile fuel can be operated at high temperatures; this leads conceptually to power conversion systems for space and terrestrial applications with performance characteristics and thermodynamic cycle efficiencies significantly improved over conventional solid fuel element nuclear reactors. In addition to aerospace propulsion applications, several new space power and/or terrestrial options are being considered, some of which use the direct coupling of energy in the form of electromagnetic radiation. These include:

(1) Direct pumping of lasers by fission fragment energy deposition in UF_6 and lasing gas mixtures;

(2) Optical pumping of lasers by thermal and/or nonequilibrium electromagnetic radiation from fissioning UF_6 and/or fissioning uranium plasmas;

(3) Photochemical or thermochemical processes such as dissociation of hydrogenous materials to produce hydrogen;

(4) MHD power conversion systems for generating electricity; and

(5) Advanced closed-cycle gas turbine driven electrical generators.

The continuous reprocessing of gaseous nuclear fuel also leads to a low steady-state fission product inventory in the reactor and limits the buildup of long half-life transuranium elements. This, together with the low critical mass, could result in increased safety and higher nuclear fuel resource utilization. References 1, 2, and 3 summarize various reactor concepts, designs, principles of operation, applications, and associated performance estimates.

A principal technology required to establish the feasibility of fissioning uranium plasma core reactors is the fluid mechanical confinement of the hot fissioning uranium plasma with sufficient containment to both sustain nuclear criticality and minimize deposition of uranium or uranium compounds on the confinement chamber peripheral walls. Figure 1 is a sketch of one unit cell configuration of a plasma core reactor (PCR). The reactor would consist of one or more such cells imbedded in beryllium oxide and/or heavy-water moderator and surrounded by a pressure vessel. In the central plasma fuel zone, gaseous uranium (injected in the form of UF_6 or other uranium compound) is confined by argon buffer gas injected tangentially at the periphery of the cell. UF_6 is a stable volatile gas at fuel injection temperatures and pressures of interest for plasma core reactors. Section AA at the bottom of Fig. 1 shows the UF_6 inlet and the on-axis and axial bypass exhaust ducts. The mixture of nuclear fuel and argon buffer gas is withdrawn from one or both endwalls at the axial centerline.

In applications in which it is desired to couple thermal radiation from the fissioning uranium plasma to a separate working fluid, the thermal radiation is transmitted through the argon buffer gas layer and, subsequently, through internally-cooled transparent walls to a working fluid channel such as shown in Fig. 1. The channels would contain particles, graphite fins, or opaque gases to absorb the radiation. For nonequilibrium, fission-fragment-induced short wavelength radiation emission applications, the working fluid channel would be removed and lasing gas mixtures would be mixed with either the uranium fuel or the buffer gas.

A long-range program plan to establish the feasibility of fissioning gaseous UF_6 and uranium plasma reactors has been formulated by NASA. Reference 4 summarizes the plan which comprises a series of experiments with reflector-moderator cavity reactors. Los Alamos Scientific Laboratory (LASL) is currently performing these cavity reactor experiments in cooperation with UTRC. Also integrated into this plan is the demonstration of an argon/UF_6 injection, separation, and recirculation system to efficiently separate UF_6 from argon in a form adaptable to subsequent recycling in the uranium plasma experiment. Figure 2 is a schematic of the system for the PCR unit cell configuration. A review of the past work is contained in Ref. 5.

Performance of static UF_6 critical experiments has been accomplished (Ref. 6). Key objectives of the initial static UF_6 and subsequent flowing UF_6 reactor experiments were to facilitate (1) research on gaseous cavity reactor physics and on non-equilibrium optical radiation from fissioning UF_6, (2) demonstration of physical applications of nonequilibrium optical radiation such as direct nuclear pumped lasers, and (3) demonstration of methods for heat extraction for low proliferation risk power generation and propulsion applications.

PCR technology studies at UTRC currently consist of several experiments and theoretical investigations directed toward evaluating the feasibility of the PCR concept. Extensive non-nuclear vortex flow and plasma fluid mechanical research has been conducted over the past fifteen years at UTRC. Past fluid mechanics (nonplasma) experiments (Ref. 7) have indicated that a radial inflow vortex is well-suited for applications which require the preferential containment of a heavy gas within a light gas created by the radial inflow vortex. A radial-inflow vortex flow pattern is characterized by an essentially laminar internal radial stagnation surface across which there is no net inward radial buffer gas flow.

Other previously reported experiments (Ref. 8) have been conducted on the confinement of argon rf plasmas. These tests were directed primarily toward development of a high-intensity, high-power-density plasma energy source (equivalent blackbody radiating temperatures >6000 K). Some of these initial exploratory tests included direct injection of very dilute mixtures of UF_6 (typically, 1 percent UF_6 in an argon carrier gas) into the argon rf plasma. Coating of the fused-silica peripheral wall occurred but short-time sustained UF_6 plasma operation was demonstrated. Particle feeder systems were also developed which permitted steady-state injection of carbon (C), tungsten (W), uranium dioxide (UO_2), and uranium oxide (U_3O_8)

into test chambers; operating pressures up to 40 atm were demonstrated. In general, these exploratory test results confirmed that simulated fuels could be confined fluid-mechanically with steep concentration gradients at the edge-of-fuel location.

Reference 9 summarizes the results of initial laboratory-scale experiments in which pure UF_6 was injected into an argon-confined, steady-state, rf-heated plasma to investigate some of the characteristics of plasma core reactors. The overall test results demonstrated applicable flow schemes and associated diagnostic techniques have been developed for the fluid-mechanical confinement and characterization of uranium vapor within the rf plasma.

The performance of high power, flowing UF_6 critical experiments requires development of reliable techniques and equipment for utilizing UF_6 over a wide range of temperatures and pressures. Also required is the associated closed-loop flow system and vortex flow confinement scheme. The results of this technology will ultimately allow operation of an approximately 5 MW self-critical fissioning uranium plasma core reactor. This research report presents results of the continuing uranium plasma confinement tests, together with the associated diagnostics and exhaust systems applicable to plasma core reactors. These tests were conducted using the UTRC 1.2 MW rf induction heater facility with pure UF_6 injected for long time periods into the steady-state, argon-confined, rf-heated plasmas.

DESCRIPTION OF PRINCIPAL EQUIPMENT

UTRC 1.2 MW RF Induction Heater

The experiments reported herein were conducted using the UTRC 1.2 MW rf induction heater system. Refer to Ref. 9 for a detailed description of the rf induction heater system. The rf operating frequency used in the experiments was approximately 5.4 MHz. The rf output power was supplied by two power amplifier tubes which drive a resonant tank circuit (resonator section) of unique design. A photograph of an assembled test configuration installed concentrically within the set of 9-cm-dia water-cooled rf work coils within the resonator section of the rf induction heater is shown in Fig. 3. The entire resonator section consisted of two arrays of ten vacuum capacitors, located (as shown in Fig. 3) within a 1.7-m-dia cylindrical aluminum test tank. Each vacuum capacitor array was connected with a single turn, silver-plated work coil.

The front of the test tank was a removable dome (shown removed in Fig. 3) containing five (10-cm-dia) view windows for observation of the test section. This permitted rapid access to the test section for inspection of uranium compound residue deposition on different test chamber and primary exhaust duct components after completion of a test.

All components of the rf induction heater were water-cooled; measurements were made of all quantities necessary for performing a component and overall system power balance on the rf equipment. An automatic twenty-four channel temperature recorder system was used to monitor all the thermocouples located throughout the rf induction heater system, the components of the rf test chamber, and the various cooling water and gas reference temperatures.

Basic Test Chamber Configuration

Figure 4 is a sketch showing a simplified cross section of the basic test chamber configuration employed in the 1.2 MW rf induction heater tests with pure UF_6 injection. Different test chamber configurations were tested before selecting the configuration and flow scheme which demonstrated the best confinement characteristics. These alternate configurations included (1) endwall injection with dual on-axis thru-flow exhaust and provision for axial bypass, (2) endwall injection with bluff-body stabilization and on-axis thru-flow exhaust, (3) endwall injection with off-axis annular exhaust, (4) peripheral wall injection, and combinations of the above. The configuration selected was based on the test results reported in Ref. 9; several desirable features are incorporated including the ability to independently vary the distribution of exhaust gas flow (axial bypass) and cooling water to the peripheral wall annulus and each endwall assembly. The peripheral wall was

comprised of a concentric set of water-cooled fused-silica tubes. The inner tube was 5.7-cm-ID x 6.1-cm-OD; the outer tube was 6.5-cm-ID x 7.3-cm-OD. The argon vortex was dr[illegible] from the right endwall only by a set of eight equally spaced stainless steel [illegible]rtex [illegible]jectors located tangent to the periphery of the endwall. The axial dist[illegible]ce betw[illegible] endwalls was fixed at 10 cm. A vacuum start technique was employed in all tests. The rf plasma was ignited at approximately 10 mm Hg using breakdown of the argon gas which occurred at a resonator voltage of about 4 kv. This technique had two advantages: (1) it eliminated the introduction of foreign materials into the test chamber; and (2) it permitted a partial purge between tests. As shown in Fig. 4, the UF_6 injector, located on-axis and concentrically within the right endwall, was fabricated from a 50-cm-long three concentric copper tube assembly; the injector tip protruded 2 cm into the test chamber from the face of the endwall. High pressure water (20 atm) heated to approximately 350 K via a steam heat exchanger flowed at 0.14 ℓ/s between the concentric tubes of the UF_6 injector. This provided cooling relative to the hot plasma environment while still maintaining a high enough temperature in the injector to permit flowing the pressurized gaseous UF_6 without solidification in the UF_6 transfer line/injector.

Argon Buffer Gas and UF_6 Supply Systems

Figure 5 is a schematic of the argon buffer gas and UF_6 supply systems. Commercial grade argon gas was supplied to the test chamber, via a filter and gas temperature conditioning system, from a 72.5×10^3 ℓ bottle supply. Flow meters were used to measure the argon mass flow rate during the tests. The exhaust gases (argon plus other volatile uranium compounds) were removed from the test chamber through exhaust ducts and, in turn, routed through an appropriate effluent gas collection system. The UF_6 exhaust system is shown in the top portion of Fig. 5. Two, 0.5ℓ collection vessels immersed in a liquid nitrogen dewar collected the condensible uranium compounds. A vacuum pump system was used for the rf plasma starting sequence and to permit outgassing the components between test series. Flow control valves were used to adjust the pressure in the rf uranium plasma test chamber. The remaining exhaust gases were finally ducted to a neutralizing ($NaOH+H_2O$) trap located on the roof of the laboratory. The UF_6 supply system is shown in the lower right portion of Fig. 5. This UF_6 handling and feeder system was developed to provide a controlled and steady flow of heated UF_6 at temperatures up to about 450 K. The principal components of the UF_6 transfer system are the UF_6 boiler, the boiler heat supply system, the flow control system, and the UF_6 condenser (exhaust) system. The boiler was a 2ℓ Monel cylinder rated at 200 atm working pressure. Monel was selected for the cylinder and feed lines because of its resistance to chemical attack by hot, pressurized UF_6. (Refer to APPENDIX A for additional details on the corrosion aspects.) A heat exchanger to provide internal heating was located within the bottom of the boiler. As shown in Fig. 5, electrical resistance heater tape was wrapped around the majority of components. An insulated 3.5 kW electrical heater surrounded the boiler and was used to reach the desired equilibrium temperature and

pressure prior to flowing the UF_6. A variable powerstat controlled the evaporation rate and temperature within the boiler. In the tests reported herein, use of the electrical heater assembly alone was sufficient to provide the required flow rates. Appropriate safety aspects were incorporated; these included (1) a removable plexiglass enclosure which surrounded the boiler and was connected via a flexible metal duct to the exhaust gas scrubber system located on the laboratory roof, and (2) a high pressure rapid cool-down system (heat exchanger coils) located within the boiler. Dual sets of welded-bellows-type shutoff valves and burst discs routed to the exhaust system were also used for added safety. A linear mass flow meter, calibrated for UF_6, provided on-line determination of the UF_6 mass flow rate prior to entering the UF_6 injector assembly. By incorporating a Monel transducer, the unit was capable of handling heated UF_6. The meter basically consisted of an electrically-heated tube and an arrangement of thermocouples to measure the differential cooling caused by the UF_6 gas passing through the tube. The thermoelectric elements generated a dc voltage proportional to the rate of mass flow through the tube. Due to partial coating of the unit throughout the test series, periodic recalibrations and chemical cleaning were required.

Based on the results of exploratory UF_6 handling and flow metering tests and test results reported in Ref. 9, the need for elimination of as much contamination as possible from the UF_6 supply and flow handling system was evident. Refer to Ref. 9 for a detailed discussion of the component preparation, cleaning procedure, and post- analysis used in the UF_6 supply system. The system was designed and tested for UF_6 mass flow rates up to about 5 g/s and subsequent possible injection of pure UF_6 into the rf plasma test chamber operating at pressures up to approximately 20 atm. For reference, the vapor pressure of UF_6 at room temperature is approximately 130 torr; at 450 K it is about 20 atm. Refer to Ref. 9, APPENDIX C, for additional details on the properties and assay of the as-received UF_6.

Test Gas Contaminant Control

A review of the available literature indicates that the uranium-oxygen and uranium-fluorine systems represent some of the most complex chemical systems known. In addition, some of the published property data (refer to APPENDIX A) are not in complete agreement between different investigators. In relation to this, many references point out the extreme importance of minimizing the presence of moisture and oxygen in the test system. To aid in reducing these contaminants, a dual trap system (as shown in Fig. 5) was fabricated and installed in a parallel arrangement with the existing argon inlet flow system. A cooled molecular sieve (alkali metal alumino-silicate) was used to trap out the moisture and a heated trap (pure copper filings at 750 K) was used to reduce the O_2 concentration. Prior to transferring the UF_6 into the boiler system, the UF_6 was filtered through a NaF trap ($T \geq 450$ K) to remove the majority of HF. To provide an indication of the H_2O levels present, two

independent calibration tests were performed. In one test, a Linberg SB dewpoint instrument was used; in another, a Panametrics Model 2000 in-situ hygrometer instrument was employed. Using the dewpoint instrument, H_2O concentration levels from about 480 to 650 ppm were recorded when no molecular sieve was used. Inclusion of the filter resulted in an approximately 100X decrease in the H_2O content. Comparison of these results with those obtained using the in-situ hygrometer instrument revealed approximately the same trend with some differences in the absolute level. These results emphasized the requirement to adequately filter all the test gases used in the test program.

Diagnostic Equipment

The total power deposited into the uranium rf plasma was obtained from an overall test chamber energy balance by summing the power lost by radiation, power deposited into the annular coolant (including the partial contribution from the radiation attenuating dye) of the peripheral wall, power deposited into the endwall assemblies, power convected out the exhaust ducts, as well as, power deposited into the exhaust heat exchanger and UF_6 injector assembly. The power radiated from the plasma was measured using a specially constructed radiometer and chopper wheel assembly. Refer to Ref. 9 for additional details. Continuous observation of the plasma during the test was accomplished using an overhead projection screen system. Photographs (using neutral density filters) taken through the various viewports were used for estimating the discharge diameter and shape. A tunable cw single-frequency dye laser system was used to provide the very narrow uranium (UI) line at λ= 591.54 nm used in the absorption reference calibration tests. Refer to Ref. 9 for a detailed description of the dye laser system and test procedure.

To permit a detailed post-test analysis of the samples of residue collected from the various components of the test chamber and primary exhaust system, the following UTRC instrumentation was employed:

1. Perkin-Elmer IR Spectrophotometer (Model 457) -- permitted identification of compounds using IR spectrophotometric absorption measurements (2.5-40 μm wavelength range) of reference material standard compounds and small samples of residue removed from test chamber and exhaust system components (see Fig. 7 for schematic of IR Spectrophotometer system).

2. Cameca Scanning Electron Microprobe (Model CAMEBAX) -- permitted determination of the elements present in the residue samples and also scanning electron micrographs. Showed topographical and compositional variations and permitted x-ray mapping of the individual elements present.

3. Norelco X-Ray Diffractometer (Mark II) -- permitted identification of compounds present in the residue samples by subjecting them to copper K_α radiation and comparing the resulting x-ray diffraction patterns with reference standards.

4. Hitachi Electron Microscope using selected area diffraction (SAD) (Model HU-11) -- permitted identification of compounds present in the residue samples by subjecting them to electron bombardment. It also provided an indication of the relative crystal structure of the material.

5. 3M Ion Scattering Spectrometer (ISS)/Secondary (or sputtered) Ion Mass Spectrometer SIMS (Model 520 B) -- permitted identification of the various elements and compounds present in the residue samples. The unique features of this instrument that distinguish it from the other instruments described above are (a) it was sensitive to just the outer monolayer of the surface, (b) its sensitivity was as high as one part of a monolayer per million, (c) it gave positive identification of the compounds, and (d) if required, it could detect hydrogen and distinguish isotopes of uranium.

Equipment and Systems for Sampling and Analyzing the UF_6 Concentration In the Effluent Gases During the UF_6 RF Plasma Tests

Figure 6 is a schematic showing the basic UF_6 exhaust gas sampling system used in both the IR spectrophotometer absorption and Time-of-Flight (T.O.F.) mass spectrometer measurements. Exploratory tests using both these type systems demonstrated the feasibility of employing either of the two above systems for off- and/or on-line UF_6 effluent gas measurements. The system shown in Fig. 6 illustrates the three different locations used with the sampling probe assembly. The sampling probe was fabricated from a 1.6-mm-OD x 1.5-mm-ID chemically cleaned stainless stell (based on availability and size) tube and located on the centerline axis of the exhaust ducts at the various locations shown in Fig. 6. An appropriate exhaust gas trap, valve assembly, and vacuum pump system was used to permit a continuous flow of sample gas through the sample cell in the case of the IR system and to the T.O.F. inlet head in the case of the mass spectrometer system. The final IR cell was fabricated from Kel-F material; Kel-F was used because it is a relatively nonreactive fluorinated polymer. A pair of AgCl (Silver chloride) windows spaced 10-cm-apart established the active path length. Where required, Kel-F oil was used to provide a seal on the valve/stopcock assembly. For calibration of both systems, a 0.5ℓ Monel supply vessel filled with filtered UF_6 was used. All line lengths were minimized to enhance the response time and the lines were surrounded by electrical heater tapes maintained at approximately 425 K.

Figure 7 is a schematic of the IR spectrometer system used for both the post-test residue analysis and the UF_6 rf plasma exhaust gas analysis. This unit provides a continuous record of the infrared transmittance of a sample (gas, solid, or liquid) as a function of wavelength. In operation, the radiation emitted by the source is divided into two beams. One beam passes through the sample, which absorbs radiation wavenumbers corresponding to its characteristic molecular vibration frequencies, while the other serves as a reference. In the photometer section the two beams are combined by a rotating semicircular sector mirror to form a single beam consisting of alternate pulses of radiation from the sample and reference beams. This combined

beam passes into the monochromator where it is dispersed by a grating into its spectral components. Afer leaving the monochromator the radiation passes through one of a set of optical filters. Finally, the transmitted radiation is focused onto a thermocouple detector. The remaining components consist of the amplifier, rectifier, modulation and servo motor systems. The recorder is mechanically linked to the attenuator, such that the pen is displaced by an amount proportional to the change in sample transmittance.

Figure 8 is a photograph of the equipment used in the on-line IR spectrophotometer absorption measurements. In these tests a portion of the exhaust stream from the rf plasma test chamber was routed into the Kel-F cell (see Fig. 6). Additional details of the Kel-F cell installed in the IR spectrophotometer sample section are shown in Fig. 9.

Figure 10 is a photograph of the T.O.F. mass spectrometer and associated equipment as used in the initial UF_6 rf plasma tests. As shown, the inlet section was located close to the exhaust duct assembly of the plasma test chamber. An oscilloscope and a strip chart recorder were used for data acquisition. For the initial tests, a 1.6-mm-OD stainless steel hypo tube sampling probe (identical to type used in IR absorption measurements described in prior section) was located downstream of the high pressure heat exchanger assembly shown in Fig. 6 and on the centerline of the on-axis exhaust duct. The interconnecting line (≈70-cm-long) of 6-mm-OD chemically clean copper tubing was surrounded by electrical heater tape and connected to a Nupro stainless steel bellows shut-off valve. See Fig. 6 for a schematic of the plumbing connections and inlet system used in these tests. The line lengths and interconnections were made as short as possible to enhance the response time. Several modifications were made to the equipment including extending the spectral range to mass numbers of approximately 400, and replacing part of the inlet system with corrosion resistant materials. Some general comments on the operation of this particular type of mass spectrometer follow. Figure 11 is a schematic representation of the T.O.F. mass spectrometer. Specifically, in a T.O.F. mass spectrometer, the gas molecules of interest are introduced into the source region and ionized by bombardment with low energy (70-100 ev) electrons, as schematically indicated in Fig. 11. Within this energy range, the molecules are usually singly ionized. In the ionization process, in addition to the removal of an electron from the molecule, rupturing of molecular bonds can also occur. This bond rupture is normally called molecular fragmentation. The ionized molecules are then pulsed out of the source region by an electric field and enter a field free region --- the analyzer. The ion source is designed so that most ions, regardless of their mass, acquire approximately the same energy. Because the drift region is field free, the ions simply coast with the lighter ions traveling faster than the heavier ones. These differences in velocity result in the arrival of isobaric (equal mass) packets of ions at the detector at different times. The detector is an electron multiplier whose first stage converts the ion packets into electron packets. The electron packets are amplified and fed into a readout or data processing unit (see bottom of

Fig. 11 for example of instrumentation output). Since these processes must take place without significant intermolecular collisions, a vacuum system is used to reduce the gas concentration around the analyzer to a level ($\approx 10^{-5}$ torr) where particle mean-free paths are long. The currents measured by the electrometer amplifier and the peak heights observed on the oscilloscope are linearly related to ion abundance and, hence, species concentration. Proper calibration of the instrument can therefore lead to reproducible quantitative measurements.

Details of UF_6 RF Plasma Test Chamber Interstage Exhaust Duct

Figure 12 is a sketch showing a cross section of the test chamber and primary interstage exhaust duct. This exhaust duct system is referred to as the interstage exhaust duct since it interfaces the test chamber with the secondary exhaust duct assembly. The test chamber endwalls incorporated provisions for locating thermocouples both within the endwall and on the surface of the endwall face exposed to the uranium rf plasma. One thermocouple tip was located flush (exposed to the UF_6 plasma region) with the face of the endwall surface at a radial distance of 1.8 cm from the on-axis centerline; the other thermocouple was located at the same radial distance from the on-axis centerline (different azimuthal location) but was recessed into a well with the tip of the thermocouple 1 mm behind the face of the endwall. The exposed thermocouple was specially constructed using a nickel sheath to better protect it from the hostile uranium plasma environment within the test chamber. (Refer to APPENDIX A for additional discussion on UF_6/F_2 corrosion effects and materials compatibility.) The endwall assemblies were also constructed and manifolded so that independent and variable cooling water flow rates could be applied to each unit as required to minimize the wall coating due to uranium compound deposition. An alternate left (exhaust side) endwall assembly was also fabricated such that a tungsten/tungsten-rhenium (W/WRh) thermocouple could be located within the on-axis thru-flow duct at the axial midplane location of the endwall assembly.

To allow estimates of the type and quantity of uranium compound residue that may deposit on the inside surface of the primary exhaust duct located immediately downstream of the left endwall assembly, a 16-mm-ID water-cooled stainless steel (304) interstage exhaust duct assembly was used. Attachment flanges were welded to each end of the 13-cm-long assembly to simplify removal of the interstage exhaust duct for post-test inspection after uranium rf plasma tests with pure UF_6 injection. The test configuration used in earlier tests (Ref. 9) employed a nonremovable 8-mm-ID water-cooled copper tube exhaust duct assembly that was silver soldered directly to the endwall assembly; this precluded removing the exhaust duct assembly for inspection and material residue analysis after the tests.

Provision was also made for locating a W/WRh thermocouple within the attached flange at the exit plane of the interstage exhaust duct. By using a swage/locking type of fitting, the tip of the thermocouple could be located flush with the inside diameter of the exhaust duct or radially indexed to the axial centerline position. As can be seen in Fig. 3, electronic ice-path compensators were used with rf-shielding and radiation insulation material surrounding the thermocouple shields, plug-ins, and leads; this helped in providing an interference-free output signal during the uranium rf plasma tests. The output from all the individual thermocouples was recorded on strip chart recorders. The UF_6 injection endwall assembly, not shown in Fig. 12, was identical to the exhaust endwall assembly except for the replacement of the axial bypass exhaust section with the argon buffer gas vortex injectors and resizing of the on-axis duct for housing the UF injector assembly (see Fig. 4). The easily removable interstage exhaust duct assembly shown in Fig. 12 could also accommodate several different types of diluent gas injectors (e.g., coaxial, radial injection, and swirl) at the upstream end. These exhaust flow schemes permitted injection of a diluent gas into the peripheral region of the interstage exhaust duct as a means of reducing the uranium compound wall coating. The assemblies also have provision for including either thermocouples or exhaust gas sampling probes at the inlet and exit plane locations. Figure 13 is a photograph of the three different diluent gas injectors used at the inlet of the interstage exhaust duct. Figure 14 is a photograph which shows the entire test chamber configuration and interstage exhaust duct/diluent gas injector assembly as used in the UF_6 rf plasma tests.

Figure 15 is a sketch of the cross section of the transpiration injection interstage exhaust duct assembly. This assembly also has provision for including either thermocouples or exhaust gas sampling probes at the inlet and exit plane locations. The dual concentric wall arrangement consists of a 16-mm-ID, 5-μm nominal pore size Monel duct (1.5-mm-wall thickness) located concentrically within a solid tube outer housing. The annular region acts as the diluent gas injection manifold. The unique feature of employing a porous wall scheme is that, in addition to reducing the bulk temperature of the stream and balancing some of the radially outward diffusion and centrifuging of the uranium compounds with the radial inward injected bleed gas, fluorine gas may be added to the bleed carrier gas to aid in regenerating the various gaseous uranium compounds back to UF_6. Figure 16 contains photographs illustrating additional details of the porous wall duct assembly. The bottom of Fig. 16 shows several of the different porosity ducts used in some of the exploratory flow visualization tests. These consisted of bench-scale tests using a mock-up assembly of the porous Monel duct scheme.

Figure 17 is a photograph showing the porous Monel interstage exhaust duct assembly connected to the downstream end of the primary interstage exhaust duct assembly as used in the UF_6 rf plasma exhaust gas tests.

DISCUSSION OF TEST RESULTS

In preparation for future interfacing of the UF_6 rf plasma experiments reported herein and near-term hot argon/UF_6 exhaust separator, recovery, and regeneration schemes, emphasis was placed on the development of techniques for minimizing the deposition of uranium and uranium compounds on the test chamber peripheral walls, endwall assemblies, and primary exhaust ducts. Figure 18 is a schematic illustrating (by letter code) the key components examined in the post-test analysis. Also shown for reference are the various possible inlet contaminants and species present within the plasma test chamber prior to entering the primary exhaust duct system. Concurrent with the requirement to minimize the uranium compound exhaust deposition is the requirement to maximize the ratio of UF_6 to UF_6 decomposition products in the effluent exhaust gas. To aid in this, different diagnostic techniques have been investigated, including both off- and on-line types, to determine the feasibility of monitoring the concentration of UF_6 and other primary and secondary (contaminants) exhaust gas constituents.

Post-Test Residue Deposition As a Function of Endwall And Interstage Exhaust Duct Operating Characteristics

To aid in estimating the effect of reducing the cooling to the endwall assemblies and interstage exhaust duct assembly on residue deposition, a series of exploratory tests were conducted using the test configuration and exhaust duct system shown in Fig. 12. See also Fig. 14 for a photograph of the assembled configuration within the 1.2 MW rf induction heater test tank.

Initial tests conducted with the uranium rf plasma operating in the 15 to 45 kW total power level range, a chamber pressure of about 2 atm, and mass flow rates of UF_6 from about 0.005 to 0.03 g/s, indicated the temperatures measured within the endwalls (recessed thermocouple location) ranged from approximately 320 K to 500 K. The corresponding temperatures at the tip of the thermocouple located flush with the face of the endwall ranged from approximately 375 K to 760 K. In these tests the argon buffer gas flow rate was maintained constant at 2.7 g/s; the rf operating frequency was 5.4328 MHz, and the annular axial bypass flow rate was preset at approximately 0.6 g/s (i.e., 22 percent of the main argon buffer gas flow rate). In these tests, the UF_6 transfer system, flow metering equipment, and exhaust duct/trap system shown in Fig. 5 were used. Also, throughout this entire test series, the on-line dye laser (uranium line $\lambda = 591.54$ nm) absorption system (see Fig. 13 of Ref. 9) was employed in selected tests to establish the reference operating conditions of the uranium rf plasma compared to prior test results (Ref. 9).

The cooling provided to each of the components was as follows:

annular cooling water flow rate - 0.75 ℓ/s;
right endwall cooling flow rate - 0.095 ℓ/s;
left endwall cooling-flow rate - 0.085 ℓ/s; and,
interstage exhaust duct cooling flow rate - 0.38 ℓ/s

These initial test results indicated that to aid in eliminating some of the post-test residue coating, the surfaces of the endwalls and exhaust duct systems would have to be operated at elevated temperatures. After completion of these tests, a post-test material analysis examination was performed to determine the type of residue coating deposited on each component. Some of the diagnostic equipment described in the 'Description of Principal Equipment' section was used in this analysis. The results indicated the surface of the UF_6 injector and the region of the UF_6 injection endwall assembly immediately surrounding the injector (to a distance of about midradius) exhibited a light coating of UO_2F_2, UF_4, and UO_2 (typically hundreds of milligrams). Figure 19 is a photograph of the rf plasma test section after a representative variable surface temperature endwall test. The post-test uranium compound coatings on the UF_6 injector and both endwall faces can be clearly seen in the photograph. The face of the left endwall assembly also displayed a light coating of primarily UO_2F_2 and UF_4 (typically 50 to 100 mgs) that also extended out to approximately midradius. Examination of the inner wall of the removable interstage exhaust duct and the endwall on-axis thru-flow duct also revealed a coating of pale green material (typically hundreds of milligrams).

To establish that the residue was indeed a coating and not a plating, part of the sample material removed was analyzed by separate emission spectroscopy. The results indicated the principal elements to be almost totally uranium, fluorine and oxygen with no significant traces of reactant wall material; a coating can be more easily removed from the wall as compared to a plating that might occur from the reaction between hot uranium compounds in the vapor state and the wall surface material.

Analysis by IR spectrophotometry revealed the residue to consist primarily of UO_2F_2 (note that UF_4 does not display a characteristic IR spectrum); analysis by electron diffraction also indicated the presence of UF_4, UO_2, and an additional amorphous material not identifiable by either the electron diffraction or IR spectrophotometer analysis techniques. In these initial tests, the thermocouples indicated temperature profiles within the interstage exhaust duct at the downstream station ranged from approximately 300 K at the wall to about 2000 K at the centerline for the lower power conditions. The W/WRh thermocouple located at the upstream station and ¼ of the distance from the centerline to the wall indicated temperatures up to about 2700 K prior to its immediate failure due to chemical attack. (See Fig. 20 for an example of the type of temperature profiles measured.) Other measurements taken at off-axis locations and used for extrapolation to the centerline, indicated centerline temperatures exceeding 4000 K occurred. Post-test examination of the tip of the W/WRh thermocouples under a high power microscope confirmed the fact that the molybdenum sheath (melting point $\approx$ 2900 K) had reacted with the hot uranium/fluorine compounds in the exhaust duct.

Part of the overall objective of this research effort was to gather information relative to the corrosive/erosive effects of hot, pressurized UF_6 and its various decomposition/reactant products (including F_2 and HF). Available information on the corrosion aspects of different materials exposed to UF_6 was presented in Ref. 9. The majority of the information relates to the rate of corrosion (μm/hr) of different materials exposed to UF_6 at a pressure of only 0.32 atm, and temperatures of about 1000 K. Over four orders of magnitude range in corrosion rate have been reported for the various materials tested (typically, 10^{-2} to 10^{2} μm/hr). These include Monel, nickel, inconel, gold, platinum, and stainless steel.

In future tests, the requirement for additional equipment being located downstream of the uranium rf plasma test chamber (e.g., exhaust gas UF_6 separator, recovery, and conditioning components) together with the need for thermocouples and other exhaust gas sampling probe devices to be located in the exhaust ducts and operated for sustained times necessitates further exploration into the corrosive aspects of the hot, pressurized UF_6 exhaust. As an example, an initial review of the literature indicates no thermocouple sheath materials are readily available that can withstand long-time, high-temperature, high pressure exposure to UF_6/fluorine. Additional information is provided in APPENDIX A.

Another important aspect of the research being conducted is in the area of contamination. Contamination in all components must be considered: the UF_6 supply itself; the UF_6 feeder and transfer system; the test chamber (e.g., minute leaks of H_2O); the argon buffer gas supply; the various components of the exhaust system; the various joints, seals, and O-ring materials; and, the handling procedures in the post-test analysis. APPENDIX A includes some additional information related to contamination. As a specific example, the elimination of all potential sources of moisture (H_2O) and/or air (O_2) is most important in this type of test series, since even small concentrations can result in several unwanted chemical reactions which can effect the quantity and type of residue deposited on the walls of the exhaust duct components and/or composition of the effluent gas. An example of such a reaction is:

$$UF_6 + SiO_2 \xrightarrow[\text{catalyst}]{H_2O} SiF_4 + UO_2F_2$$

In this case, the source of the SiO_2 is the inner fused-silica peripheral wall of test chamber.

Test results indicated a molecular sieve and oxygen trap system, of the type shown in Fig. 5, was required in the inlet argon buffer gas supply system to significantly reduce the contamination level. The effectiveness of the filter/trap system was verified in the following set of tests. A parallel connection arrangement was used such that the argon inlet filter/trap system could be activated only when desired. The configuration used in these tests is shown in Fig. 5. The discharge was operated at a power level of approximately 45 kW, a chamber pressure level of 1.75 atm, and

an argon buffer gas flow rate of 3.04 g/s. For this series of tests, these operating conditions were maintained constant to permit a direct comparison of the argon buffer gas inlet system operating both with and without the filter/trap system. The test results are shown in Fig. 21. At a UF_6 mass flow rate of 1.8×10^{-2} g/s, an axial bypass flow of 0.57 g/s, and test times of approximately three minutes, typically 600 to 750 mgs of residue coating was deposited on the inner wall of the removable interstage exhaust duct assembly. In these tests, the cooling water injection flow rate to the interstage exhaust duct assembly was maintained constant at 0.38 ℓ/s. Two additional tests at approximately the same test conditions resulted in a reproducibility of the deposited residue within 10 percent (refer to upper right portion of Fig. 21). When both the molecular sieve and oxygen trap system were activated, a factor of approximately 2.5X reduction in the total quantity of residue deposited on the inside surface of the exhaust duct occurred. During these tests, measurements were also made of the quantity of residue deposited on the faces of both endwall assemblies and the UF_6 injector (refer to data key of Fig.21). In the tests not employing the filter trap system, up to about 10 mg was deposited on the exhaust endwall, up to about 20 mg on the face of the injection (argon inlet) endwall, and up to 40 mg on the UF_6 injector assembly that protruded 2 cm into the test section. When the argon inlet trap systems were used, an approximate factor of 2X reduction in the quantity of material deposited on these components was measured. These results confirm the fact that using traps on the inlet gas system help to reduce the quantity of residue deposited on the surfaces of the test chamber.

A series of tests was also conducted to permit an estimation of the degree of wall coating as a function of the water-cooling flow rate applied to the interstage exhaust duct assembly. These corresponded to a fixed test time of three minutes (total UF_6 mass flow of 3240 mg); all other conditions were maintained approximately constant. The results are illustrated in Fig. 21. The high pressure cooling water flow rate applied to the interstage exhaust duct was throttled down in discrete steps from the maximum of 0.38 ℓ/s to approximately 0.088 ℓ/s (85 percent reduction). This was the lowest level determined by heat transfer calculations to be safe for the steady-state operation without possible component failure. At this condition, approximately 25 mg of residue was deposited (relatively uniformly) onto the interstage exhaust duct.

In one test, the cooling water flow rate was reduced still further; this led to a weep-type water leak at the welded junction between the inner and outer concentric tube assemblies of the interstage exhaust duct. This leak was discovered during rf plasma vacuum start procedure; it also showed up at a water pressure check at 30 atm. This temperature induced failure served as an example of the importance of verifying that all sources and traces of contamination and/or impurities are reduced to the lowest possible levels prior to conducting a given test series; if not, questionable data interpretation may occur which would not be representative of the selected test parameters used.

The results obtained indicate the desirability to operate the endwall assemblies and the interstage exhaust duct assembly at as high a temperature as possible compatible with the structural material limitations.

Tests With Variable Flow Exhaust Duct Interstage Assemblies

Figure 12 shows the configuration used in the tests with the removable, water-cooled interstage exhaust duct assembly which could incorporate different types of exhaust flow augmentation schemes (i.e., coaxial injector, radial injector, and swirl injector). Figure 13 is a photograph showing details of the different design diluent gas injector assemblies. Each assembly had an inside diameter of 1.6 cm; the thickness of the radial injector unit was 0.6 cm, the other two units were 0.95 cm in thickness. The injection cross-sectional area of each component was selected based on flow calculations and estimates of the hot flow test conditions inside the exhaust duct inlet. Five equally-spaced 1-mm-dia orifices were employed in the radial injector scheme, one annular injector ring (annular slot height 1.6 mm) in the coaxial injector scheme, and four equally-spaced tangential injectors (1.2-mm-ID) in the swirl injector scheme (see Fig. 13).

Figure 14 is a photograph showing the entire test configuration installed in the 1.2 MW rf induction heater test tank. In this particular photograph, the coaxial injector scheme was installed and the photograph was taken immediately following one of the uranium rf plasma tests. Visible in the photograph is a light coating of residue material on the UF_6 injector assembly and a very light coating on the inner radius section of the left endwall assembly. An example of the test results is shown in Fig. 22. The weight of residue deposited on the ID of the interstage exhaust duct assembly is shown versus the argon flow rate through the particular diluent injector assembly used. The range of test conditions are shown in the figure along with the corresponding key to the type of injector assembly used. To provide a reference base for the no argon diluent flow case in addition to a reproducibility check, several data points are shown in the upper left corner of Fig. 22. The reproducibility was approximately $\pm$15 percent. Bearing in mind the entire test chamber and exhaust duct system were disassembled and cleaned after each hot flow test, this type of reproducibility was considered good. As can be seen in Fig. 22, the introduction of as little as 0.14 g/s of argon diluent resulted in an approximate order of magnitude reduction in wall coating on the interstage exhaust duct. Further increases in the argon diluent flow rate did not have as pronounced an effect on continuing to reduce the wall coating; thus, changing exhaust conditions may be the dominant effect on the coating level.

At argon diluent injection flow rates of >0.6 g/s, some oscillations were noted in the uranium rf plasma discharge. Apparently, as the flow rate of the diluent gas approached about one-third of the total mass flow rate (without injection) the exhaust conditions were changed sufficiently to result in upstream perturbations on the discharge. These test results show that within the range of

test conditions used, the use of either a swirl or coaxial type diluent gas injector reduces the residue coating on the inside surface of the interstage exhaust duct. Therefore, this or a similar type of exhaust system flow scheme or a combination thereof may be employed in the near-term interfacing tests of the uranium rf plasma system with an argon/UF_6 separation and recovery system.

Tests With Diluent Gas Injection Porous Exhaust Duct Assembly

An alternate scheme investigated to further reduce the uranium compound residue coatings on the inside wall of the interstage exhaust duct assembly was to use a porous duct (i.e., transpiration injection flow system). The basic configuration is shown in Fig. 15. APPENDIX B contains supporting calculations and an analysis of swirling hot flow within a porous duct with radial transpiration injection. Extensive studies have been published on the heat and mass transfer aspects of hot vortex flow within tubes but little, if any, have been published for the case of a plasma vortex flow within a duct with transpiration injection. The unique feature of employing a porous duct assembly as part of the exhaust duct system is that, in addition to providing the required bulk gas cooling and aid in reducing the uranium compound wall coating, different concentrations of F_2 could be doped into an argon carrier gas, for example, to assist in the possible conversion of some of the UF_6 decomposition products back to UF_6.

Bench-scale exploratory cold flow tests were conducted using a mock-up assembly of the porous duct scheme shown in Fig. 15. Figure 16 is a photograph showing several of the different size porosity ducts tested. The custom fabrication of sintered Monel (desirable from the standpoint of corrosion resistance to hot, pressurized UF_6) tubing in a variety of relatively uniform and small pore sizes, permitted conducting a series of comparison tests. TABLE I lists the metallurgical composition and basic property data of the Monel 400 material used. Mock-up assemblies of porous ducts with nominal pore sizes ranging from 40 μm down to 5 μm were tested using flow visualization techniques. Gaseous hydrogen chloride and ammonia were used as the two reactant gases, with a dense smoke occurring from the reaction. Based on visual observations, the 5 μm nominal pore size Monel tube resulted in a very uniform central core of gases flowing within the duct and confined away from the inside diameter of the tube. The exact confinement core sizes were dependent upon the flow conditions selected, and were representative of those anticipated in hot flow tests. Based on these test results, several removable porous Monel (5 μm nominal pore size) interstage exhaust duct assemblies were fabricated for hot flow testing. The top portion of Fig. 16 is a photograph illustrating their construction. The materials and fabrication techniques (including electron-beam welding) were chosen based on compatibility under the expected operating environment. However, the exact determination of the axial and radial temperature distributions present in the uranium plasma exhaust duct assembly is difficult and is further complicated by the presence of the vortex flow in the exhaust duct assembly. The latter effect alone can significantly increase the heat transfer coefficient at the surface of the Monel duct.

During the initial hot flow tests (argon only) conducted using the basic configuration shown in Fig. 15, a hairline circumferential crack developed in the inner Monel tube (approximately 1/5 of the way down the duct from the inlet location). This was apparently caused by thermal stress (tensile) in the inner Monel tube assembly. Partial redesign (free floating end scheme) followed by a different welding procedure, appeared to alleviate this problem. However, several follow-on tests later, a similar circumferential crack again developed near the inlet section. Based on the porous duct analysis results reported in APPENDIX B, and the interstage exhaust duct test results reported in the prior section, it was decided to relocate the porous duct exhaust assembly immediately downstream of the interstage exhaust duct. This new test geometry is shown in the photograph of Fig. 17. As can be seen in Fig. 17, surrounding the porous duct assembly, water-cooled coils were silver soldered directly to the outer wall to alleviate the high heat loads, particularly near the end flange locations. This was also required to provide additional protection for the O-ring seals used at the junction of the different flange assemblies.

A series of tests were conducted using this test configuration to determine if the porous Monel duct assembly performed as well as anticipated. The results are shown in Fig. 23. In this figure, the total weight of residue collected from the porous Monel duct is shown versus the test time in minutes. TABLE II is a summary, including the corresponding test conditions, of the data shown in Fig. 23. After completion of the first test, it became obvious that only very small amounts of residue were being deposited on the inside surface of the porous Monel duct. This emphasized the importance for careful removal of the residue for weighing on a balance that was capable of accurate measurements down to micrograms. In these tests, laboratory distilled and deionized water was used to wash off the coatings from the porous duct assembly. After filtering and drying, the residue weight was determined. In selected tests, post-test analysis was conducted using the various diagnostic instruments discussed in the 'Description of Principal Equipment' section. Using the configuration shown in Fig. 15, W/WRh thermocouples were used to provide an estimate of the temperature within the porous duct exhaust assembly (centerline location) during an actual hot flow test. For typical operating conditions corresponding to the tests shown in Fig. 23, the centerline temperature was approximately 1800 K at the downstream location. Near the wall the temperature was approximately 850 K.

Note that as shown in Fig. 23, the test case corresponding to a low UF_6 injection resulted in the lowest residue coating on the wall of the porous duct (72 μg). Alternately, a reduction in the argon diluent gas injection flow rate through the porous duct resulted in a noticeable increase in the post-test wall residue. An indication of the effectiveness of the porous duct for longer test times at approximately the same test conditions is illustrated by the square data points in Fig. 23. An increase in the weight of post-test residue (within the experimental error) is noted as the test time was increased from 2.5 minutes to over eleven minutes. The approximately 150 μg of coating determined was virtually

nondetectible by visual observation. Figure 17 is a photograph illustrating the type of coatings that occurred in the UF_6 rf plasma tests with the porous Monel duct (Test Case 1, TABLE II). The left endwall had less than 1 mg of coating, the UF_6 injector and right endwall assemblies had less than 10 and 3 mg, respectively. The fused-silica peripheral wall had less than 4 mg (a slight whitish coating is observable in Fig. 17 adjacent to the left O-ring assembly) and the porous Monel duct assembly had $\approx$0.23 mg. Based on these results, it appears that use of a porous Monel duct assembly acting as part of the interstage exhaust duct between the uranium rf plasma test chamber and future Ar/UF_6 separation and recovery systems will permit transport of the majority of hot UF_6 and UF_6 composition products out the exhaust duct to a region where they can be efficiently recovered and reprocessed.

Exhaust Gas Sampling Tests Using Off- and On-Line IR Absorption Techniques

A series of exploratory tests were first conducted to provide an initial estimate of the detectibility and type of gaseous constituents present in the effluent flow within the exhaust duct during the actual uranium rf plasma tests. This information is required at different axial locations within the on-axis exhaust duct as well as within the off-axis axial bypass exhaust duct system pending future integration with a hot Ar/UF_6 separator and reclaimation system.

A review of the literature indicated useful information was available on the infrared (IR) spectra of UF_6 between 2 to 40 μm (Ref. 10). In all cases reported, considerable effort was required regarding purity to obtain consistent test results. For example, the exposure to fused-silica was minimized (note that the peripheral walls of the test chamber used in this test series are high grade fused-silica) and only those results with little or no traces of SiF_4 were documented in the literature. The SiF_4 results from the reaction between UF_6, fused-silica (SiO_2), and traces of moisture. Small amounts of HF are always present and extremely difficult to eliminate completely.

Figure 24 shows the infrared absorption spectrum of room temperature UF_6 over a wavelength range from about 1200 to 500 cm^{-1} (8.5 to 20 μm) as reported in Ref. 10. The reported path length was 10 cm. Note the very intense band at about 623 cm^{-1} and the moderately strong band ($\approx$2 orders of magnitude less) at about 676 cm^{-1}.

A stainless steel hypo tube (304 type) sampling probe (1.6-mm-OD) was used in these exhaust duct system tests. By using an appropriate exhaust gas trap, valve assembly, and vacuum pump system (see Fig. 6) a continuous flow of sample effluent gas could be drawn through a small (approximately 50 cm^3 volume) sample test cell. The initial cell was fabricated from fused silica (2.5-cm-ID cylinder) and had an active path length of 10 cm between a pair of AgCl windows. A pair of fused-silica stopcocks with Kel-F oil were also installed on the peripheral wall of the sample

cell to isolate the collected sample in preparation for the off-line analysis using the IR spectrophotometer. Considerable calibration testing was required before proceeding with an actual hot flow uranium rf plasma test. Two Monel 0.5ℓ canisters containing filtered (using NaF traps) UF_6 (approximately 10 gms net) obtained from the main UF_6 supply vessel were prepared as standard sources. Electrical heater tapes were wrapped around all the connection lines and valves to maintain temperatures sufficient to eliminate possible UF_6 condensation and solidification in the transfer lines. Figure 25a is an example of the IR absorption trace obtained for the evacuated (No UF_6 -- 10 μm) fused-silica sample cell with AgCl windows. In all cases, the path length was 10 cm; a Perkin Elmer Model 457 IR spectrophotometer was used for making the IR absorption measurements. Figure 7 is a schematic diagram of the basic components of the spectrophotometer. The presence of H_2O (moisture) and CO_2 (carbon dioxide) in the reference beam were detectible at the corresponding wavelengths shown at the bottom of Fig. 25a. A trace of a hydrocarbon impurity at about 3.5 μm was also evident. The AgCl window transmission cutoff was at approximately 20 μm as shown at the right side of Fig. 25a. Figure 25b shows the corresponding IR absorption spectrum obtained when the fused-silica cell was filled with approximately 0.5 gm of filtered UF_6 and maintained at room temperature. Considerable care was taken in cleaning and thoroughly outgassing and baking the vessel prior to filling. The labels at the bottom of Fig. 25 indicate the trace impurities occurring at the corresponding wavelength. The distinct absorption peaks corresponding to both UF_6 and SiF_4 are shown by the vertical arrows at the bottom of Fig. 25b. Recall, the SiF_4 is attributed to the reaction between UF_6, fused-silica, and a trace of moisture. Based on results reported in the literature indicating the critical requirement of eliminating all traces of SiF_4, it was decided to fabricate a new test cell out of Kel-F material. This material is a fluorinated polymer that is relatively nonreactive with UF_6 and associated fluorine compounds at near room temperature. Unfortunately, it has a melting point of approximately 450 K, therefore care must be exercised with its use in moderate temperature environments. Additional follow-on tests were conducted with the Kel-F sample cell replacing the fused-silica cell. A special fixture was fabricated to permit centrally attaching the AgCl windows, using Kel-F wax to the ends of the Kel-F cylinder. Figure 9 is a photograph showing the Kel-F cell, filters, valves, and AgCl windows installed in the test section of the IR spectrophotometer. The use of the Kel-F cell eliminated the SiF_4 contamination found in the earlier tests and consistent calibration data were obtained (similar to that shown in Fig. 24). Subsequently, a series of tests were conducted using the test configuration shown in Fig. 6.

A 20-cm-length of chemically-cleaned 6.4-mm-dia copper tubing wrapped with electrical heater tape connected the sampling probe to the Kel-F sample collection cell. The sampling probe was fabricated with a 90 deg bend near the end to permit a direct flow of effluent gas into the probe. By carefully controlling the valve sequence using the system shown in Fig. 6, several samples of the effluent exhaust gas were collected from actual hot flow uranium rf plasma tests. The three exhaust gas sample probe locations indicated in Fig. 6 were used. In all cases, the tip of the sampling probe was located on the centerline axis of the particular exhaust

duct being investigated. Operating conditions used were similar to those shown in Fig. 21. The sole exception was that the chamber pressure was reduced to approximately 1.2 atm to eliminate the possibility of over pressure damage to the AgCl window seal. Figure 25c illustrates the type of off-line IR absorption spectrum obtained. Note the positive identification of the UF_6 peaks (623 cm^{-1} and 676 cm^{-1}) when compared to those shown in Fig. 24. The time interval from actual sample collection to start of sample analysis in the chemistry laboratory using the IR spectrophotometer varied somewhat, but was normally about ten minutes. The results shown in Fig. 25c were obtained with the sampling probe located in the upstream position of the on-axis thru-flow duct, as shown in Fig. 6. Similar results were observed for the downstream location but of a slightly reduced magnitude. A series of calibration tests were also completed to verify the negligible effect of varying the test cell temperature and pressure on the IR absorption spectrum of UF_6. The test range included cell pressures between 125-800 Torr and cell temperatures between about 300 K - 400 K. When the sampling probe was located in the annular axial bypass exhaust duct, no trace of UF_6 was detected in any of the tests. This is of particular importance, since it provides a quantitative measure of the uranium confinement characteristics of the vortex flow employed in the UF_6 rf plasma test chamber. Additional tests using off-line wet chemical analysis techniques (total uranium analysis) substantiated the findings of the IR spectrophotometric analysis. The elimination of all the SiF_4 absorption bands indicated the choice of Kel-F material combined with careful removal of major contaminants was adequate in providing a good reproducible spectrum. These results indicated the feasibility of using IR spectrophotometric measurement techniques for estimating the UF_6 concentration in the exhaust gas system.

To extend this technique to include on-line determination of the gaseous UF_6 concentration in the effluent gas, the Perkin-Elmer Model 457 IR spectrophotometer was adapted onto the exit duct/sampling probe assembly of the uranium rf plasma test configuration. Figure 8 is a photograph illustrating this particular on-line test configuration. The major advantages of employing an on-line diagnostic scheme such as this are: a large amount of valuable data can be acquired in a relatively short time span; and, the elimination of possible nonrepresentative sample acquisition due to the occurrence of post-test chemical reactions within the sample cell. Location of the relatively large IR spectrophotometer instrumentation adjacent to the exhaust duct assemblies of the 1.2 MW rf induction heater test tank required considerable rearrangement of equipment. Also a number of preliminary calibration tests were required to verify adequate shielding of the instrumentation from the plasma radiation and stray rf fields. The valving and line interconnections were similar to those shown in Fig. 6 but, due to physical constraints, a longer ($\approx$50 cm) 6.4-mm-dia copper line connecting the sampling probe assembly to the valve on the Kel-F sample cell was required. Electrical resistance heater tape ($\approx$425 K) surrounded the connecting line to reduce the possibility of constituent deposition on the walls from the effluent gas. This configuration permitted a continuous flow of sample effluent gas through the 50 cm^3 volume Kel-F cell while making the on-line IR absorption measurements. Tests were conducted using both the

623 cm^{-1} and the 676 cm^{-1} wavelengths since these wavelengths possessed the strongest UF_6 absorbance in the IR range investigated. Figure 26 is an example of the output absorbance signal obtained for the 623 cm^{-1} wavenumber. In these tests, the x-axis normal wavelength output of the recorder was converted to a linear time scale and the IR spectrophotometer was locked onto the 623 cm^{-1} wavenumber (determined from prior calibration measurements). The first portion of the trace shows the evacuated Kel-F cell condition ($\approx 10\ \mu m$), which is followed by an argon only (cold flow -- no rf plasma) test condition. The next sequence illustrates a typical reference operating condition with the argon rf plasma only (no UF_6 injection). Some additional signal noise was expected and is noticeable under the rf hot flow test condition. During the next sequence, increasing quantities of UF_6 were injected into the rf plasma in three steps and maintained constant for a sufficient time (typically 30 s) to allow the output absorbance signal to level off. (Refer to TABLE III for additional details.) Immediately following this, the UF_6 injector valve was closed and the rf plasma was manually extinguished. As noted in Fig. 26, the post-test vacuum condition agreed reasonably well with the pretest vacuum calibration; however, a slight realignment of the Kel-F cell was required to bring the signal back to near its original level. Careful post-test inspection of the AgCl window revealed a minute trace of coating which also may have accounted for the inability to achieve the exact pretest calibration level. The data shown in TABLE III illustrate the approximate concentrations measured and confirm the feasibility of using an on-line IR absorption technique for establishing the quantity of UF_6 present in the effluent exhaust gas. The definite advantages of such a system are (1) the ability to collect and analyze a considerable amount of data in a short time (this is particularly important in an experiment such as this wherein several complicated systems must all simultaneously perform correctly (i.e., UF_6 transfer system, 1.2 MW rf induction heater system, single-frequency narrow band dye laser system, and all associated electronic monitoring equipment)), and (2) the potential for eliminating post-test chemical reactions within the sample cell. The experience gained using this system also revealed several potentail disadvantages if used in a near-term 1.2 MW rf uranium plasma/UF_6/argon separator system application: (1) the measurements are primarily limited to UF_6 only; (2) there are cell optical alignment problems and associated AgCl window degradation due to coating and attack by UF_6/UF_6 decomposition products; (3) there are installation problems related to the physical size of the IR cell and required close proximity of the associated equipment; (4) measurements obtained are weighted-averages and do not provide a true radial concentration profile; and, (5) the limited pressure and temperature range associated with use of the Kel-F cell. Because of these potential disadvantages, an alternate technique was investigated and the results reported in the following section.

Exhaust Gas Sampling Tests Using Off- and On-Line Mass Spectrometer Techniques

In preparation for near-term interfacing of a hot argon/UF_6 separator system with the 1.2 MW rf uranium plasma test facility, a second exhaust gas analysis technique was investigated. This technique involved use of a Time-of-Flight (T.O.F.) mass spectrometer. Review of its capabilities indicated the instrument can be adapted for high resolution, rapid scanning over a wide spectral range (mass numbers), and also possesses the flexibility to analyze both major and minor constituents (e.g., minor contaminants in the UF_6/argon system). This is a unique and important feature not possible with the IR spectrophotometer system discussed in the prior section. The instrument selected was a modified Bendix commercial MA-1 unit. In its standard form the instrument is capable of quantitative analysis of samples as small as 10^{-15} moles in as short a time as 20 s. Refer to Figs. 10 and 11 and 'Description of Principal Equipment" section for additional discussion.

Special applications such as this are possible because the T.O.F. uses a straight-line trajectory for all the ions, employs a planar grid ion source, and collects all the ion masses on each cycle of the instrument by the magnetic electron multiplier detector. Thus, by means of an oscilloscope, every mass peak may be monitored at an interval of 100 μs. Using an appropriate strip chart recorder, the analog output system provides permanent recordings of the mass spectra.

An alternate candidate instrument for use in this unique application of analyzing hot, high pressure UF_6/UF_6-decomposition-products in an argon carrier gas is the quadrupole mass spectrometer. Reference 11 and personal communications with the author revealed considerable modifications are required, in conjunction with a molecular beam type inlet system and a liquid nitrogen cold trap to make the quadrupole mass spectrometer reasonably compatible with UF_6. The measurements reported in Ref. 11 were for on-line analysis of UF_6 in gaseous diffusion cascades. The measurements and test results indicated that the apparent high resolution of the quadrupole could not be realized with UF_6, primarily due to inadequate sensitivity and low signal-to-noise ratio. The conclusion reached was that considerable more development would be required to adapt this instrument to the isotopic analysis of UF_6. In the course of evaluation, considerable modifications were completed to the instrument, including modifications to the source structure (Monel filter rods and a nichrome source) and the ionization chamber, in addition to the molecular beam type inlet and cold trap system referenced above. From the standpoint of duty cycle, initial source life of the quadrupole, during exposure to UF_6, was limited to a few hours (analyzer pressures $<10^{-8}$ torr). Although reasonably encouraging data were obtained after extensive modifications to the quadrupole system, overall performance was still considerably below that required for the intended application. Since maximum sensitivity was required, operation of the quadrupole with UF_6 required repeated adjustment of many parameters to minimize the rate of formation of UF_6 reaction products on the ion sources. At

pressures $>10^{-8}$ Torr in the main body of the analyzer these deposits formed very rapidly. In general, reproducibility of desired conditions from day-to-day was unsatisfactory. Noise was difficult to control due to changing surface conditions on the filter poles. Based on these results and the in-house experience with T.O.F. systems and the associated servicing aspects, the T.O.F. mass spectrometer was chosen for application to the PCR research effort.

A review of the literature indicated very few reports exist containing the relative mass spectral intensities for inorganic fluorine containing vapors and gases, in particular, for UF_6. The reason is due to problems related to corrosion and safety. One such report (Ref. 12) was the result of work done in 1974 at Los Alamos Scientific Laboratory. This report points out the difficulties associated with the corrosion/impurity aspects. The corrosion subsequently leads to contamination of the sample by volatile impurities.

Various techniques can be used for obtaining reliable detailed mass spectra of corrosive fluorine containing gases such as hot, pressurized UF_6. These may include elaborate passivation techniques for the surface of the various components (Ref. 13), employment of cryogenic inlet systems (Ref. 14), and use of molecular beams (Ref. 15). The scope of the present effort does not include such an extensive developmental effort at this time, since the main emphasis is on determining the feasibility and practicality of the applicable techniques. Therefore, much of the equipment was adapted with as many fluorine/UF_6 compatible materials available as possible.

Good quantitative analytical measurements using a mass spectrometer system in this type of application require extensive calibration procedures; this allows comparing the spectra taken under similar conditions and, in particular, with the same instrument. Based on the literature search, many of the inorganic fluorine-containing gases (heavy atomic mass) have not been standardized from the standpoint of calibration operating conditions and tabulated ion abundance levels in the mass spectra. This lack of standardization of operating conditions in reporting the spectra make ion abundance levels unreliable for quantitative analysis. The results reported in Ref. 12 present the first extensive cataloging of the ion relative abundance and sensitivities of about twenty-four fluorine-containing gases in a systematic manner. All the measurements were made using a modified Bendix T.O.F. mass spectrometer similar to that used in the tests reported herein. The inlet was constructed entirely of fluorine-compatible materials (primarily nickel and Monel with welded joints). Another subtle but important modification was the use of Kel-F material for the line connecting the molecular leak to the source. Reference 12 indicates that until these modifications were made, introduction of UF_6 generated many impurity peaks.

Figure 27 is a plot, assembled from some of the tabulated experimental data reported in Ref. 12, illustrating the relative sensitivity and relative abundances for UF_6. The sensitivity factor, relative to nitrogen, S (equal to 0.16 for UF_6), is defined as the ratio of the peak height of the largest peak (e.g., Intensity = 100 for UF_5^+) to the peak height of an equivalent pressure of N_2 at its largest peak, m/e = 28. The data key shown within the vertical brackets of Fig. 27 indicates the relative intensity, atomic mass, and corresponding species, respectively. These data were obtained at an ionizing voltage of 70 ev; this is approximately the same level as that employed in the current tests. Personal communication with the author of Ref. 12 again emphasized that use of high purity UF_6 (obtained from Union Carbide Corp.), the modifications described previously, and an extensive passivation procedure (details contained in Ref. 13) first using fluorine and then UF_6, resulted in the elimination of the majority of the large impurity peaks. The gases were sampled several times followed by a nitrogen purge to obtain the relative sensitivities. Reference 12 indicates that the sensitivity was found to decrease slowly with exposure to the samples, particularly for the heavy metal fluorides. This was primarily due to adsorption of compounds on the surface of the glass strip electron multiplier. Reference 12 reports the reproducibility of the relative peak heights was ≤ 2 percent for major peaks and less for minor peaks. The impurity peaks were identified from their relative abundance patterns and subtracted from the spectra. All impurity peaks with relative abundances >0.5 (on a scale of 100) were taken into account. The most frequently observed impurities reported were N_2, O_2, and HF. These were probably introduced from air leaks and reactions with adsorbed water during manufacture, storage, and transfer.

Figure 28 is an example of the type of mass spectral relative intensities obtained from one of the many calibration tests conducted prior to connecting the T.O.F. system to the sampling probe assembly. In this particular test, 100 mm Hg of filtered (using NaF trap system) UF_6 in a 0.5ℓ canister was topped off with 660 mm Hg of filtered argon. These tests included several samplings at the same conditions (T.O.F. unit operated at 5×10^{-6} mm Hg and a scan rate of 100 amu/min) followed by complete transfer line purging with argon for checking relative sensitivities. Results of the calibration tests indicated resonably good reproducibility for the major and minor peaks. The Hg^+ and Hg^{++} lines observed and shown in Fig. 28 were due to the mercury used in the diffusion pump. A number of unidentified impurity peaks can be seen in Fig. 28 (e.g., m/e = 229, 155, 96, 85, 81, 77, 73, and 47). Examination of Ref. 16, which contains a comprehensive index of approximately 8000 mass spectra, did not permit positive identification. The spectral data presented in Ref. 16, consist of the six strongest peaks in each spectrum and their relative intensities, along with the name of the compound. Seven separate indexes are based on molecular weight, most intense peak, and second peak through the sixth peak. Personal communication with the author of Ref. 12, however, revealed a similar grouping of unidentified impurity peaks occurred until such time as all the modifications to the T.O.F. mass spectrometer system mentioned previously were completed. Since the scope of the present effort did not permit

these extensive modifications, these impurities were to be expected. Note that the abundances of all the ions of the UF_6 decomposition species are clearly evident in Fig. 28, with the exception of UF_6^+ and F^+. These would not have been expected in these tests since they have relative abundances approximately an order of magnitude less than the UF_4^{++} peak (1.1 units relative intensity) shown at the atomic mass location of 157 in Fig. 28.

Figures 29 and 30 are two typical examples of the mass spectral relative intensities obtained in the 1.2 MW uranium rf plasma tests using the on-line T.O.F. mass spectrometer system shown in Fig. 10. The data in Fig. 29 are from a test with the sampling probe located in the on-axis exhaust duct directly behind the [illegible] pressure water-cooled heat exchanger, as shown in Fig. 6. The data shown in Fig. 30 are from a test with the sampling probe located in the axial bypass exhaust duct. In all tests conducted, no trace of UF_6* (corresponding to UF_5^+ peak) was detected in any of the measurements taken with the sampling probe located in the axial bypass exhaust duct at the centerline location. This result was also confirmed using the on-line IR absorption technique described in the previous section.

TABLE IV summarizes some of the results obtained using the T.O.F. mass spectrometer system. The data reduction used incorporated the ratio of Ar^{36} to Ar^{40}, since in the majority of tests conducted the magnitude of the Ar^{40} relative intensity was considerably above that of adjacent series. Also included in the data reduction was the cross section difference correction between the argon and nitrogen. TABLE IV shows that the highest concentration of UF_6 determined was of the same order as that determined using the alternate IR spectrophotometer absorption technique. This is believed to be the first time T.O.F. mass spectrometer equipment has been used for on-line measurement of hot, pressurized uranium species from the exhaust of a UF_6 plasma. These results are encouraging from the standpoint that this system represents a flexible and powerful technique for obtaining quantitative measurements of the chemical composition in different sections of the exhaust system and is also applicable to future hot UF_6/argon separator and UF_6 reprocessing system components.

Residue Analysis of Long Run Time Tests Using Selected Configuration and Operating Parameters

A series of tests were performed to investigate the effect of extended test times on the residue wall coatings of the various components. TABLE II summarizes the results. The test times ranged from 2.5 to 11.2 minutes; the UF_6 injection mass flow rate ranged from 1.9×10^{-2} to 6.4×10^{-2} g/s. As previously discussed in the 'Tests With Porous Exhaust Duct Assembly' section, typically 0.1 to 0.2 mg of residue coating was left on the porous Monel interstage exhaust duct. This level of coating was almost nondetectible by visual observation thus demonstrating the effectiveness of the porous wall technique in allowing transport of the majority of the hot UF_6/UF_6 decomposition products to a downstream location where efficient recovery and reprocessing techniques can be applied.

* < 500 ppm --- lower detectability limit of existing gas sampling/T.O.F. system.

TABLE V is an example of a complete post-test analysis conducted that corresponds to the test Case IX shown in TABLE II. In this example the total test time was 11.2 minutes. Refer to Fig. 18 for a schematic of the components examined. Figure 31 contains photographs showing the test chamber before and after this long run time test. Close observation reveals a light coating visible on the UF_6 injector that protrudes into the test chamber from the right endwall. A very light residue coating is also visible on the faces of both endwalls. At the specified UF_6 flow rate of 6.4×10^{-2} g/s, the 11.2 minute test corresponds to a total UF_6 injected mass of 43 gms. Based on the post-test residue analysis, approximately 13 percent of the total UF_6 injected was deposited on the comporents upstream of the cold trap system. The majority of this was deposited on the walls of the high pressure water-cooled secondary exhaust duct (see Fig. 18). Less than 0.1 percent was deposited within the confines of the rf plasma test chamber; approximately 0.6 percent was deposited within the axial bypass exhaust duct.

Based on the results of the different diagnostic techniques employed, the CAMECA Scanning Electron Microprobe (SEM) provided much worthwhile information. This included identification of the elements present in the residue samples as well as the associated scanning electron micrographs/x-ray distributions. Figures 32 through 34 are examples of the type of information obtained for the long run test test using the SEM system. In these examples, a magnification of 500X was used. Both the electron micrographs and the corresponding x-ray distribution for the major component (U) are shown. The results shown in Fig. 32 corresponding to sample residue removed from the surface of the test chamber (UF_6 injector and left endwall). The back-scattered electron micrographs shown in Fig. 32a and 32c illustrate the typical topographical variations present. Figures 32b and 32d show the accompanying x-ray maps corresponding to uranium. At the magnification of 500X, the predominance of uranium, as shown by the white areas, is evident. Figure 33 shows results obtained from electron photomicrographs and x-ray maps taken of residue removed from the axial bypass exhaust duct and the interstage exhaust duct. In the case of the x-ray map for uranium, Fig. 33b illustrates the minor contribution due to uranium. As expected, the sample residue removed from the axial bypass exhaust duct was different than that removed from the on-axis exhaust duct components; the reason is attributed to the bulk temperature differences. The temperature within the axial bypass exhaust duct is considerably lower (5-10X) than that of the thru-flow exhaust. In general, a hotter exhaust combined with downstream water-cooled exhaust ducts/heat exchangers (as in the main exhaust duct system) will result in a more rapid quench effect. This manifests itself as an amorphous residue deposit on the component. Also noted were differences in the sample morphology relative to the axial location in the test component from where the particular sample was taken. This may be related to the type of axial temperature gradient present.

The presence of minor amounts of iron (Fe) and/or copper (Cu) as detected in several of the SEM post-test analyses (see Figs. 32b, 33d, 34b, and 34d) would tend to indicate some reaction with the wall material may have taken place. This was

not confirmed, however, by the IR spectrophotometer absorption and ISS/SIMS measurements or the other diagnostic techniques used. As indicated within the third column of TABLE V different complementary diagnostic techniques were employed to aid in defining the major and minor constituents. These are indicated in the fourth column of TABLE V; the minor constituent is shown within the parentheses. The far right column of TABLE V contains information on visual observations and the accompanying coating pattern observed during the post-test analysis. Because of the possibility of chemical and/or catalytic reactions between the various uranium species and the constituents (including impurities) of the exhaust duct materials, additional material reference samples were prepared and analyzed using both the IR spectrophotometer and the ISS/SIMS techniques. These included standard and anhydrous forms of CuF_2, FeF_2, FeF_3, NiF_2, and $NiSiF_6$. Several of these compounds possess a distinct characteristic spectrum but these absorption bands were not found in any of the post-test analyses conducted during the UF_6 rf plasma exhaust duct tests (see TABLE VIII).

To further the understanding of the types of compounds forming on the surfaces of the various components, additional supporting tests were conducted using the ISS/SIMS technique. The IR absorption technique readily identifies the presence (qualitatively) of the UO_2F_2 but UF_4 possesses no characteristic spectrum in the 2.5 to 40 μm wavelength range. The presence of amorphous material also precludes the use of the electron or x-ray diffraction techniques. Therefore, additional reference samples were prepared of the two predominant fluorides (UO_2F_2 and UF_4) and the three oxides (UO_2, UO_3, and U_3O_8) as potential contributors to possible residue coating; these were analyzed by the ISS/SIMS system. TABLE VI is a summary of available information pertinent to the several dominant oxides and fluorides of uranium. As noted in TABLE VI, the decomposition aspects of several of the compounds complicates the ability to determine what compounds may be initially formed on the walls of the test chamber compared to those determined during post-test analysis after exposure to moist air. The ISS/SIMS system provides two techniques for performing detailed chemical analyses of surfaces. Depending on the system used, the readout of the secondary ion current versus mass number leads to identification of the elements and compounds leaving the surface. Both the sputtered yield and the degree of ionization depend both on the ion being measured and on the properties of the substrate. As a consequence, reference standards are required to do quantitative analysis with the ISS and SIMS. Preliminary cataloging of these standards was initiated during this test program. To provide an indication of the type of analysis results obtained with both the ISS and SIMS instrumentation, Fig. 35 gives an example of the type of intensity versus E/E_o (energy ratio of scattered/incident ion) profile obtained from the ISS system for a reference sample corresponding to UF_4. The locations corresponding to uranium, fluorine oxygen, and copper are labeled on the abscissa. This information forms part of the uranium compound reference standards and diagnostic techniques at UTRC applicable for post-test characterization and quantitative identification of the residue coatings possible on the current and future test configurations.

Figure 36 shows two examples of the surface chemical analysis of some uranium compound residues removed from the wall of the interstage exhaust duct obtained using the SIMS system. These examples show the relative intensity versus the atomic mass units (AMU) (225 to 300). Figure 36a was obtained for the test case wherein the interstage exhaust duct was operated relatively hot. Figure 36b corresponds to a case where the exhaust duct operated at a relatively low temperature and the argon inlet trap system was not employed. A distinct difference in the relative intensity peak heights is noticeable, particularly at AMUs of 257, 273, and 292. Part of this difference may be attributed to the influence of contaminants in the case where the inlet trap system was not activated.

Analysis of the ISS/SIMS test results combined with the IR absorption and the other complementary measurements indicates that the residue deposited (relatively uniformly) on the walls of the exhaust duct is composed almost entirely of UO_2F_2 and UF_4. Based on the limited number of tests conducted, insufficient data are available at present to quantitatively determine the ratio of UF_4 to UO_2F_2 but preliminary analysis using the ratios of UF_2/UOF, UF_3/UF_2, and UF/UF_2 of the test results obtained in this test program would indicate a 50:50 to 70:30 breakdown appears likely. To further improve the ability to quantitatively ascertain the ratio of the uranium compounds present, considerably more reference samples would have to be prepared using different ratios of UF_4 and UO_2F_2 and also some with the inclusion of small percentages of the several oxide compounds. This effort was not within the scope of the present program but may be included in future work.

Refer to APPENDIX A for a complete cataloging of the IR reference sample test results. Reference 9 also contains a summary of an additional thirty reference compound standards used in the IR spectrophotometric analysis.

TABLE VII provides an overall summary of the post-test residue analyses: it also indicates the progress made to date in reducing the residue coatings that occur on the various components used in the UF_6 rf plasma confinement and exhaust duct tests. In general, use of upstream filter and trap systems (for both the argon and UF_6) has aided in eliminating some of the contaminants and subsequent residue coatings. Selecting the inlet flow conditions in the UF_6 rf plasma test chamber with appropriate axial bypass flow has permitted reducing the residue coating that occurs on the fused-silica tube peripheral wall. Employing Kalrez O-ring material (perfluoroelastomer) and using a sparing amount of Kel-F oil on the O-rings used for sealing the fused-silica tube peripheral wall to the endwalls has also helped in minimizing the residue deposited on the peripheral wall. The very light coating that still appears near the ends of the peripheral wall (see Fig. 14) is principally UO_2F_2. This may be attributed to the trace amounts of H_2O in the fused-silica tube being baked out during hot flow tests and, in turn, reacting with the UF_6 in the boundary to form UO_2F_2 and HF according to the reaction $UF_6 + 2H_2O \longrightarrow UO_2F_2 + 4HF$. It is also possible that the moisture consumed in this reaction is regenerated by the following reaction: $SiO_2 + 4HF \longrightarrow SiF_4 + 2H_2O$. Thus trace amounts of moisture are capable of reacting with relatively large amounts

of UF_6. To combat this, more elaborate procedures could be employed in the fused-silica tube precleaning and bakeout but the disassembly of the entire test chamber between every test with replacement of O-rings, Kel-F oil, etc. would nullify the added effort. Prior to all UF_6 rf plasma hot flow tests conducted, the fused-silica tubes were thoroughly washed with trichlorethylene and outgassed under vacuum for an approximately four hour time interval.

As shown in TABLE VII, the approximate order of magnitude reduction in residue wall coatings on the endwall assemblies for the specific configuration tested has been achieved primarily by operating the endwalls at as high a temperature as possible ($\approx$ 700 K) subject to heat transfer and material limitations. The left endwall assembly (exhaust side of the test chamber) inherently operates at a slightly higher temperature ($\approx$ 800 K) than the right endwall and correspondingly the associated wall coatings are less. The right endwall assembly incorporates both the UF_6 injector and the argon vortex buffer gas injectors with their associated secondary flow patterns. These secondary flow patterns in the vicinity of the endwall surface also effect the coating pattern observed (see TABLE V, Component B). Attempts to operate the left endwall assembly at still higher temperatures ($\geq$800 K using a steam augmentation scheme) resulted in severe erosion/corrosion of the inside diameter of the endwall exhaust duct with subsequent failure of the component. Figure 37 illustrates the extremes of these erosion/corrosion aspects.

Based on the overall results of these tests, it appears that the typical milligrams of coating occurring on the left endwall assembly represent about the minimum levels obtainable using this test configuration and operating within the test conditions employed. Further reductions could be achieved by employing porous endwall assemblies and maintaining a bleed flow of argon gas through the surface in contact with the plasma. As shown in TABLE VII, post-test residue analysis of the interstage exhaust duct in the early exploratory tests revealed coatings of typically 600-800 mg. Use of reduced cooling to this component (i.e., operating at higher wall temperatures) combined with upstream injector flow augmentation has reduced these coatings by approximately a factor of 300X. Incorporating a porous Monel interstage exhaust duct assembly with argon bleed flow resulted in another approximate order of magnitude (10X) reduction in the residue wall coating. These levels of coating (i.e., hundreds of micrograms range) are nearing the practical detectibility limit of the measuring instruments and represents an extremely small fraction ($\approx 5 \times 10^{-6}$) of the total UF_6 flow injected into the test chamber. As indicated in TABLE VI, with the exception of the UF_6 injector assembly, the major constituents deposited (not plated -- as determined from separate emission spectroscopy measurements) on the various components were UO_2F_2 and UF_4. UO_2 was also found as a major constituent on the UF_6 injector assembly.

These results are encouraging from the standpoint of minimizing the wall coatings to relatively low levels but also in application to future tests employing batch and/or on-line UF_6 reprocessing-recirculation systems. The presence of only several major constituents each capable of reconversion back to UF_6 should aid in permitting design and development of an efficient UF_6 regeneration exhaust gas system.

REFERENCES

1. Rodgers, R. J., et al.: Investigation of Applications for High-Power, Self-Critical Fissioning Uranium Plasma Reactors. NASA CR-145048, Sept. 1976.

2. Thom, K. and F. C. Schwenk: Gaseous Fuel Reactor System for Aerospace Applications. AIAA Conference on the Future of Aerospace Power Systems, Paper No. 77-513, St. Louis, MO., Mar. 1977.

3. Kendall, J. S. and R. J. Rodgers: Gaseous Fuel Reactors for Power Systems. Paper Presented at 12th Intersociety Energy Conversion Engineering Conference, Washington, D.C., 29 Aug. - 2 Sept. 1977.

4. Rodgers, R. J., et al.: Preliminary Design and Analyses of Planned Flowing Uranium Hexafluoride Cavity Reactor Experiments. United Technologies Research Center Report R76-912137-1, Mar. 1976.

5. Thom, K., et al.: Gaseous-Fuel Nuclear Reactor Research for Multimegawatt Power in Space. International Astronautical Federation XXVIIIth Congress, Prague, 25 Sept. - 1 Oct. 1977.

6. Barton, D. M., et al.: Plasma Core Reactor Experiments. Paper 3D-13 1977, IEEE International Conference on Plasma Science, May 1977, Rensselaer Polytechnic Institute, Troy, N.Y.

7. Mensing, A. E. and J. S. Kendall: Experimental Investigation of Containment of a Heavy Gas in a Jet-Driven Light-Gas Vortex. United Technologies Research Laboratories Report D-910091-4, Mar. 1965. Also issued as NASA CR-68926.

8. Roman, W. C. and J. F. Jarinet: Development of RF Plasma Simulations of In-Reactor Tests of Small Models of the Nuclear Light Bulb Fuel Region. United Aircraft Research Laboratories Report L-910900-12, Sept. 1972.

9. Roman, W. C.: Laboratory-Scale Uranium RF Plasma Confinement Experiments. United Technologies Research Center Report R76-912205, Sept. 1976. Also issued as NASA CR-145049, Sept. 1976.

10. Burke, T. G., D. F. Smith, and A. H. Nielsen: The Molecular Structure of MoF_6, WF_6, and UF_6 From Infrared and Raman Spectra. Journal of Chemical Physics, Vol. 20, No. 3, Mar. 1952.

11. Jones, H. C.: Evaluation of a Quadrupole Mass Spectrometer for the Isotopic Analysis of Uranium Hexafluoride. Union Carbide Report K-1072, Mar. 1975.

REFERENCES (Continued)

12. Beattie, W. H.: Mass Spectral Intensities of Inorganic Fluorine-Containing Compounds. Applied Spectroscopy, Vol. 29, No. 4, 1975.

13. Svec, H.: Mass Spectrometry, R. I. Reed, Ed., Academic Pressure, London, England, 1965, p 233.

14. Cristy, S. S. and G. Mamantov: Cryogenic Mass Spectrometry of Reactive Fluorine Containing Species. International J. of Mass Spectrometry Ion Physics, Vol. 5, 1970, p 309.

15. Vosile, M. J., G. R. Jones, and W. E. Falconer: Application of a Molecular Beam Source Mass Spectrometer to the Study of Reactive Fluorides. International J. of Mass Spectrometry Ion Physics, Vol. 10, 1972, p 457.

16. Anon: Index of Mass Spectral Data. American Society of Testing and Materials Report AMD-11 (Including the Goteborg Univ. Mass Spectral Data Collection).

17. Katz, J. J. and E. Rabinowitch: Chemistry of Uranium. USAFC, Technical Information Service, Oak Ridge, TN., 1958.

18. Dewitt, R.: Uranium Hexafluoride: A Survey of the Physico-Chemical Properties. Goodyear Atomic Corp., Portsmouth, OH., Report GAT-280, Aug. 1960.

19. Hildenbrand, D. L.: Thermochemistry of the Gaseous Uranium Fluorides. Stanford Research Institute Report PY-64822, June 1976.

20. Leng, B. and J. H. Moss: The Fluorination of Uranium and Vanadium Oxides With Some Metal Fluorides. Journal of Fluorine Chemistry, Vol. 8, 1976 (Printed in Netherlands).

21. Steindler, M. J. and R. C. Vogel: Corrosion of Materials in the Presence of Fluorine at Elevated Temperatures. Argonne National Laboratory Report ANL 5662, 1957.

22. Myers, W. R. and W. DeLong: Fluorine Corrosion. Chemical Engineering for Progress, Vol. 44, 1948.

23. Baxter, J. P.: Fluorine Technology. Rev. Pure and Applied Chemistry (Australia), Vol. 2, No. 4, Dec. 1952.

24. Michallet, M.: Action of UF_6 on Some Metallic Fluorides. Commissariat a L'Energie Atomic (Saclay), C.E.A. Report 2110, 1961.

REFERENCES (Continued)

25. Langlois, G.: Corrosion of Metalic Materials by UF_6 at High Temperatures. Commissariat a L'Energie Atomic (Saclay), C.E.A. Report 2385, 1963 (In French).

26. Dixmier, J., et al.: Corrosion Par L'Hexafluoriurne D'Uranium. J. of Nuclear Materials, Vol. 3, No. 1, 1961.

27. Hale, C. F., et al.: High Temperature Corrosion of Some Metals and Ceramics in Fluorinating Atmospheres. Union Carbide Nuclear Co., Oak Ridge, TN., Report K-1459, 1960.

28. Daniel, P. L., et al.: Halogen Corrosion of Metals. Advances in Corrosion Science and Technology, Vol. 5, Plenum Press, N.Y., 1976.

29. Brown, M. H.: Resistance of Materials and Fluorine and Hydrogen Fluoride. AEC REPORT No. MDDC-144, 1952.

30. Jarry, R. L., et al.: The Mechanism and Kinetics of the Reaction Between Nickel and Fluorine. Argonne National Laboratory Report ANL-6684, 1963.

31. McKinley, J.: Mass-Spectrometric Investigation of the Nickel-Fluorine Surface Reaction. Journal of Chemical Physics, Vol. 45, No. 5, Sept. 1966.

32. Skrivan, J. F. and W. VonJaskowsky: Heat Transfer from Plasmas to Water-Cooled Tubes. IEC Process Design and Development, Vol. 4, No. 4, Oct. 1965.

33. Johnson, J. R., N. M. Choksi, and P. J. Eubank: Entrance Heat Transfer from a Plasma Stream in a Circular Tube. IEC Process Design and Development, Vol. 7, No. 1, Jan. 1968.

34. Schmidt, P. S. and G. Leppert: Heat Transfer from Plasma in Tube Flow. ASME Transactions Paper 69-WA/HT-54, ASME Winter Annual Meeting, Nov. 1969.

35. Eckert, E. R. G. and J. N. B. Livingwood: Comparison of Effectiveness of Convection, Transpiration, and Film Cooling Methods with Air as Coolant. NACA Report 1182, 1954.

36. Olson, R. M. and E. R. G. Eckert: Experimental Studies of Turbulent Flow in a Porous Circular Tube with Uniform Fluid Injection Through the Tube Wall. Journal of Applied Mechanics, Transactions of the ASME Paper No. APM-24, Mar. 1965.

REFERENCES (Concluded)

37. Yuan, S. W.: Cooling by Protective Fluid Films. Section G - Turbulent Flow and Heat Transfer, Edited by C.C. Lin. Princeton University Press, Princeton, N.J., 1959.

38. Leadon, B. M.: The Status of Heat Transfer Control by Mass Transfer for Permanent Surface Structures. Aerodynamically Heated Structures, Edited by P. E. Glaser, Prentice-Hall, Inc., Englewood Cliffs, N.J., 1962.

39. Anderson, O. L.: Users Manual for a Finite-Difference Calculation of Turbulent Swirling Compressible Flows in Axisymmetric Ducts with Struts and Slot Cooled Walls. Ft. Eustis TR-74-50, 1974.

LIST OF SYMBOLS

AMU	Atomic mass unit, dimensionless
E/E_o	Energy ratio of scattered to incident ions, dimensionless
f	RF operating frequency, MHz
I	Intensity, arbitrary units
I_o	Incident or source intensity, arbitrary units
I/I_o	Transmission, dimensionless
$\log_{10}(I/I_o)$	Absorbance, dimensionless
L	Path length, cm
ℓ	Liters
m	Particle mass, g
m/e	Atomic mass
$\dot{m}_{Ar}$	Argon buffer gas flow rate, g/s
$\dot{m}_{Ax}$	Axial bypass flow rate, g/s
$\dot{m}_{UF_6}$	UF_6 flow rate, g/s
P	Pressure, atm, mm Hg, or Torr
P_c	Chamber pressure, atm
Q	Power, kW
Q_R	Power radiated, kW
Q_T	Total rf discharge power, kW
R	Radius, cm

LIST OF SYMBOLS (Concluded)

r	Radial distance, cm
S	Sensitivity factor, dimensionless
T	Temperature, deg K
T_s	Wall temperature, deg K
t	Time, minutes (m) or seconds (s)
kV	Voltage, kilovolts
V_ϕ	Swirl velocity, m/s
V_z	Axial velocity, m/s
W	Weight of residue material, mg
X	Mole fraction, dimensionless
Z	Axial length, m
λ	Wavelength, nm or microns Wavenumber, cm^{-1}
$\Delta\lambda$	Wavelength band, nm

APPENDIX A: SUPPORTING INFORMATION ON THE CORROSION/CONTAMINATION ASPECTS OF UF_6 AND ASSOCIATED REACTANT SPECIES

To aid in the analysis of the present and future tests, continued supporting research was conducted and information cataloged pertinent to UF_6 and other candidate reactant uranium compounds and derivatives, the compatibility with different materials, and the associated corrosion/contamination aspects. This APPENDIX highlights some of this information.

With respect to basic properties, UF_6 is, at atmospheric conditions, a crystallized translucid solid (orthorhombic structure). It is unique in being the only uranium compound that has the property of subliming, under normal pressure, at about 329 K. Refer to Refs. 17 and 18 for detailed discussions of the properties of UF_6 and the other related intermediate fluorides. Reference 19 contains a complete discussion of the thermochemistry of the gaseous uranium fluorides.

The complexity of the U-O-F system and the associated properties of UF_6, particularly at elevated temperatures and pressures, make a complete understanding of the corrosion aspects extremely difficult. This is because any reaction, whatever the mechanism, will permit the metal coming into contact with the UF_6 to also react with the fluorine or reactive fluoride from the UF_6. References 21, 22, and 23 discuss the aspects of fluorine technology, fluorination, and fluorine corrosion. Intermediate fluorides may also be present within the gas-metal interface. These intermediates may or may not participate in the actual corrosion reaction, but they will react with the gaseous phase to yield equilibrium products at the particular temperature and pressure conditions. Another complication is that any trace of moisture as an impurity can generate hydrofluoric acid which can also significantly modify the corrosion rate.

Several topics were of interest relative to the type of tests conducted in this research program. The first was the question of impurity and contamination of the UF_6 and other reacting gases and materials. Second was the question of the accuracy of the published property data (much being in disagreement between different investigators), and third was the area of corrosion relative to high temperature, high pressure operation with UF_6 and its decomposition/reactant constituents.

From the standpoint of impurities, a detailed assay of the UF_6 used in the tests reported herein is documented in Ref. 9. Throughout the course of the test program it became obvious that it was extremely important to try and eliminate as much of the moisture, oxygen, and HF present as possible. UF_6 reacts vigorously with H_2O according to the equation: $UF_6 + 2H_2O \rightarrow UO_2F_2 + 4HF$. The incorporation of the traps and getters as used on the supply systems throughout the test program aided in reducing these impurities to tolerable levels. Filtering the as-received

UF_6 through a anhydrous NaF powder trap was effective in reducing the amount of HF contained in the UF_6. There is still a need for additional improvements in the area of contamination.

The chemical state of the metal surface is also of importance with respect to the level of attack by the UF_6. For example, any trace of organic matter (e.g., fingerprints deposited during disassembly/assembly) are a site for preferential attack. The adsorbed water will lead to an immediate decomposition of UF_6 together with the attendant formation of HF. It may be possible to significantly reduce the corrosion by using mechanical polishing of the machined metal surface of the test component. However, a mechanically-polished surface may still contain physical imperfections. Electrolytic polishing would be an alternate scheme for possible elimination of the crystalline layer in question. The presence of thin surface oxides on the initial metal surface may also influence the corrosion rate depending upon the composition, structure, and thickness of the oxide layers.

TABLE VI shows a comparison of several of the physical and chemical properties of the various oxide and fluoride compounds of uranium that are relevant to this research program. As noted in TABLE VI, the decomposition of several of the compounds complicates the ability to determine what compounds may be initially formed on the walls of the test components during testing as opposed to those determined during the post-test analysis using different diagnostic techniques.

Additional reference data were also acquired during this test program using the IR absorption spectrophotometer system. TABLE VIII is a summary of the material reference samples that were examined and cataloged. The majority display a distinct absorption spectrum between 2-40 μm. Should any of these compounds form on the surface of the test components in future tests, a positive identification will be possible. Also included for reference are several of the copper, iron, and nickel fluorides which may form as a surface layer during fluorine passivation conditions.

Before an assessment can be made of potential corrosive situations, information is required on the composition of the constituents at the operating temperatures and pressures in question. Figure 38 is an example of the type of data that have been generated and cataloged. This figure shows the equilibrium composition of a UF_6/argon mixture as a function of temperature. The total pressure of 2 atm is typical of the pressures employed in actual hot flow UF_6 rf plasma tests. Three different UF_6 partial pressures, ranging from 1 Torr to 10^{-2} Torr are included. The temperature range in the actual experiments extended from room temperature to levels approaching 10^4 K within the rf plasma test chamber. In the UF_6 feeder system, typical temperatures were about 450 K, while in the primary exhaust ducts a radial temperature profile was present (as illustrated in Fig. 20) which ranged from about 350 K at the wall to greater than 3000 K on-axis.

The actual UF_6 corrosion process is characterized by the reaction between an anhydrous gaseous phase and a solid phase. This process is comparable to the dry oxidation of metals. Refer to Refs. 24, 25, and 26 for a detailed discussion of UF_6 attack on metals and metallic fluorides. During some of the early tests with the UF_6 transfer system, post-test examination revealed some etch pits after the deposits were removed. Attack by UF_6 can proceed by micropitting; this may be related to the well known fact that halogens in solution also cause pitting. Based on the similarity to dry oxidation depth growth curves, the growth in depth would be expected to follow parabolic time laws. In future experiments, the Secondary Ion Mass Spectrometer (SIMS) could be used to analyze the formation of these fluoride monolayers. The corrosion layers obtained will depend primarily on the nature of the metal (or alloy), its structure and the associated temperature regime. Preliminary observations of some of the test components revealed a powdery layer adjacent to the metal. During other inspections, a somewhat crystalline layer was observed, while in some of the higher temperature regions, a crust-like coating was occasionally present.

At relatively high temperatures (>500 K) and in some locations the surface of the metal appeared to be covered only by the metal fluoride. If this layer is in the powder form, then it would no longer provide a protective coating. As far as the intermediate uranium fluorides are concerned, they most likely will occur on the highly cooled surfaces of the experiment. This can be attributed to their considerable vapor pressure, even at the relatively high temperatures.

The key problem that was present throughout the test program was the occasional clogging of the UF_6 shutoff and flow control valves (see Fig. 5). In spite of strict precleaning, handling, and assembly, plugging of the valves did occur several times throughout the test series. The cleaning procedure employed an acid-flush technique. The component was first cleaned with 0.1 N HCl solution, followed by trichlorethylene, and then a heated bakeout (≈ 500 K). This was followed by outgassing under vacuum conditions for approximately four hours. Other parts of the UF_6 canister and transfer system showed signs of partial attack by UF_6; this included a failure of the nickel tube adjacent to the exit of the UF_6 boiler. The tube contained a 90 deg bend with associated thin wall and residual stresses induced by the stretch bending. The failure was a combination of erosion/corrosion occurring in the vicinity of the high stresses. X-ray and IR spectrophotometer analysis of the material from this and other components of the system (including the plugged valve assembly) indicated UF_4, UO_2F_2, UO_2, and occasionally a fourth unidentified (amorphous structure) compound may be present. After removal of the material, some areas showed signs of micropitting. Under a UF_6 environment, very small (<0.1 μm deep) micropits can start to appear at relatively low temperature (<400 K). Other points of preferential attack are surface defects, such as grinding marks, scratches, etc., or phases out of solid solution. At higher temperatures, the grain boundaries are subject to attack. Reference 26 points out that some of the impurities in the material itself can also be preferentially attacked (e.g., in the steels it is the

sulfides which are most reactive). Oxide inclusions are attacked at higher temperatures along with the silicates. In the case of stainless steels, the attack occurs on sulfides, carbides, and oxides. In copper, Cu_2O is preferentially attacked. With Monel (of the type used in the porous wall duct), the titanium carbonnitrides and magnesium oxides or sulfides are preferentially attacked.

In addition to the temperature and exposure-time factors, the progress of UF_6 corrosion may be influenced by other factors which are external to the metal. These would include purity of the gas phase and pressure. At low and moderate temperatures, pressure is not that significant as reactions are dominated by the diffusion phenomena in the corrosion layers. At higher temperatures pressure becomes more important through the volatility of the reaction products in equilibrium with UF_6. As mentioned previously, the purity of the gas phase is quite difficult to control since there are always some impurities in the UF_6 (particularly HF). Even small quantities of HF can effect the corrosion rate in a significant manner.

The details of UF_6 corrosion aspects are probably most critical when viewed from the safety aspect. Reliable data must be made available to permit judicious selection of the material (and/or combinations of materials) to use for the various test components in order to minimize the corrosion problem and subsequent failure of the component. Due to the unavailability of experimental data on the corrosion aspects of hot, pressurized UF_6, some preliminary information has been accumulated. Some of this may be applicable to future high temperature, high pressure UF_6 plasma experiments. Reference 9 contains an example of corrosion rate data for different materials as a function of temperature. The preferred use of nickel or Monel was obvious when compared to other materials. For example, at 1000 K, there is greater than four orders of magnitude (10^4X) difference between the rate of corrosion of 316 stainless steel compared to nickel. In the regime of UF_6 pressures of about 0.3 atm, typical rates of corrosion are 10^2 μm/hr for stainless steels and 10^{-2} μm/hr for nickel. The progress of the reaction is generally revealed by a weight gain of the material in question. To establish maximum test time safety criteria, measurements could also be made of the depth of the corrosion as a function of test conditions.

Where possible, the majority of the key components exposed to UF_6 and used in the experiments have incorporated nickel or Monel material. A survey of the literature (Refs. 27, 28, and 29) and personal communications with UTRC Materials Laboratory personnel revealed the most corrosion resistant materials to be nickel or nickel alloys (including NiAl). Alternate materials may also be required since nickel possesses a relatively high capture cross section for thermal neutrons, thereby restricting its application in full-scale PCRs to perhaps a thin plating.

A search of the literature revealed very little quantitative experimental data on the UF_6-Ni system. Reference 27 indicates that if proper prepassivation techniques are employed, the reaction of UF_6 with Ni can be significantly reduced, particularly at high temperatures ($\approx$1000 K). Similarly, Ref. 24 indicates that UF_6 does not react with the metallic difluorides (assumed low temperature regime).

At the high temperatures and pressures of interest, the UF_6, F_2, HF, and most of the lower fluorides formed from the dissociation of UF_6 (see Fig. 38) are all relatively corrosive. Since F_2, F, and some HF may be present, they will be the more reactive species. Therefore, the materials used in the different test components should also be capable of long term survival under the fluorine environment.

Most of the research on fluorine corrosion of difference materials has been done at relatively high fluorine pressures. The experiments reported herein and the actual designs for full scale plasma core reactors may operate at considerably lower pressures of fluorine. Lower rates of fluorine attack on the materials should accompany the lower pressures.

A considerable amount of information is available in the literature (see Refs. 28 and 30) on the corrosion of nickel by fluorine. The F_2 occurring from the thermal dissociation of the UF_6 while the HF occurs due to the H_2O contamination reaction with UF_6. Reference 28 contains data on the influence of tmeperature on the corrosion of Ni by F_2. An example is shcwn below.

Temp. °K	P_{F_2} (atm)	Test Time (min)	Estimated Loss of Metallic Nickel for 1 Year Long Exposure (μ)
357	0.92	110	0.21
773	0.92	1800	3.0
913	1.0	150	140
1083	1.0	100	310

Note that increasing the temperature from 357 K to 773 K results in an approximate factor of 15X increase in the corrosion. Extending the temperature to 1083 K results in another two orders of magnitude increase in loss of nickel. The mechanism of the corrosion resistance of nickel to fluorine is one of passivation of the nickel surfaces by NiF_2. The fluorination rate of nickel appears to be sensitive to small amounts of impurities. Most impurities or alloying materials used with nickel (e.g., carbon, iron, sulfur, silicon) degrade the corrosion resistance to fluorine. Figure 39 illustrates the effect of temperature and fluorine on nickel material structural strength. Electrolytic grade nickel 200 starts to exhibit a complete loss in its yield strength at temperatures of about 1200 K; this is also the onset of extensive chemical attack.

Reference 31 contains the results of T.O.F. mass spectrometer measurements made of the reaction of polycrystalline nickel with fluorine. The temperature range was 900-1600 K, the corresponding fluorine pressures were between 10^{-7} and 10^{-4} Torr. The major products were gaseous NiF_2, NiF, and fluorine. These were formed rapidly on the surface at rates linear with the fluorine pressure. NiF

was found to be present on the surfaces over the entire temperature range and desorbed above 1373 K. NiF_2 formation and desorption were found to be important between 900-1600 K. The rate-limiting step in the formation of NiF_2 is probably dissociation of fluorine on the surface.

Based on the above information, it is obvious that considerably more data will be required over a wide range of operating conditions to fully document the possible corrosive effects that long time exposure to high temperature, high pressure UF_6, fluorine, HF, and the intermediate fluorides can have on the various materials proposed for use as components in continued experimental tests. In the limited tests conducted in this program, the periodic post-test inspection of different components has only provided a qualitative indication of the degree of corrosion attack that occurred.

APPENDIX B: SUPPORTING ANALYSIS OF HEAT AND MASS TRANSFER ASPECTS OF SWIRLING HOT FLOW WITHIN A POROUS DUCT WITH BLEED FLOW AUGMENTATION

One of the key components used in the UF_6 rf plasma exhaust gas tests reported in this research program was the porous Monel interstage exhaust duct assembly. Prior engineering analyses and experimental studies have been conducted on the heat transfer from a plasma or high temperature axially flowing gas to the confining walls of a water-cooled tubular test section (Refs. 32, 33, and 34). Additional work has also been published on the aspects of using a porous surface to thermally protect it from an adjacent hot fluid flow (Refs. 35 and 36). This method is known as transpiration cooling. Extensive studies have also been made of both the fluid dynamic and heat transfer effects of transpiration cooling by injecting either the same or a foreign gas through a porous surface into an external flow. These have included both laminar and turbulent boundary layers, in subsonic as well as supersonic flows, with zero as well as nonzero pressure gradients in the direction of flow. (Refer to Refs. 37 and 38 for extensive bibliographies.) Numerous analytical solutions have also been obtained for laminar flow in tubes, between parallel plane walls, and in annuli for transpiration injection through porous walls. In contrast, essentially nothing has been published for the case of swirl flow within a duct with the addition of transpiration injection. Therefore a preliminary supporting analysis was conducted* using a modified existing computer code developed in the Fluid Dynamics Laboratory of UTRC (Ref. 39). Because of the complexity of the problem, only argon gas was considered for both the main carrier gas and the transpiring coolant. Also not included in this preliminary analysis was the additional complex uranium chemistry and possible homo-/heterogeneous reactions and catalytic effects that may occur.

The objective of this analysis was to establish some initial trends which might aid in selecting the flow parameters and configurations to be used in forthcoming UF_6 rf plasma experiments. Experimental test results reported herein have already indicated the feasibility of employing a 5-μm nominal pore size Monel duct to aid in reducing the uranium compound coatings deposited on the walls of the primary exhaust duct. Another attractive feature of employing a porous duct scheme is that it also permits the addition of different concentrations of fluorine gas (F_2) to the diluent argon carrier gas as an aid in converting some of the uranium compounds back to UF_6 while still in the flowing gaseous state. Considerable more analysis and experiments will be required to permit selection of a system that has optimized flow conditions for maximum UF_6 regeneration while simultaneously minimizing the wall coating effect.

*Analysis conducted by O. L. Anderson.

Required inputs to the program were: geometry, physical dimensions of the exhaust duct, gas properties, total inlet mass flow rate, inlet axial and swirl velocity parameters (velocity profiles $V\phi$ and V_Z), inlet temperature profile, wall temperature, and total transpiration mass flow rate (uniformly injected).

The program calculated: the radial temperature and velocity profiles at different axial locations, the heat flux to the wall, the bulk Reynolds and Nusselt numbers, and additional information on the boundary layer parameters. For the purpose of this APPENDIX, it will suffice to include several of the key results and trends determined for future comparison of these to the type of actual hot flow test results obtained in continuing UF_6 rf plasma exhaust system experiments.

Figure 40 is an example of several of the basic test configurations investigated. The first case shown is representative of the type of solid wall, water-cooled interstage exhaust duct assembly used in several of the actual UF_6 rf plasma hot flow tests with swirl. The significant dimensions and test conditions were selected as being representative of those used in the actual hot flow UF_6 rf plasma tests. The second case shown is geometrically similar to the first, but the solid wall has been replaced with a porous wall to permit uniform transpiration injection along the entire length, Z. The third case shown in Fig. 40 is actually a composite of the prior two (i.e., a porous duct has been located immediately downstream of the cooled, solid wall assembly). This geometry closely approximates that used in the group of long run time hot flow test series conducted in this portion of the research program and, therefore, is the case of most relevance.

Due to previously discussed difficulties with corrosion/erosion of the thermocouples used to measure the temperatures at several selected locations within the exhaust duct, the temperature profile was estimated and extrapolated from the limited data available for a low power test case.

For estimating the velocity profiles, a DISA anemometer system and a Thermo-Systems Inc. hot-film probe (2-mil-dia) transducer was used in several of the exploratory tests to measure the approximate isothermal velocity profiles of the argon buffer gas exiting the interstage exhaust duct. Equipment availability and test schedules did not permit extensive measurements, therefore, as with the temperature determinations, additional estimates were also included to account for the influence of higher temperatures.

Figure 41 is a composite plot illustrating the effect of increasing only the transpiration bleed flow rate through the porous duct on the velocity and temperature distributions for the last case shown in Fig. 40 (refer to TABLE II (last case) and Fig. 15 for details of test configuration, significant dimensions, and test conditions). The assumed wall temperature (T_s) was 700 K. The highest transpiration injection bleed flow rate shown (4.3 g/s) corresponds to the actual test condition used in several of the UF_6 rf plasma hot flow tests. It can be seen in Fig. 41c

that increasing the bleed flow rate to this level has resulted in a definite leveling off of the temperature from about the r/R = 0.75 position to the wall location (r/R = 1.0). The effect of the bleed flow on minimizing the wall coating was demonstrated in the experimental results; thus it appears that the diffusion of the uranium compounds toward the wall can indeed be counter-balanced by the radial transpiration injection of the argon bleed gas through the porous wall.

If required in the future, additional refinements could be made to this operational computer program to permit a detailed parametric analysis of the combined effects of varying wall temperature, radial flow rate, and vortex swirl/velocity parameters. This would permit a complete optimization of the test conditions required, within the physical constraints allowable, for minimizing the wall coating due to uranium compound deposition.

TABLE I

SUMMARY OF PHYSICAL AND MECHANICAL PROPERTY DATA FOR MONEL 400
(Ref. - Mech. Engr. Design Handbook)

COMPOSITION, %	Ni 66.5, Cu 31.5, Fe 1.25, Mn 1, Si 0.25, C 0.15, S 0.12
PHYSICAL PROPERTIES	
Density, lb/in.^{3}	0.319
Melting Range, F	2370-2460
Permeability (70 F, H=200 oersted)	-
Annealed	-
Age Hardened	-
Specific Heat (70 F), BTU/lb/^{o}F	0.102
Coefficient of Thermal Exp., in./in./^{o}F	
70-200 F	7.7×10^{-6}
70-1000 F	9.1×10^{-6}
Thermal Conductivity, BTU/ft^2/hr/hr/^{o}F	
70 F	12.6
1000 F	22
Electrical Resistivity, ohms/cmf	
70 F	307
1000 F	367
MECHANICAL PROPERTIES	
Modulus of Elasticity (70 F), psi	
Tension	26×10^6
Torsion	10×10^6
Ult Ten Str, 1000 psi	
70 F	70-1000
500 F	77
1000 F	45
Yld Str (0.2% offset), 1000 psi	
70 F	25-100
500 F	24
1000 F	22
Elongation (in 2 in.), %	
70 F	22-60
500 F	50
1000 F	30
Hardness (70 F), Brinell	110-241

TABLE II

SUMMARY OF UF_6 RF PLASMA TESTS CONDUCTED IN 1.2 MW RF INDUCTION HEATER USING POROUS MONEL EXHAUST DUCT CONFIGURATION

See Fig. 15 for Details of Test Configuration

Test Case	RF Operating Frequency (f-MHz)	Argon Buffer Gas Flow Rate ($\dot{m}_{Ar}$-g/s)	Axial Bypass Flow Rate ($\dot{m}_{AX}$-g/s)	Chamber Pressure (P_c-atm)	RF Discharge Power, Q_T, (kW)	Discharge Diameter d (cm)	Porous Duct Bleed Flow Rate ($\dot{m}_B$-g/s)	UF_6 Injection Mass Flow Rate ($\dot{m}_{UF_6}$-g/s)	Inlet Mass Ratio (UF_6/Ar)	Total Test Time (t-min)	Weight of Residue Deposited on Porous Duct (W_p-mg)
I	5.4325	3.20	0.65	2.7	49	3.0	3.60	0.038	0.012	2.5	.229
II	5.4260	2.85	1.12	2.8	37	3.1	4.27	0.019	0.007	4.2	.072
III	5.4298	3.04	1.15	3.1	47	3.1	3.22	0.028	0.009	6.0	.295
IV	5.4304	3.04	1.12	~ 6	48	3.2	4.27	0.034	0.011	6.0	.132
V	5.4320	3.04	0.90	2.7	48	3.05	4.27	0.022	0.007	10.2	.210
VI	5.42.5	2.95	1.07	2.4	41	3.25	4.27	0.027	0.009	5.6	.188
VII	5.4332	3.10	0.82	2.8	47	3.0	4.27	0.060	0.023	2.5	.110
VIII	5.4310	3.04	0.85	3.4	51	3.2	5.45	0.062	0.020	5.3	.151
IX	5.4288	3.04	1.13	2.6	43	3.15	4.27	0.064	0.021	11.2	.207

TABLE III

EXAMPLE OF TEST RESULTS FROM ON-LINE IR SPECTROPHOTOMETER ABSORPTION MEASUREMENTS

See Fig. 6 for Schematic of Sampling System --
Sampling Probe Located at Position B Downstream of
Low Pressure Heat Exchanger Assembly -- 623 cm^{-1} Wavenumber Used
Operating Frequency, f_o, =5.4362 MHz, P_c = 1.3 atm, IR Cell Pressure ≈1.0 atm
See Fig. 26 for Example of Absorption Measurements Corresponding to A, B, C

	Discharge Power Q_T, (kW)	Sampling Test Time t, (sec)	Argon Buffer Gas Flowrate $\dot{m}_{Ar}$ (g/s)	Axial Bypass Flowrate $\dot{m}_{AX}$ (g/s)	UF_6 Injection Flowrate $\dot{m}_{UF_6}$ (g/s)	Mass Ratio (UF_6/Ar)	Dye Laser Reference Beam Transmission (I/I_o) λ=591.54 nm	Partial Pressure of UF_6 in Kel-F IR Cell, P_{UF_6} (mm Hg)	UF_6 Concentration (ppm)
A	24	50	3.04	1.03	0.008	0.003	0.86	0.07	92
B	36	27	3.04	1.03	0.019	0.006	0.69	0.19	250
C	44	24	3.04	1.03	0.039	0.013	0.44	1.02	671

TABLE IV

EXAMPLE OF RESULTS OBTAINED USING THE T.O.F. MASS SPECTROMETER SYSTEM INTEGRATED ON-LINE WITH THE UF_6 RF PLASMA EXHAUST SAMPLING TESTS

See Fig. 10 for Photograph of System
See Fig. 6 for Schematic of Exhaust Gas Sampling System
See Figs. 29 and 30 for Examples of Mass Spectral Intensity Outputs

	f_o (MHz)	Q_T (k'	P_c (tm)	$\dot{m}_{Ar}$ (g/s)	$\dot{m}_{AX}$ (g/s)	$\dot{m}_{UF_6}$ (g/s)	Mass Ratio UF_6/Ar	Test Time (min.)	Exhaust Location	T.O.F. Instrument Ref. Settings	Measured UF_6 Concentration (ppm)
A	5.42'0	48	2.48	2.86	0.6	0.024	0.008	5	Centerline of on-axis thru-flow duct -- upstream location A (See Fig. 6)	mult. gain=6 scan rate=4 $P_{c_{T.O.F.}}$ = 5×10^{-6} mm Hg	≈500
B	5.4199	45	2.20	2.86	0.58	0.014	0.005	3	Centerline of on-axis thru-flow duct -- downstream location B (See Fig. 6)	mult. gain=6 scan rate=4 $P_{c_{T.O.F.}}$ = 5 $)^{-6}$ mm Hg	<500
C	5.4230	43	2.35	2.86	1.03	0.014	0.005	6	Centerline of axial bypass duct -- Location C (See Fi . 6)	mult. gain=6 scan rate=4 $P_{c_{T.O.F.}}$ = 5.2×10^{-6} mm Hg	<500

TABLE V

SUMMARY OF POST-TEST ANALYSIS CONDUCTED AFTER LONG RUN TIME UF_6 RF PLASMA TEST

See TABLE II, Case IX for Corresponding Test Conditions
See Fig. 18 for Schematic of Components Examined

Component	Weight of Residue (mg)	Diagnostic Techniques Employed	Constituents	Visual Observation/Coating Pattern
A-UF_6 Injector	17.5	SEM	U(O,F,Cu)	Light brown, grey coating in vicinity of tip, mint green coating near face of endwall, clean copper on face of tip exposed to plasma.
		IR	UO_2^{2+}	
B-Right Endwall Assembly	6.6	SEM	U(F,Cu)	White mist coating on argon vortex injectors, light brown/green/white coating extending to approximately midradius, inner portion more green/brown.
		IR	UO_2^{2+}	
		Electron Diffraction	Trace UF_4 + amorphous material.	
C-Fused-Silica Peripheral Wall	9.2	SEM	U(O,Si,F)	Trace of white misty residue near left end in area adjacent to O-ring, similar pattern at extreme right end with additional evidence of swirl pattern.
		IR	UO_2^{2+}	
		Profilometer	≤ 1 μm coating	
		Electron Diffraction	Trace UF_4 + amorphous material.	
D-Left Endwall Assembly	1.4	SEM	U(F,O)	Essentially clean, also true for region inside endwall exhaust duct.
		IR	UO_2^{2+}	
E-Axial Bypass Exhaust Duct	240.3	SEM	O,F(U)	Whitish/pale green very light coating uniformly deposited on inside diameter.
		IR	UO_2^{2+}	
F-Interstage Exhaust Duct	11.7	SEM	U,O,Fe(Cu,Si,F)	Whitish colored light coating uniformly deposited over entire inside diameter.
		IR	UO_2^{2+}	
		Wet Chem.	UO_2F_2	
		SIMS/ISS	UO_2F_2,UF_4	
G-Porous Monel Duct	0.2	SEM	U,Fe(F,O)	Barely visible whitish mist coating at extreme downstream end of duct.
		IR	UO_2^{2+}	
		Emission Spectroscopy	Majority U trace of reactant wall material.	
H-High Pressure Water-Cooled Secondary Exhaust Duct	5490.	SEM	U,(F,O)trace Cu	Mist green coating deposited relatively uniformly on inside diameter.
		IR	UO_2^{2+}	

TABLE VI

COMPARISON OF SEVERAL PHYSICAL AND CHEMICAL PROPERTIES OF VARIOUS OXIDE AND FLUORIDE COMPOUNDS OF URANIUM

Element/ Component	Color	Stability to Moist Air at Room-Temp.	M.P. (°C)	B.P. (°C)	Solubility in H_2O (Hot/Cold)
U	Bright silver (prior to tarnishing in air)	$+H_2O$, $+O_2$ $\longrightarrow$ UO_2 <200°C	1132	3818	No
UO_2	Brown-Blue	Stable	2500	—	No
UO_3	Yellow-Red	Stable	Decomposes	—	No
U_3O_8	Olive Green-Black	Stable	Decomposes (1300 $\longrightarrow$ UO_2)	—	No
UF_3	Viole Red-Black	Unstable	Decomposes at >1000		Slightly soluble (Decomposes)
UF_4	Green	Stable	960	No Reliable Data Available	Very slightly Soluble($\approx$100 mg/ℓ)
UF_5	White	$+H_2O \longrightarrow UO_2^{+2} + UF_4$	—		Decomposes
U_2F_2	Black	$+H_2O \longrightarrow UO_2^{+2} + UF_4$	—		Decomposes
UO_2F_2	Pale Yellowish-White	Depends on Preparation 1) low temp. prep. $\longrightarrow$ hygroscopic 2) high temp. hydro-fluorination $\longrightarrow$ no deliquescence	Decomposes (>120)	—	Yes

TABLE VII

OVERALL SUMMARY OF POST-TEST RESIDUE ANALYSIS RESULTS FROM UF_6 RF PLASMA TESTS

See Fig. 18 for Schematic of Components Examined

Component	Early Tests (Including Exploratory)		Tests To Date	
	Residue Weight (mg)	Major Constituent	Residue Weight (mg)	Major Constituent
Fused-Silica Peripheral Wall	50-600	UO_2F_2,(trace UF_4), UO_2, γUO_3, O-ring decomposition products	4-30	UO_2F_2,(trace UF_4)
Left Endwall	25-100	UO_2F_2,UF_4 UO_2	0.1-3	UO_2F_2,UF_4
Right Endwall	90-200	UO_2F_2,UF_4 UO_2	4-20	UO_2F_2,UF_4
UF_6 Injector	200-400	UO_2F_2,UF_4 UO_2, αUO_3,unidentified compound,(trace Cu)	10-50	UO_2F_2,UF_4,UO_2
Axial Bypass Exhaust Duct	—	UO_2F_2,UF_4,(trace U_3O_8)	100-300	UO_2F_2,UF_4
Interstage Exhaust Duct	600-800	UO_2F_2,UF_4,(trace U_3O_8)	7-250	UO_2F_2,UF_4
Interstage Exhaust Duct Flow Augmentation	—	———	0.15-2.5	UO_2F_2,UF_4
Porous Monel Exhaust Duct	—	———	0.07-0.3	UO_2F_2,UF_4

Average Test Time 3 minutes (range 1-11.2 minutes)

TABLE VIII

SUMMARY OF KEY MATERIAL REFERENCE SAMPLES USED IN IR SPECTROPHOTOMETRIC ANALYSIS

(Refer to TABLE VI of Ref. 9 for additional list of cataloged reference samples.)

Sample	Available Within UTRC	IR Spectrum Completed	Displays Distinguishable Spectrum
KBr	Yes	Yes	Standard Blank--No
Kel-F Oil	Yes	Yes	Yes
UO_2	Yes	Yes	No
UO_3-amorphous	Yes	Yes	Yes
UO_4	Yes	Yes	Yes
U_3O_8	Yes	Yes	Yes
$UO_2F_2(UO_2^{2+})$	Yes	Yes	Yes
$UO_2 \cdot nH_2O (n=3,6)$	Yes	Yes	Yes
USi_2	Yes	Yes	No
CuF_2 anhydrous	Yes	Yes	? - highly reactive
$CuF_2 \cdot 2H_2O$	Yes	Yes	Yes-weak-reactive
FeF_2 anhydrous	Yes	Yes	No
$FeF_3 \cdot 3H_2O$	Yes	Yes	No
FeF_3 anhydrous	Yes	Yes	Yes-weak
$NiF_2 \cdot 4H_2O$	Yes	Yes	Yes
NiF_2-anhydrous	Yes	Yes	Yes-weak
$NiSiF_6 \cdot 6H_2O$	Yes	Yes	Yes
UF_6	Yes	Yes	Yes
UF_5	No	No	-
UF_4	Yes	Yes	No
Silicon O-ring decomposition products	Yes	Yes	Yes
Kalrez O-ring decomposition products	Yes	No	-

FIG. 1

PLASMA CORE REACTOR UNIT CELL CONFIGURATION

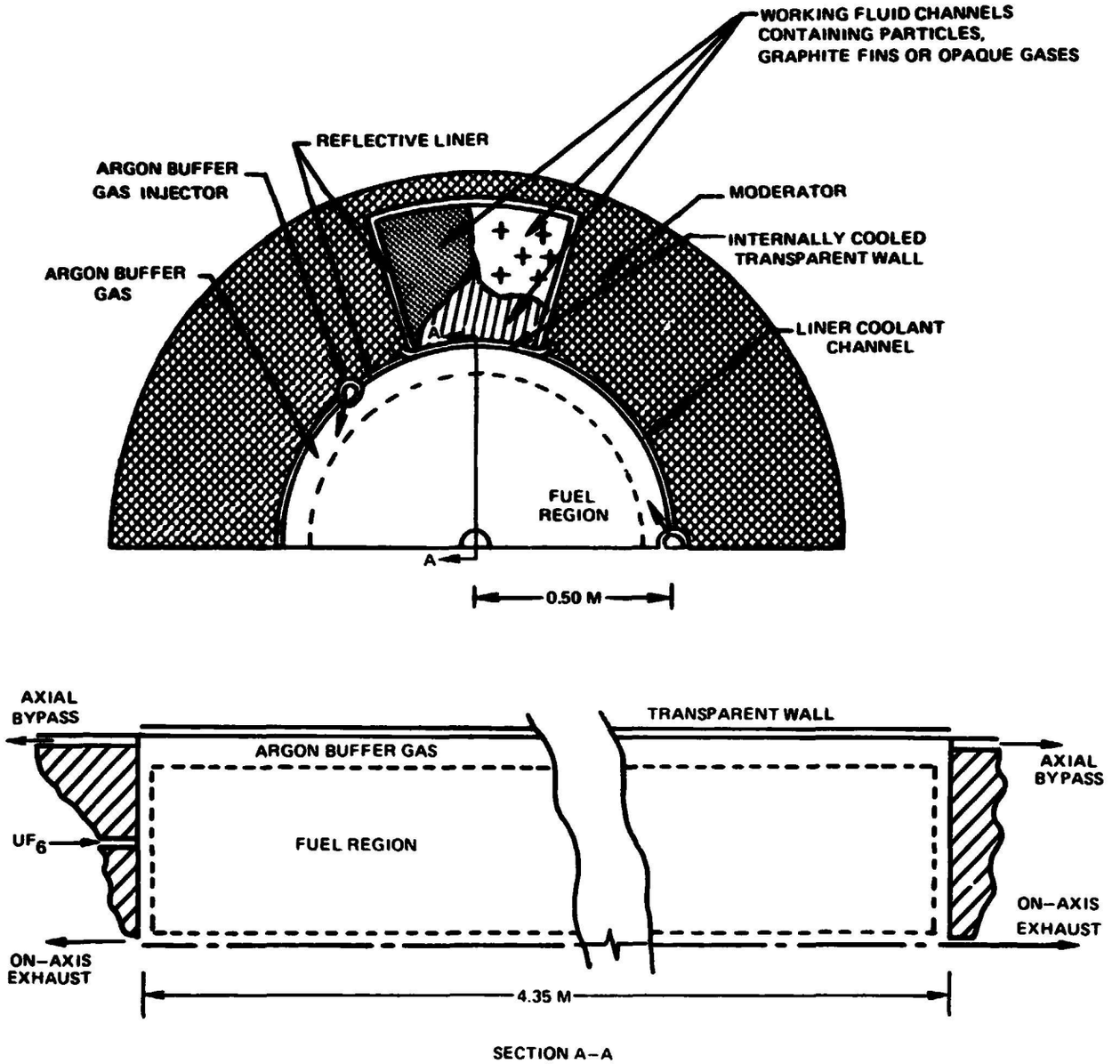

SECTION A–A

SCHEMATIC OF ARGON/UF_6 SEPARATION AND RECIRCULATION SYSTEM FOR PCR UNIT CELL CONFIGURATION

SEE FIG. 1 FOR UNIT CELL CONFIGURATION

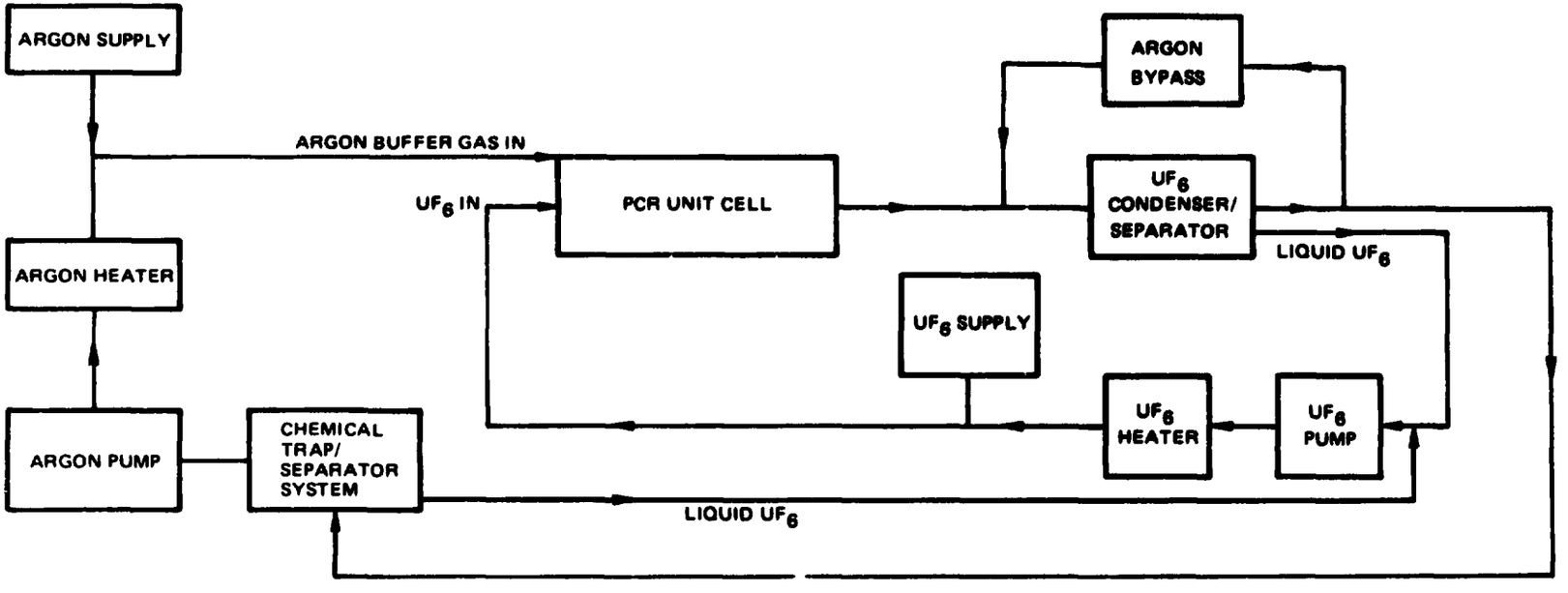

FIG. 2

PHOTOGRAPH OF BASIC TEST CHAMBER CONFIGURATION AND EXHAUST SYSTEM USED IN UF_6 RF PLASMA TESTS

(SEE FIG. 4 FOR SKETCH OF BASIC TEST CHAMBER CONFIGURATION)

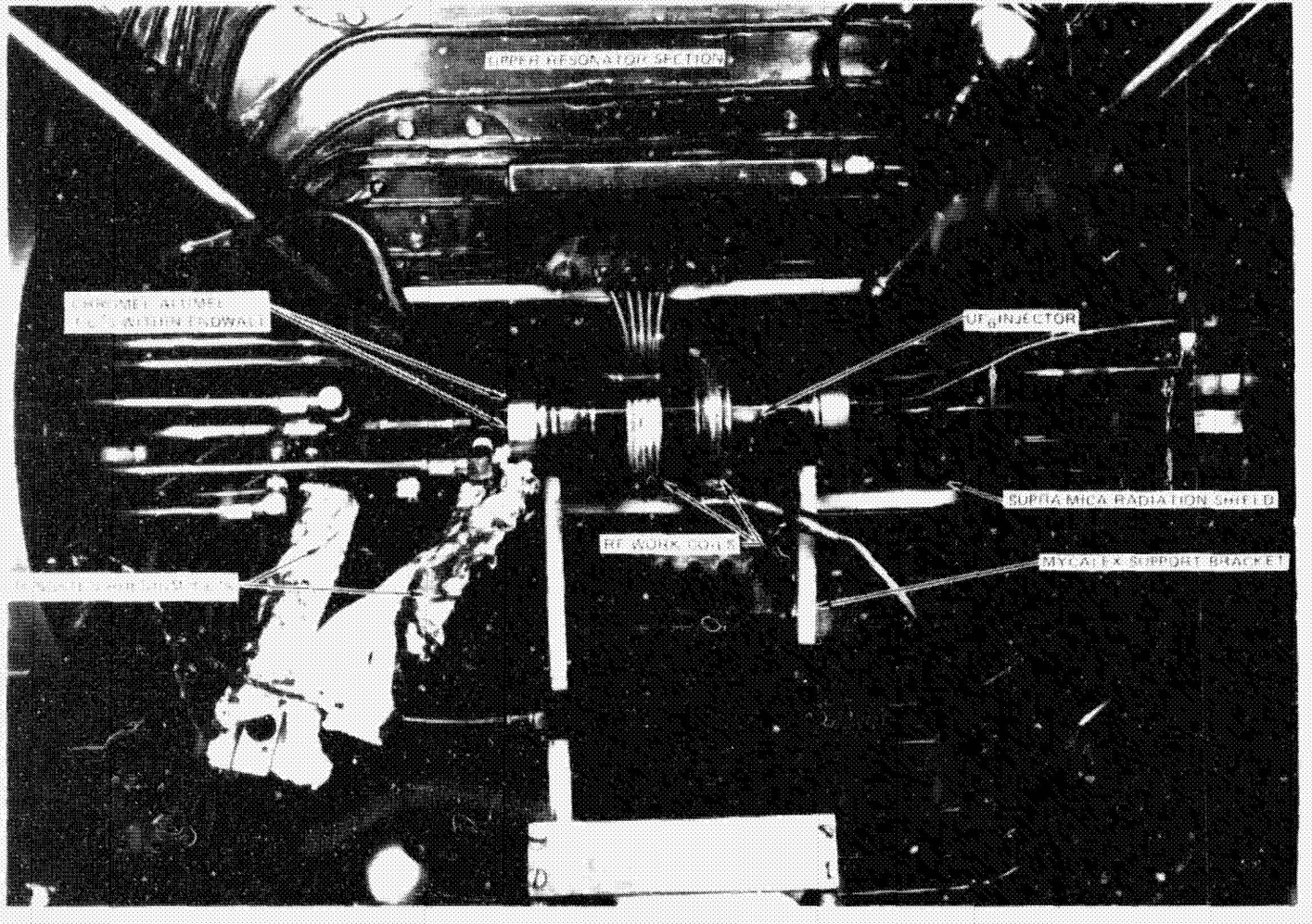

FIG. 3

SKETCH OF BASIC TEST CHAMBER CONFIGURATION USED IN UF_6 RF PLASMA TESTS

(SEE FIG. 3 FOR PHOTOGRAPH OF TEST CHAMBER CONFIGURATION INSTALLED IN 1.2MW RF INDUCTION HEATER TEST TANK)

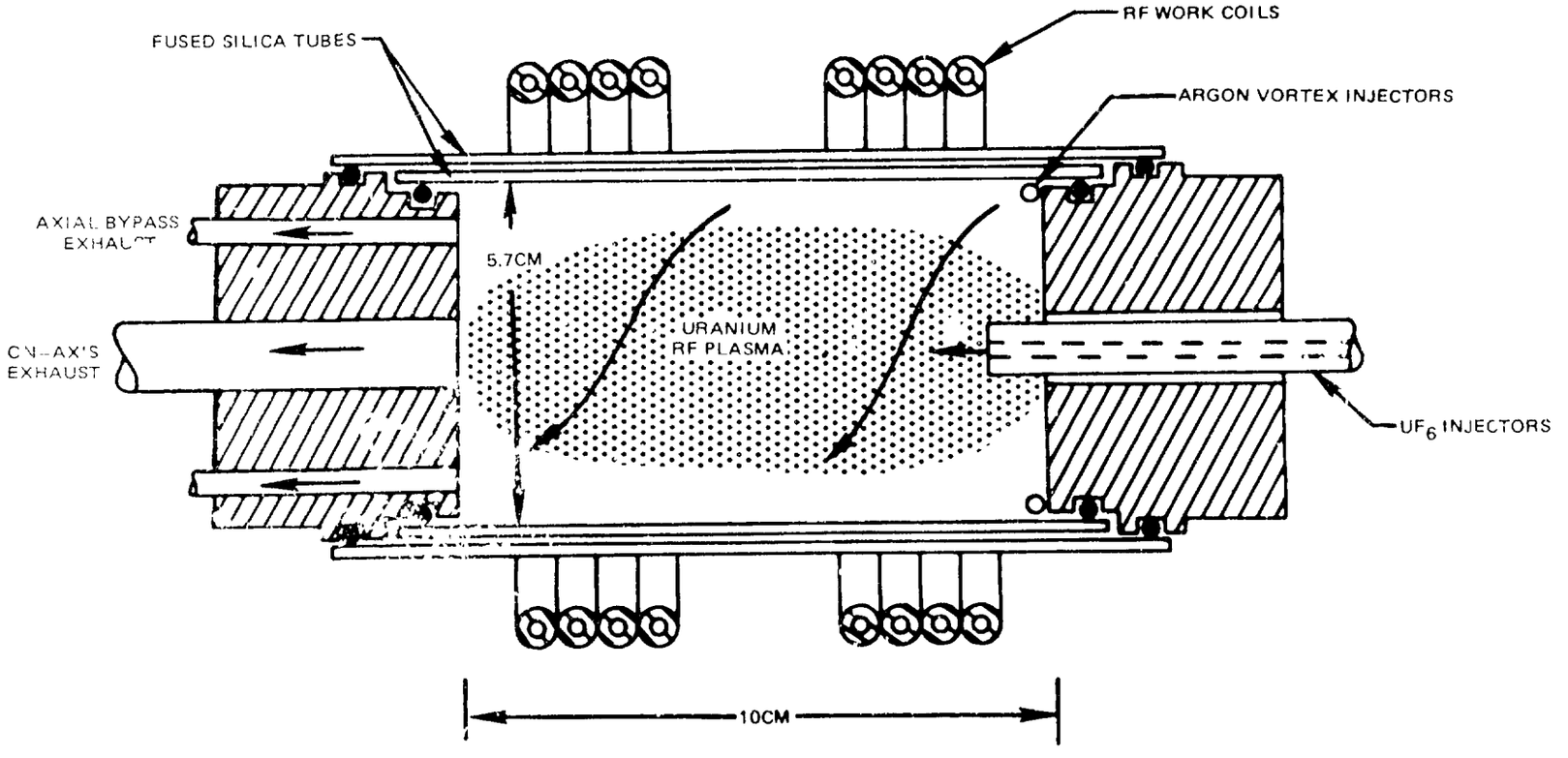

(NOT TO SCALE)

FIG. 4

SCHEMATIC OF ARGON BUFFER GAS AND UF_6 SUPPLY SYSTEMS

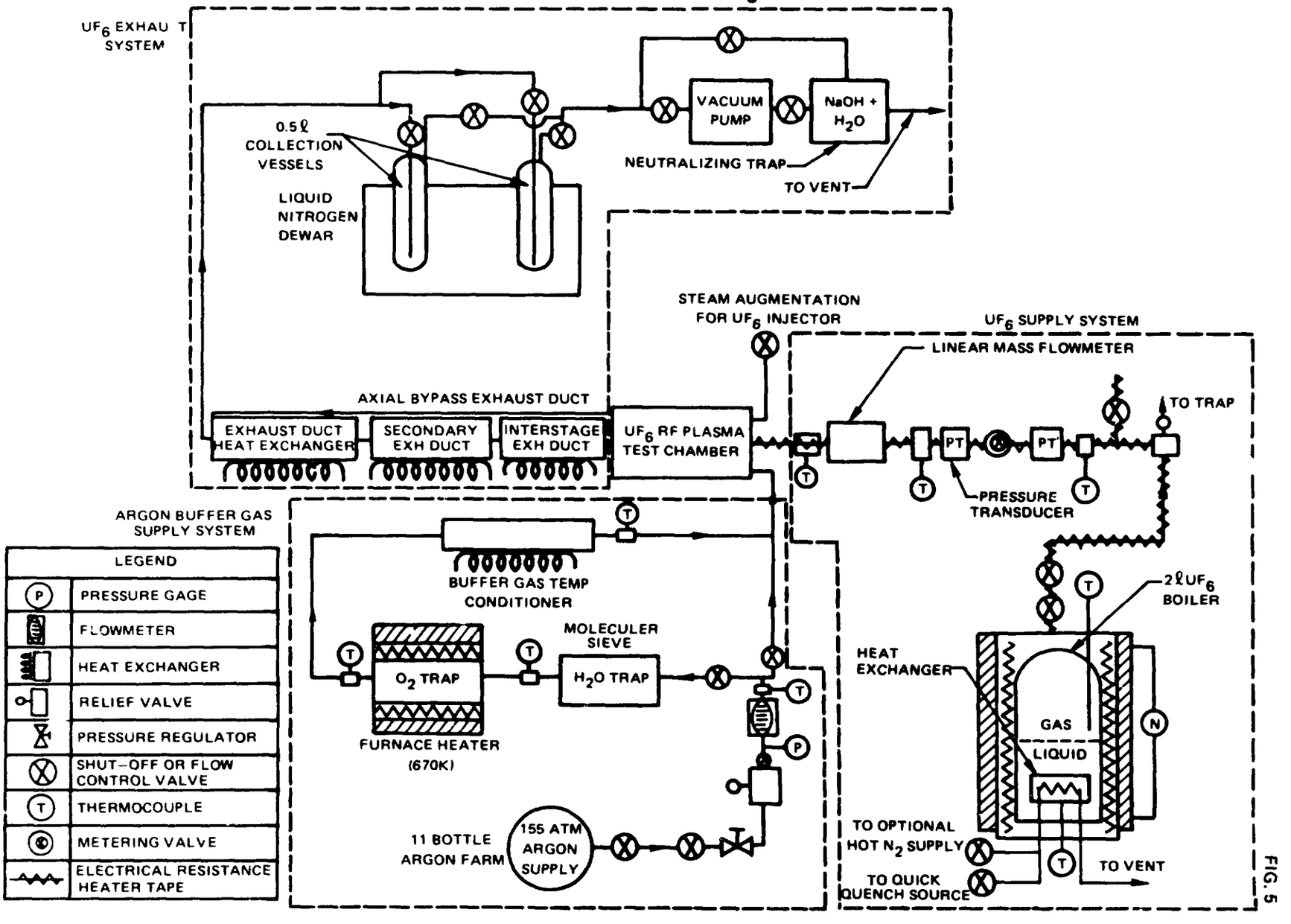

FIG. 5

SCHEMATIC OF UF_6 EXHAUST GAS SAMPLING SYSTEM USED IN BOTH IR SPECTROPHOTOMETER ABSORPTION AND T.O.F. MASS SPECTROMETER MEASUREMENTS

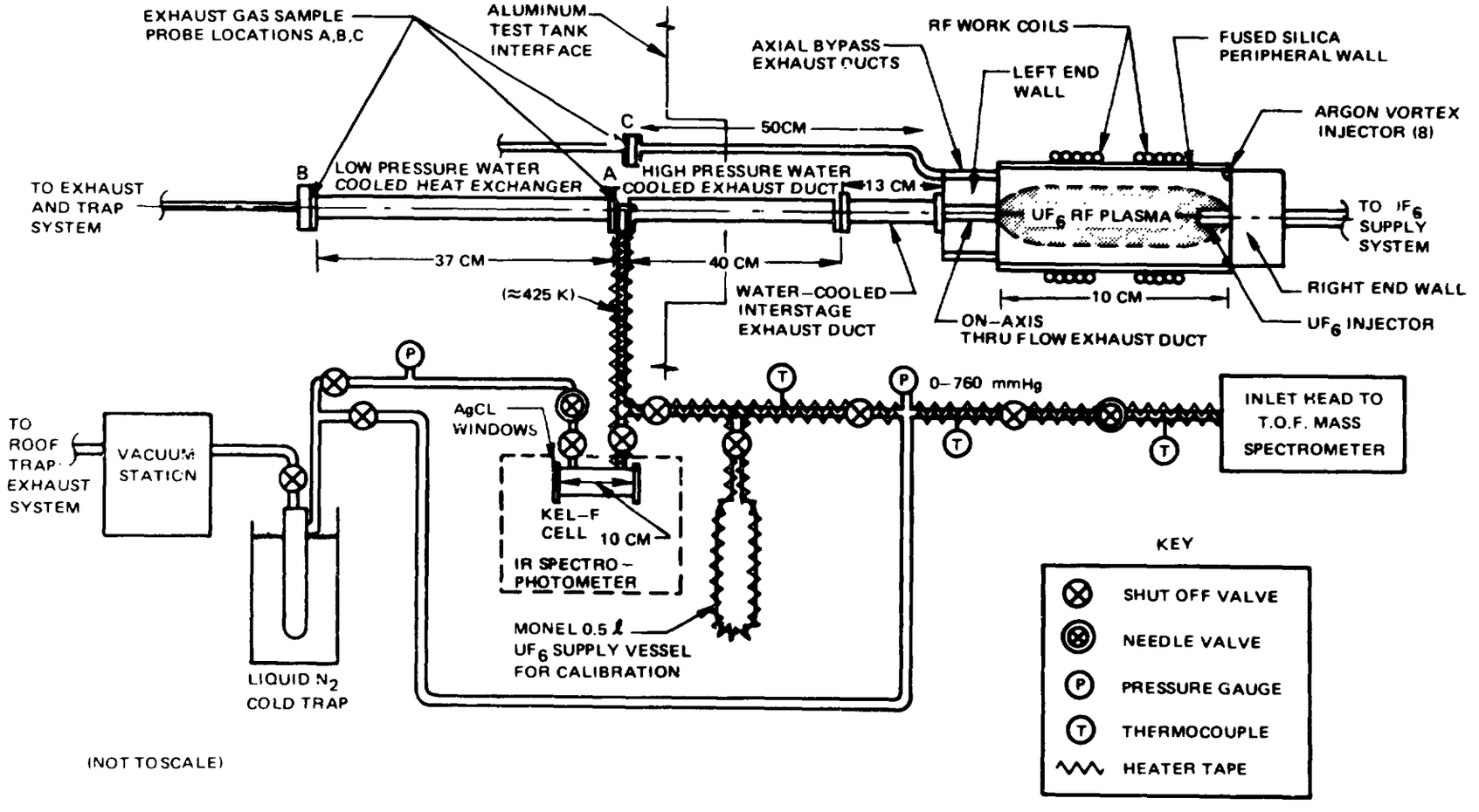

FIG. 6

SCHEMATIC OF IR SPECTROPHOTOMETER SYSTEM USED IN UF_6 RF PLASMA EXHAUST GAS AND POST TEST RESIDUE ANALYSIS

SEE FIG 18 FOR PHOTOGRAPH OF SYSTEM

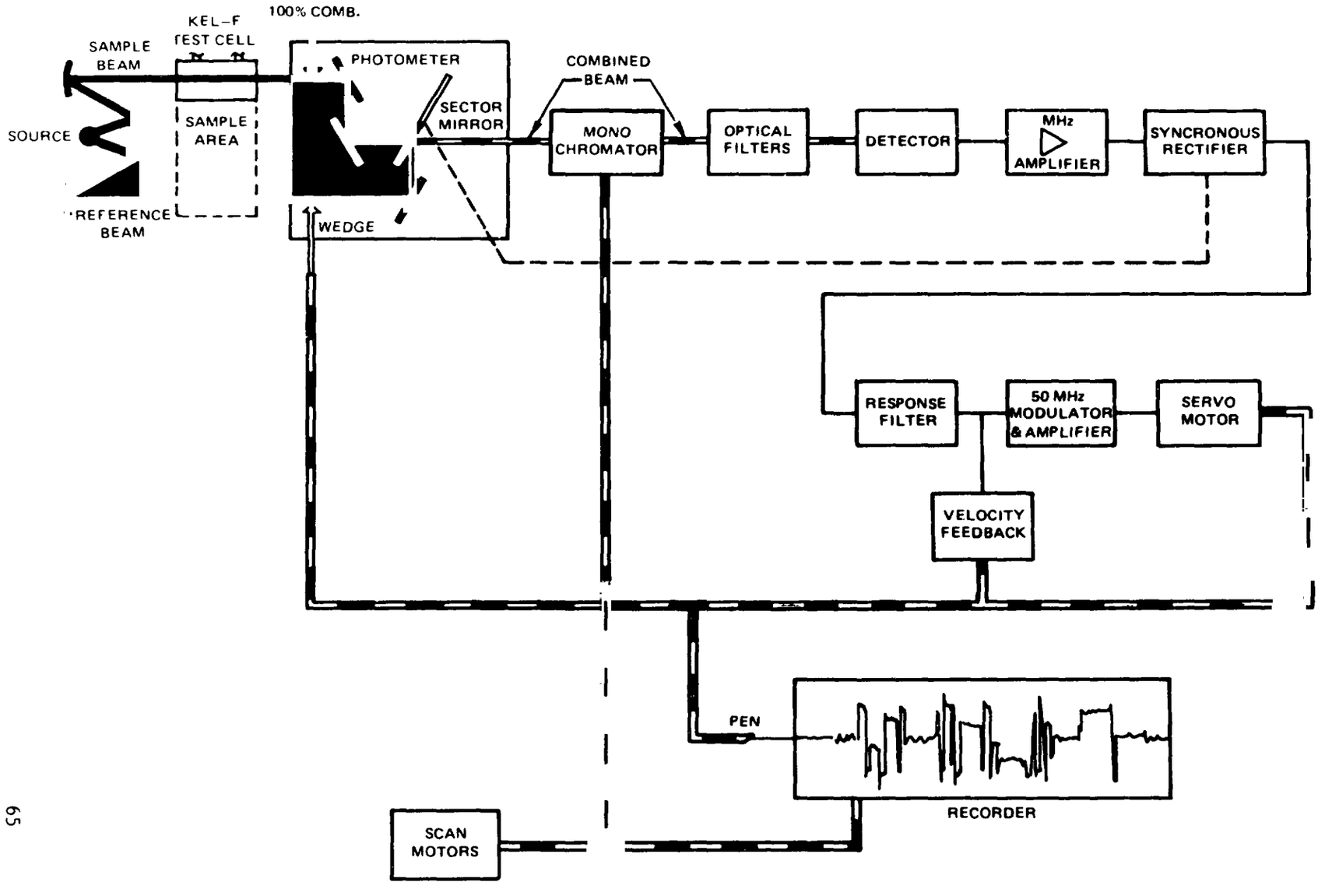

FIG. 7

PHOTOGRAPH OF EQUIPMENT USED IN ON-LINE IR SPECTROPHOTOMETRIC ABSORPTION MEASUREMENTS OF EXHAUST GAS FROM UF_6 RF PLASMA TESTS

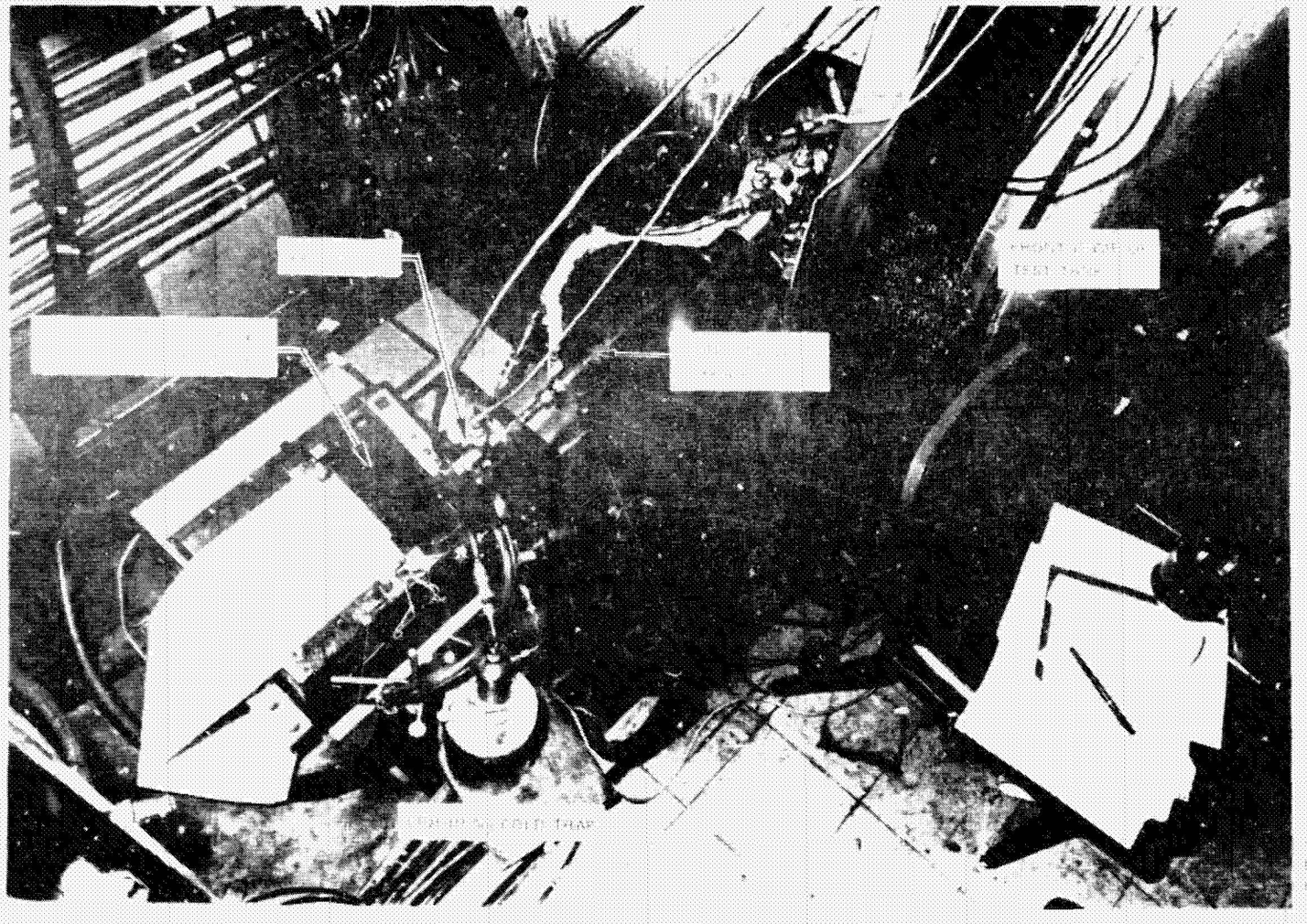

FIG 9

PHOTOGRAPH OF KEL-F CELL AS USED IN EXHAUST GAS
IR ABSORPTION MEASUREMENTS

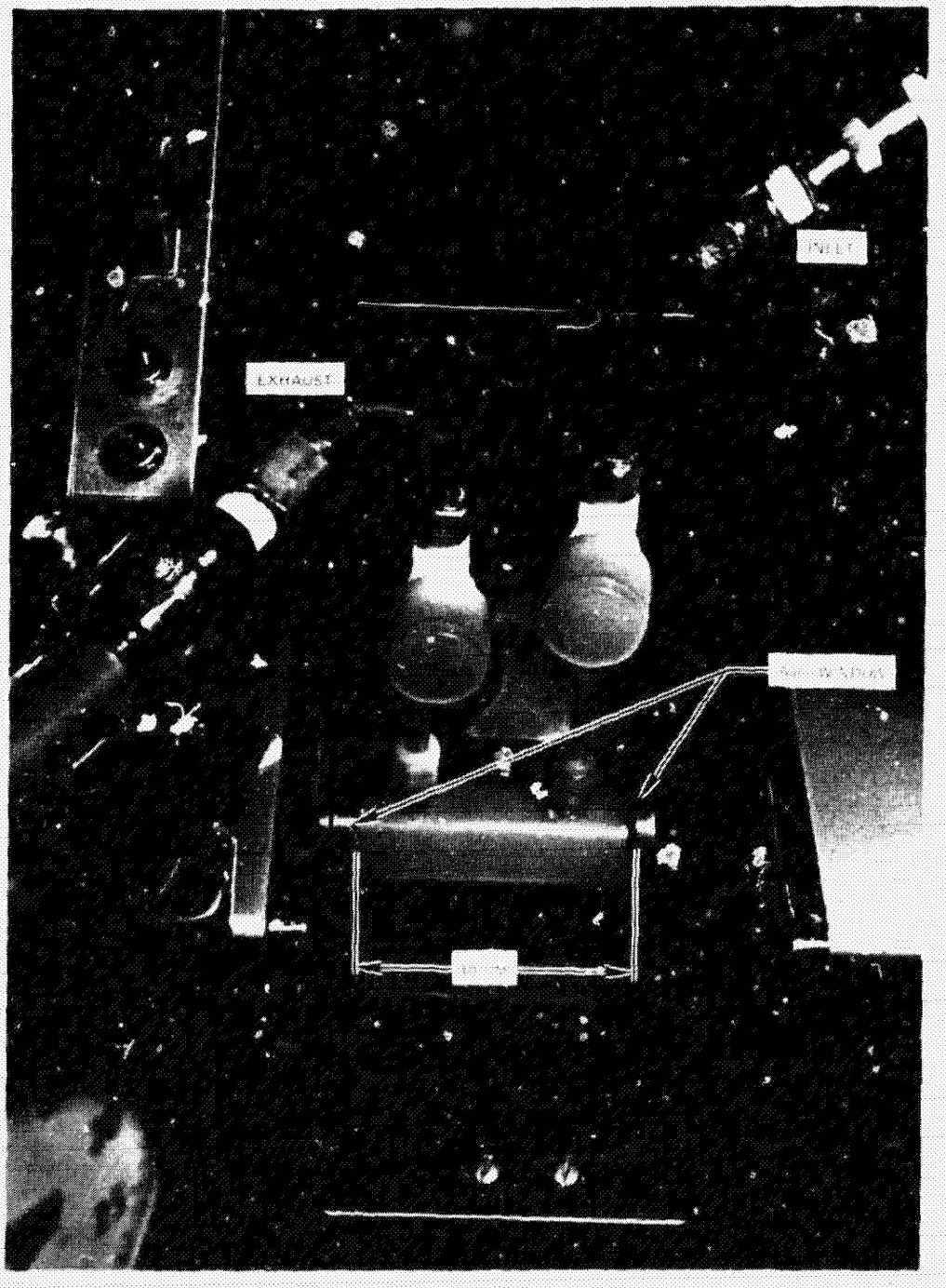

PHOTOGRAPH OF TIME OF FLIGHT MASS SPECTROMETER EQUIPMENT USED IN UF_6 RF PLASMA TESTS

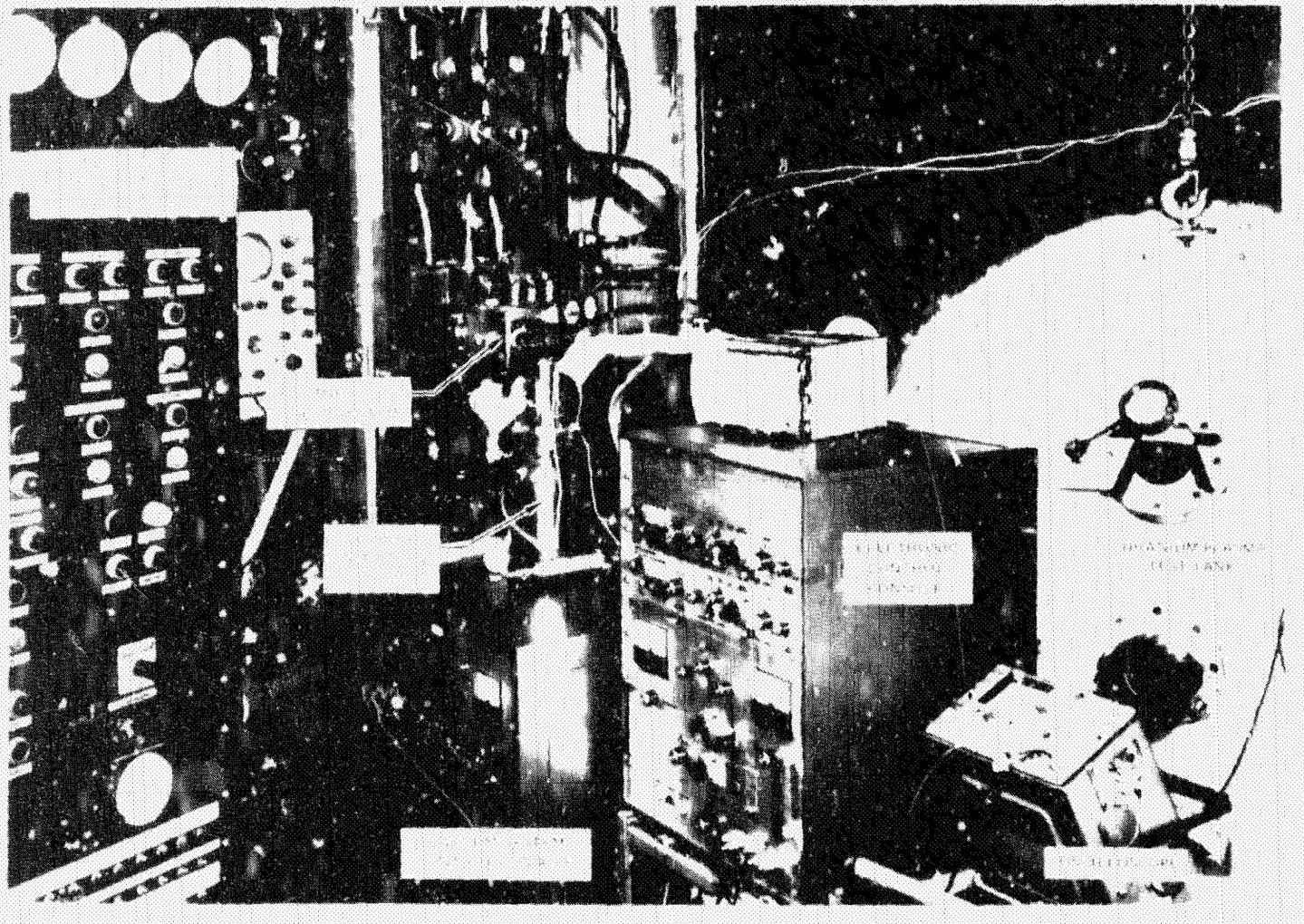

FIG 10

SCHEMATIC REPRESENTATION OF A TIME–OF–FLIGHT (TOF) MASS SPECTROMETER

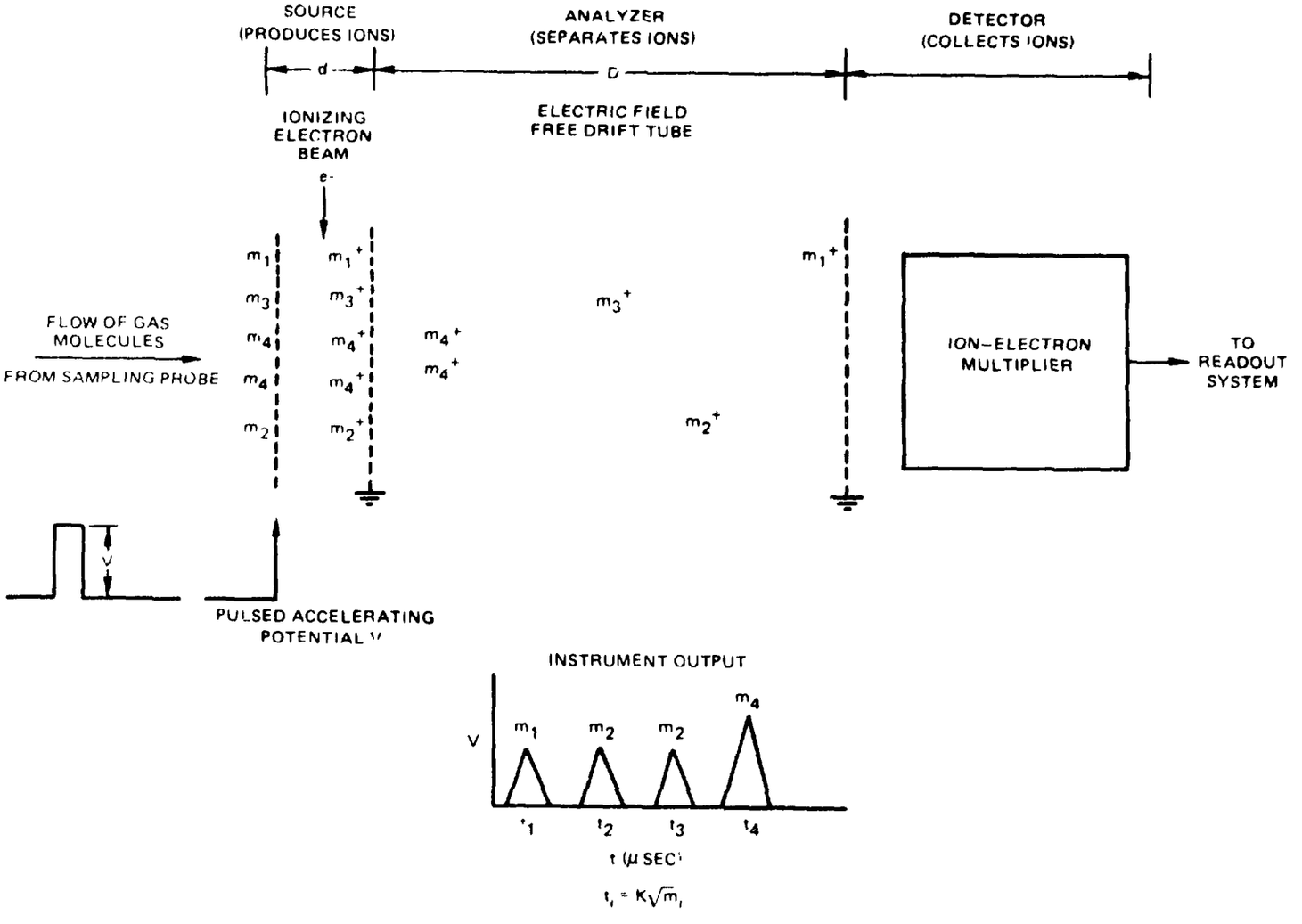

FIG. 11

SKETCH OF CROSS-SECTION OF UF_6 RF PLASMA TEST CHAMBER AND INTERSTAGE EXHAUST DUCT

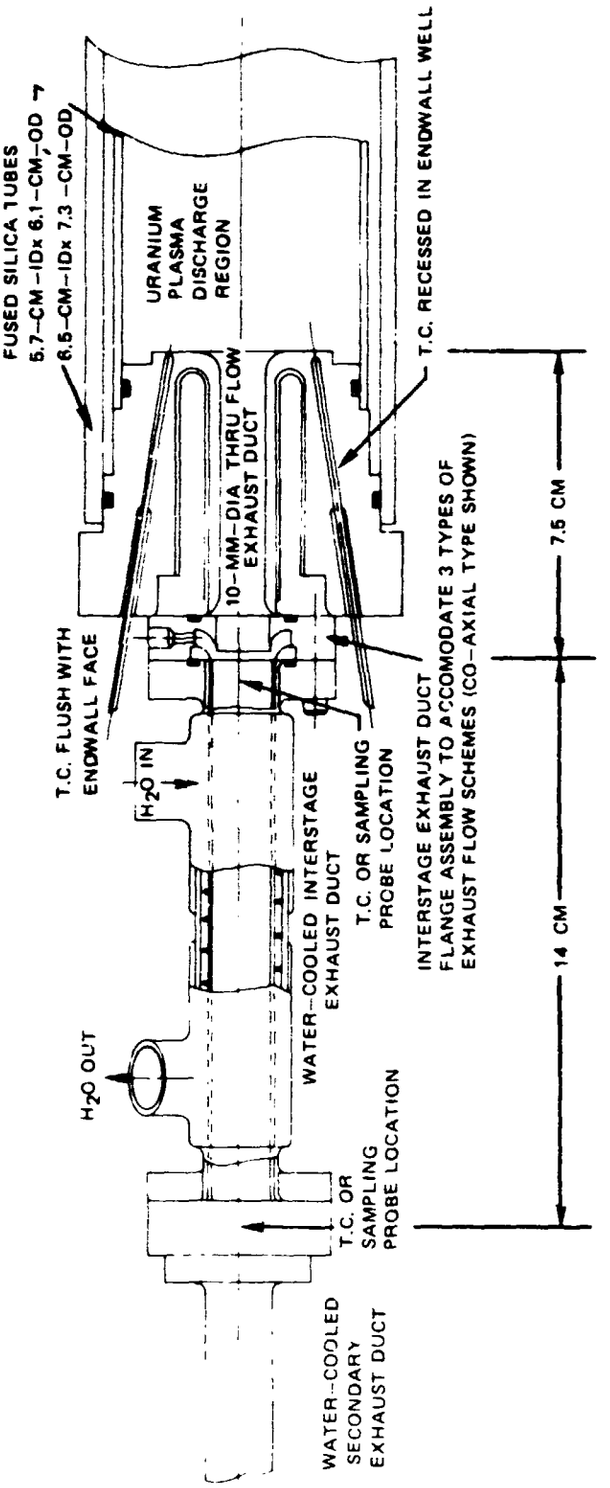

FIG. 12

PHOTOGRAPH OF 3 DIFFERENT DILUENT GAS INJECTORS USED IN INTERSTAGE EXHAUST DUCT UF_6 RF PLASMA TESTS

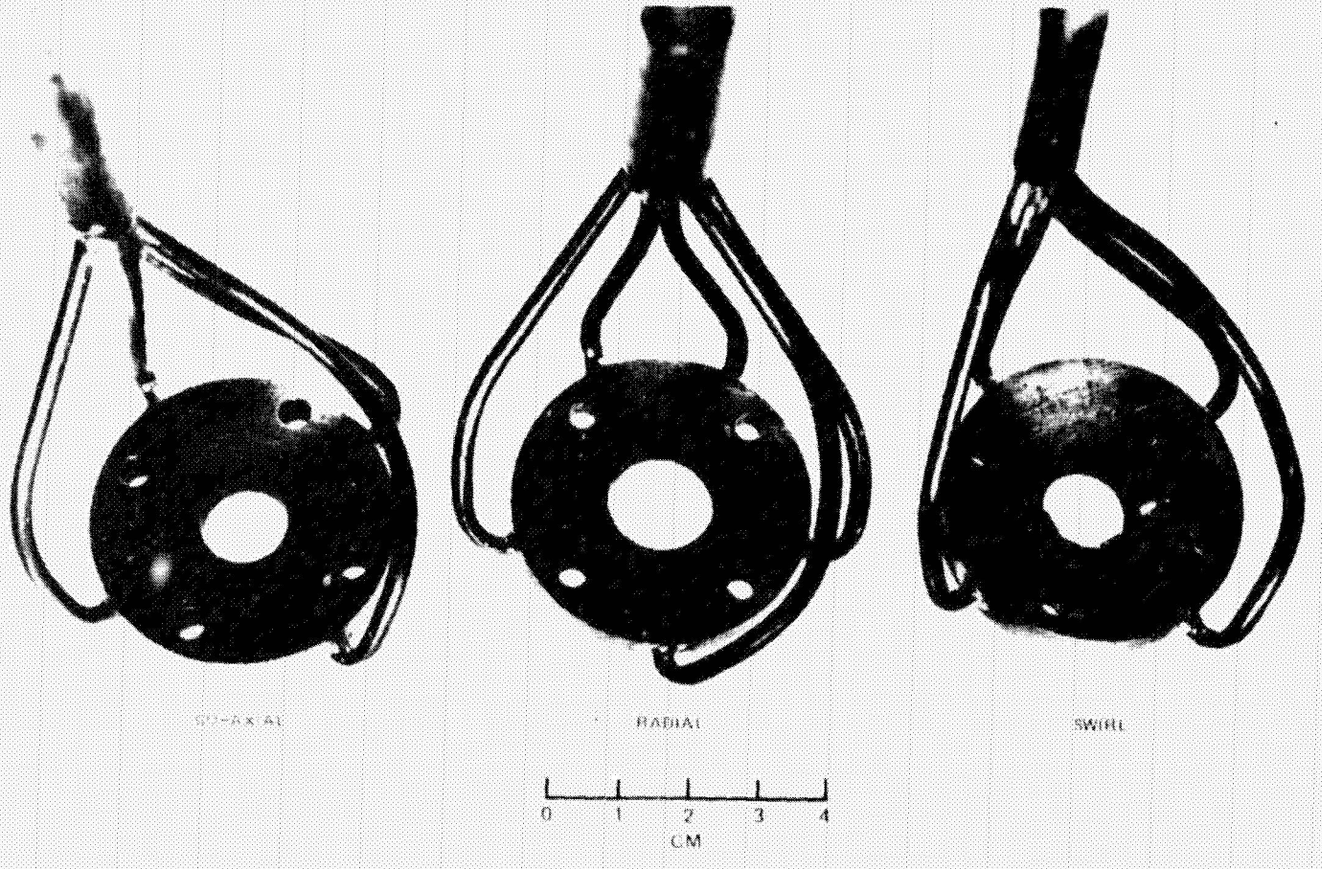

FIG. 13

POST TEST PHOTOGRAPH OF TEST CHAMBER CONFIGURATION AND INTERSTAGE EXHAUST DUCT/DILUENT GAS INJECTOR ASSEMBLY USED IN UF_6 RF PLASMA TESTS

SEE FIG. 11 FOR COMPONENT IDENTIFICATION

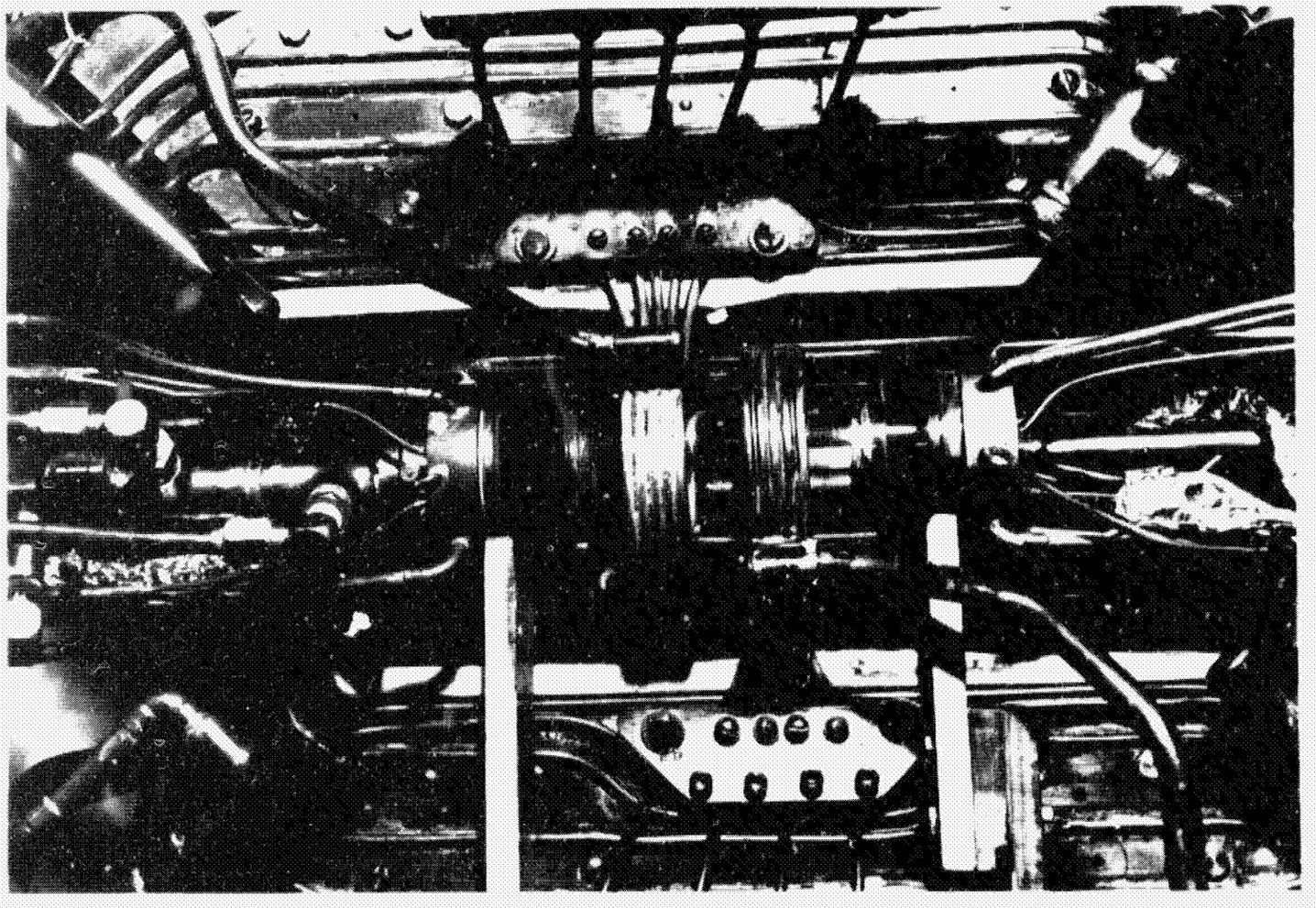

FIG. 11

SKETCH OF CROSS–SECTION OF UF_6 RF PLASMA TEST CHAMBER AND TRANSPIRATION INJECTION EXHAUST DUCT

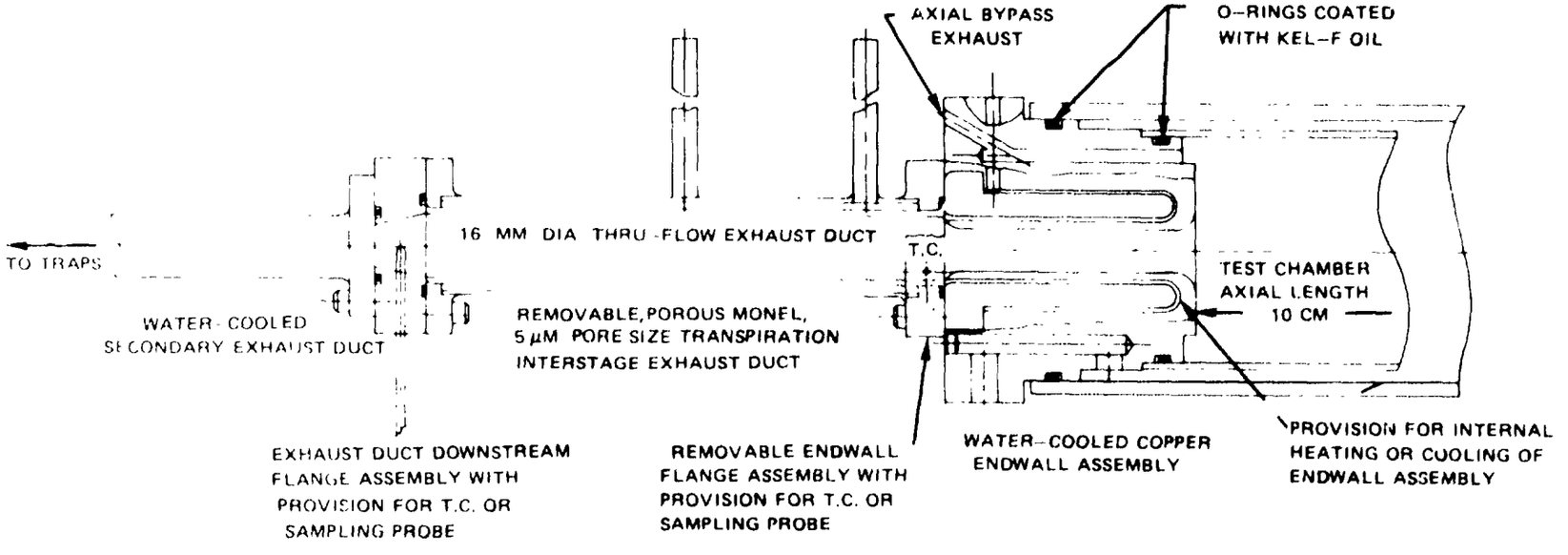

FIG. 15

FIG. 16

PHOTOGRAPHS OF POROUS MONEL INTERSTAGE EXHAUST DUCT AND DIFFERENT POROSITY TUBES USED IN EXPLORATORY TESTS

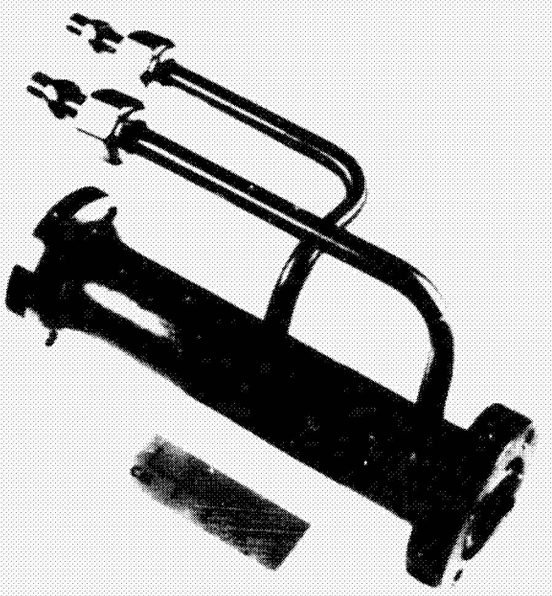

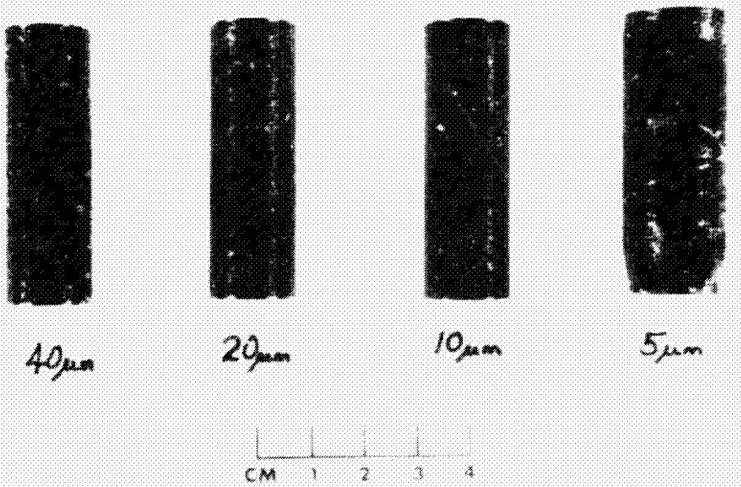

POST TEST PHOTOGRAPH OF TEST CHAMBER AND POROUS MONEL INTERSTAGE EXHAUST DUCT SYSTEM USED IN UF_6 RF PLASMA EXHAUST GAS TESTS

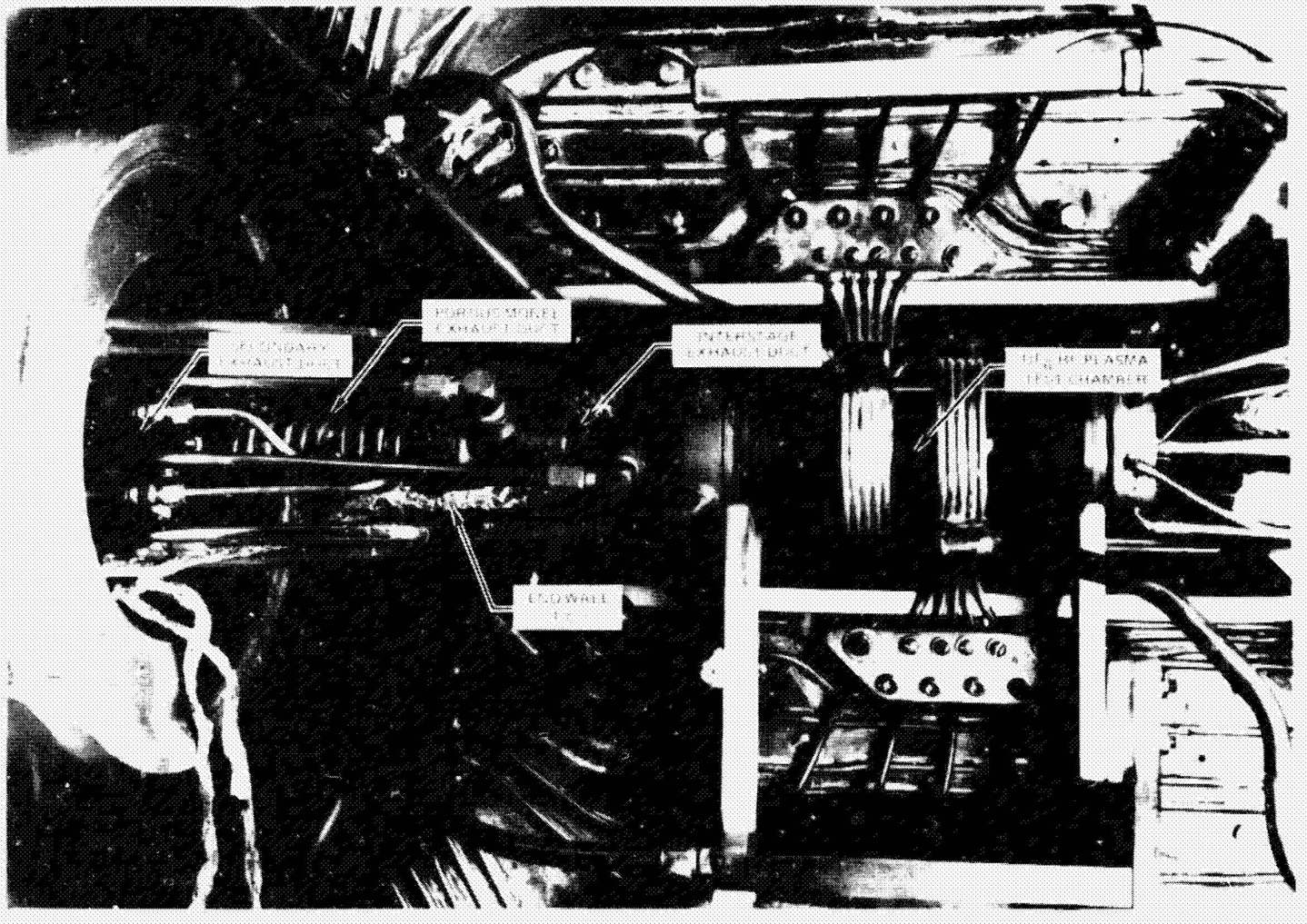

FIG. 17

SCHEMATIC OF COMPONENTS EXAMINED IN POST TEST ANALYSIS OF LONG RUN TIME TEST

SEE TABLE II FOR RANGE OF TEST CONDITIONS

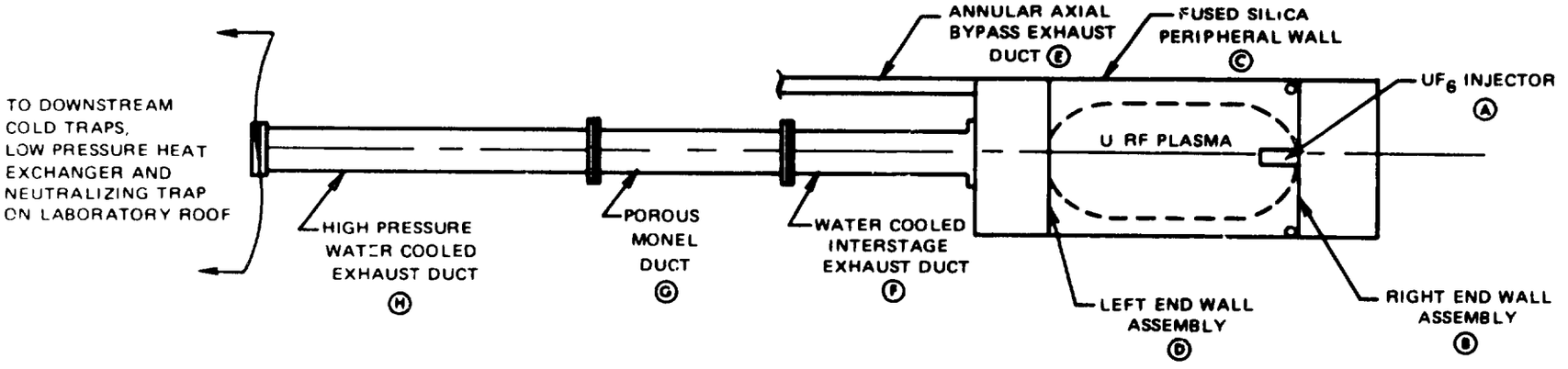

PERIPHERAL WALL, SiO_2 (ALSO SOURCE OF O_2)

POSSIBLE SPECIES WITHIN PLASMA TEST CHAMBER

$UF_6, UF_5, UF_4,$
$UF_3, U, U^+,$
$U^{++}, U^{+++}, F,$
F^-, F_2, UO_2F_2
UO_x

POSSIBLE INLET CONTAMINANT

HF
O_2
H_2O
HYDROCARBONS

FIG. 18

FIG 19

PHOTOGRAPH OF TEST SECTION SHOWING RESIDUE PATTERN AFTER VARIABLE SURFACE TEMPERATURE ENDWALL TEST

FIG. 20

EXAMPLE OF MEASURED RADIAL TEMPERATURE PROFILES ACROSS INLET AND EXIT LOCATION OF INTERSTAGE EXHAUST DUCT ASSEMBLY

SEE FIG. 12 FOR SCHEMATIC OF CONFIGURATION; W/W Rh T.C.'s EMPLOYED IN THESE MEASUREMENTS
ARGON ONLY LOW POWER RF PLASMA TEST CASE

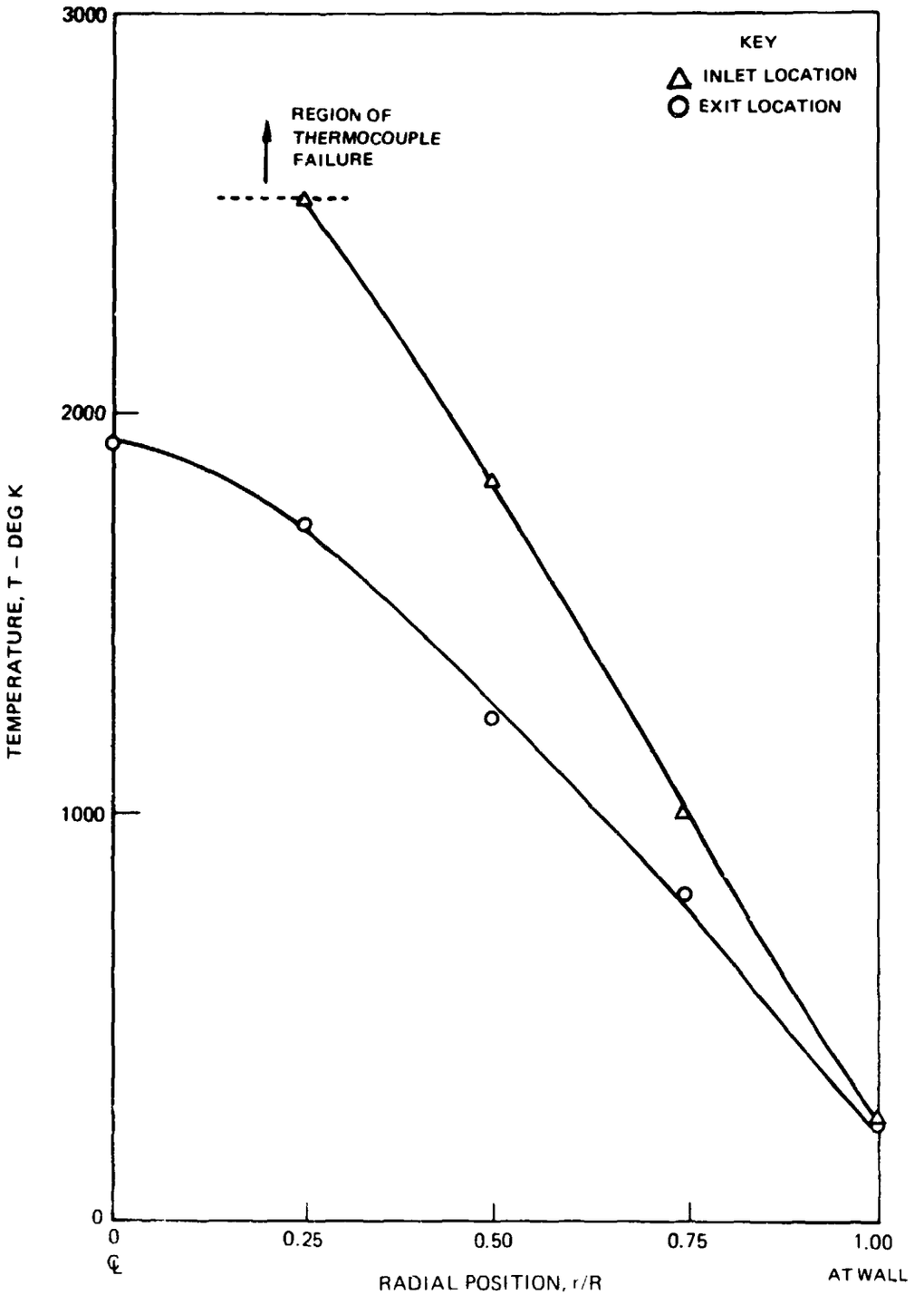

FIG. 21

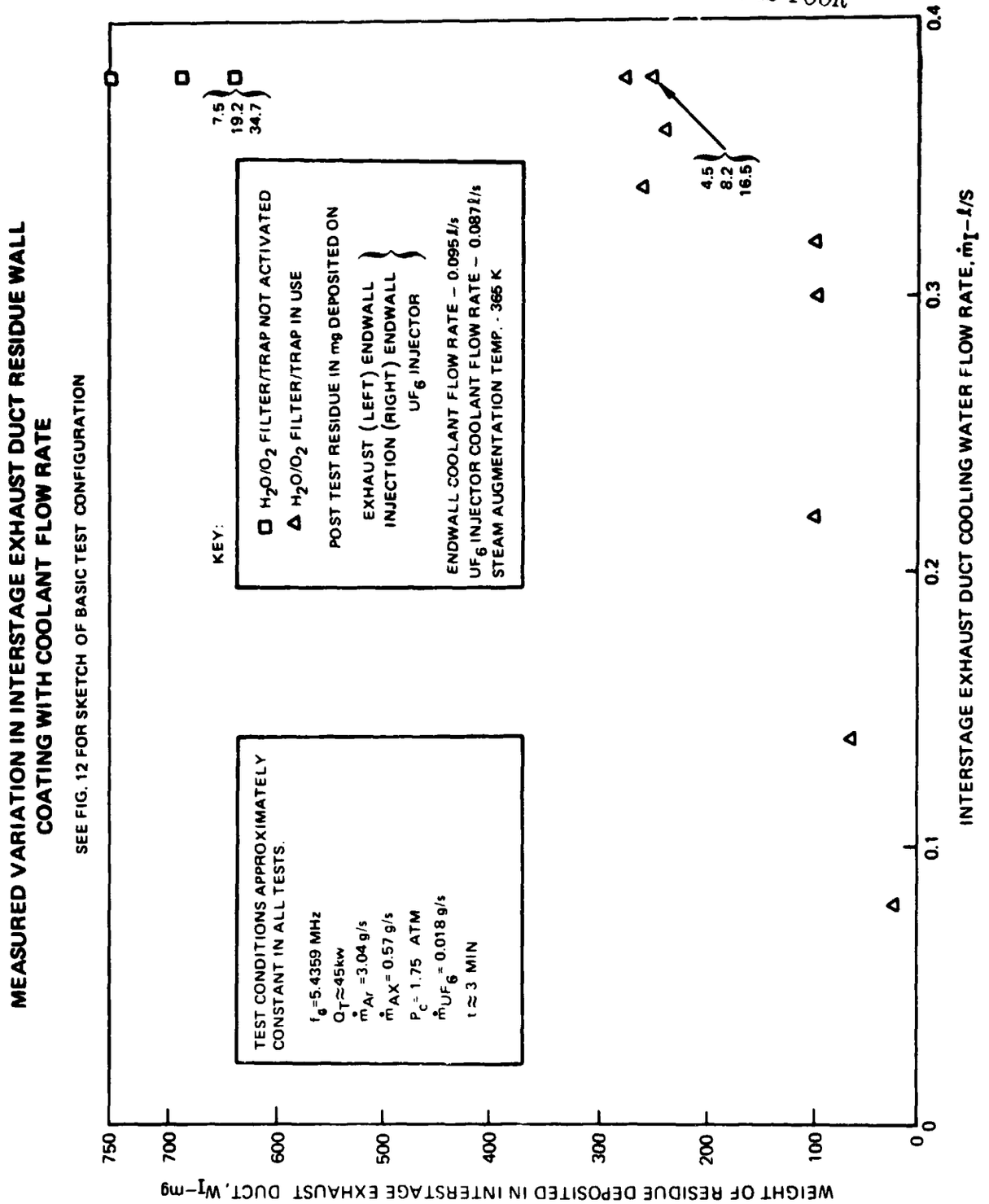

FIG. 22

MEASURED VARIATION IN INTERSTAGE EXHAUST DUCT RESIDUE WALL COATING WITH DILUENT GAS INJECTOR FLOW RATE

SEE FIG. 12 FOR SKETCH OF TEST CONFIGURATION
SEE FIG. 14 FOR PHOTOGRAPH OF TEST CONFIGURATION

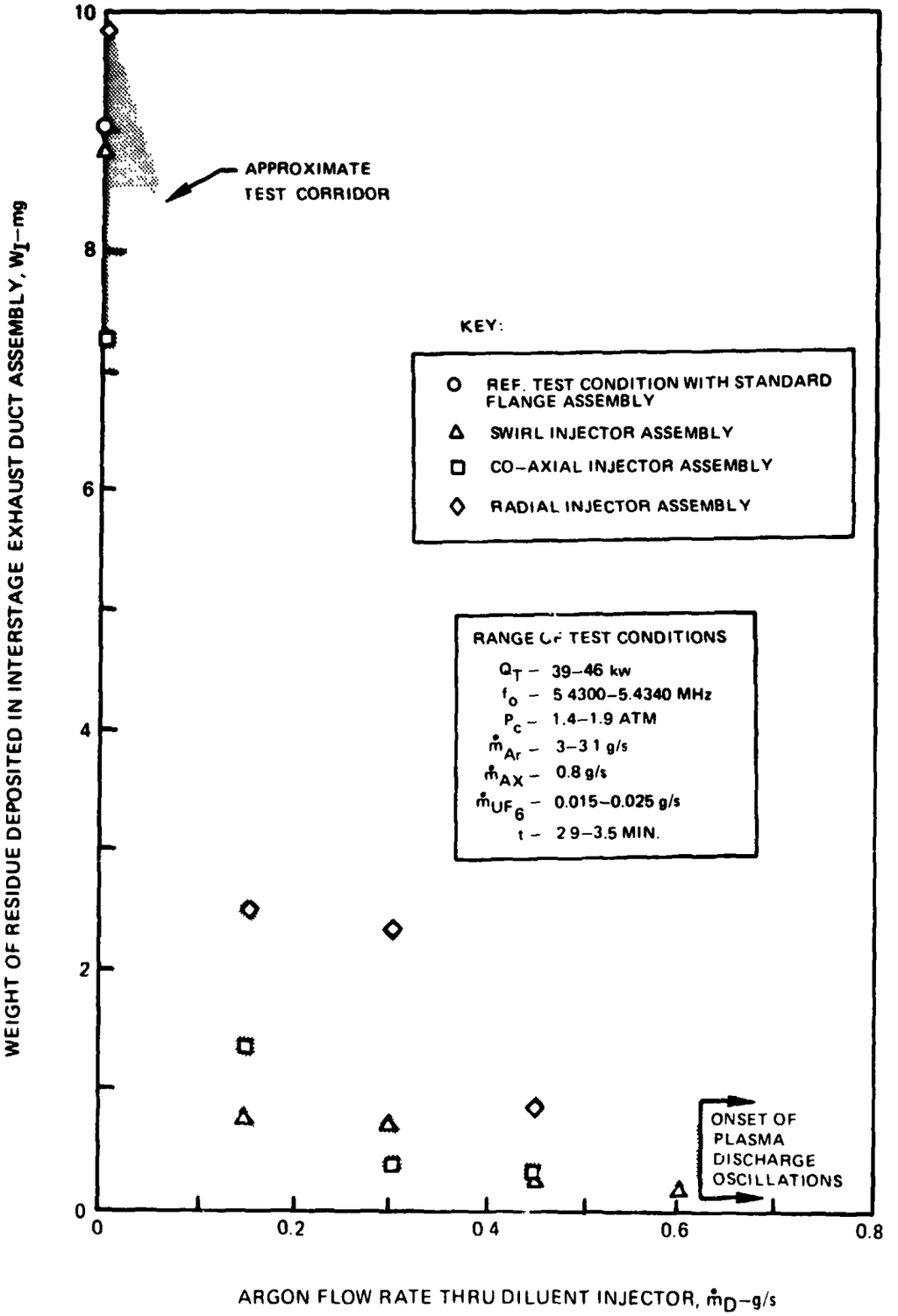

EXAMPLE OF POROUS MONEL EXHAUST DUCT RESIDUE WALL COATING VERSUS TEST TIME

SEE FIG. 15 FOR DETAILS OF TEST CONFIGURATION

SEE TABLE II FOR CORRESPONDING TEST CONDITIONS

[NOTES TESTS AT APPROXIMATELY CONSTANT UF_6 MASS FLOW RATE

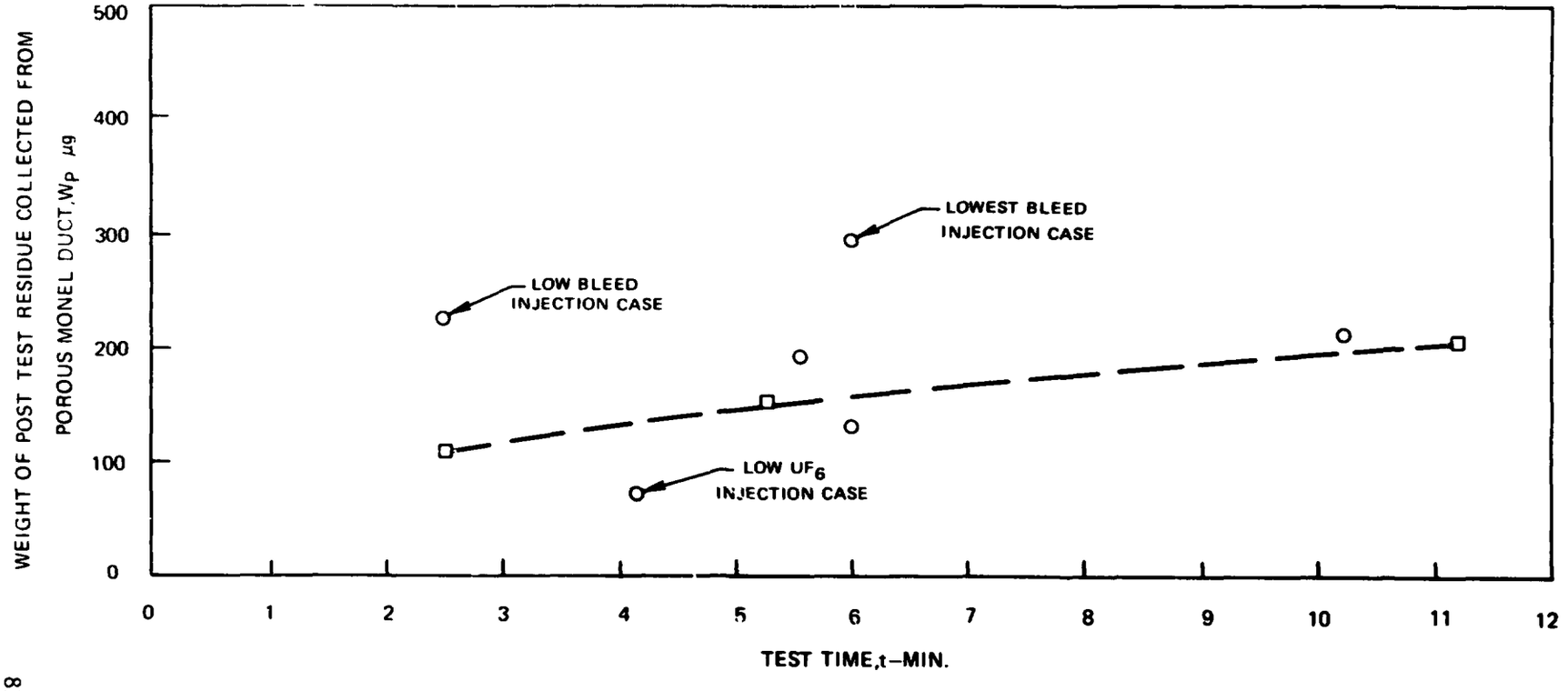

FIG. 23

FIG. 24

INFRARED SPECTRUM OF UF_6

GASEOUS STATE
ROOM TEMPERATURE
10 CM CELL LENGTH

DISPERSING ELEMENT
REF. 10
{ NaCl PRISM 8.5–15 μM
{ KBr PRISM 15–20 μM

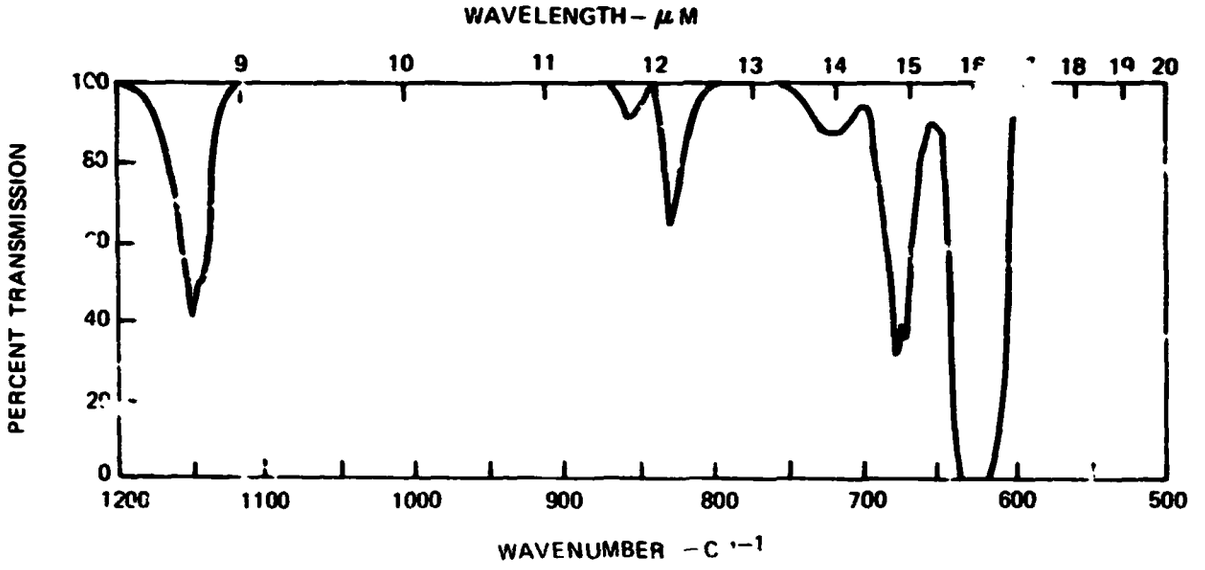

FIG. 25

EXAMPLES OF IR SPECTROPHOTOMETRIC ABSORPTION MEASUREMENTS

PERKIN ELMER MODEL 457

PATH LENGTH=10CM

a) EVACUATED (10μM) FUSED SILICA CELL WITH AgCl WINDOWS

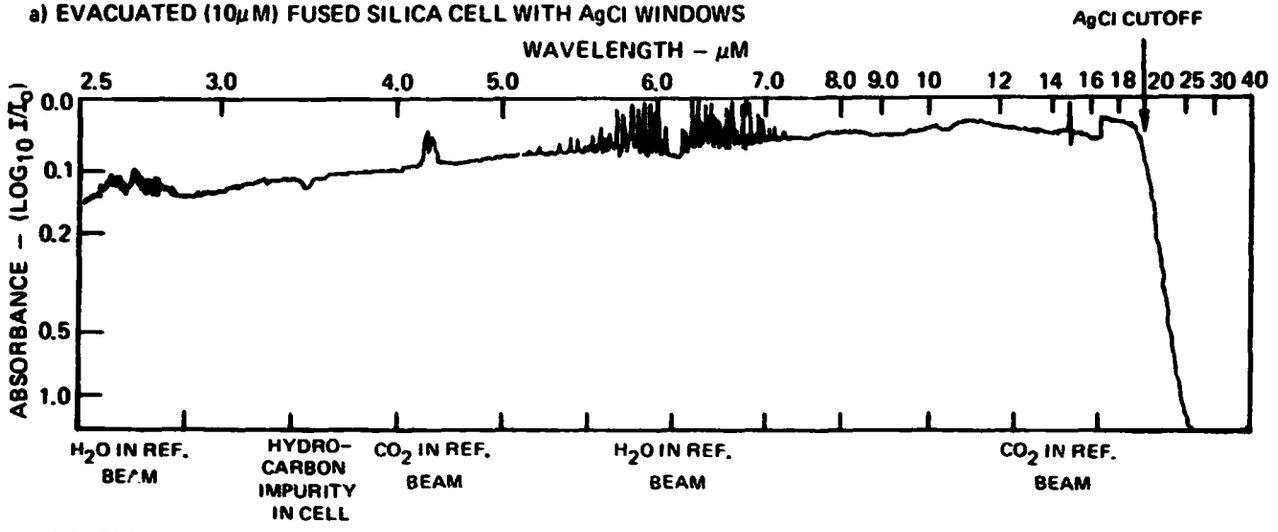

b) FUSED SILICA CELL WITH AgCl WINDOWS FILLED WITH 0.5 GMS OF FILTERED UF_6

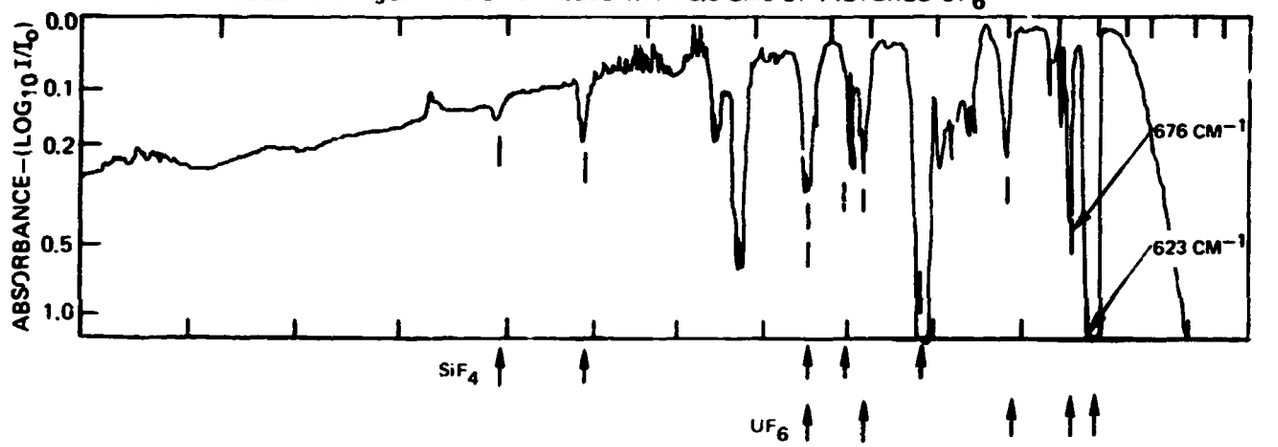

c) KEL–F CELL WITH AgCl WINDOWS CONTAINING OFF–LINE SAMPLE OF EFFLUENT EXHAUST GAS FROM RF URANIUM PLASMA TEST

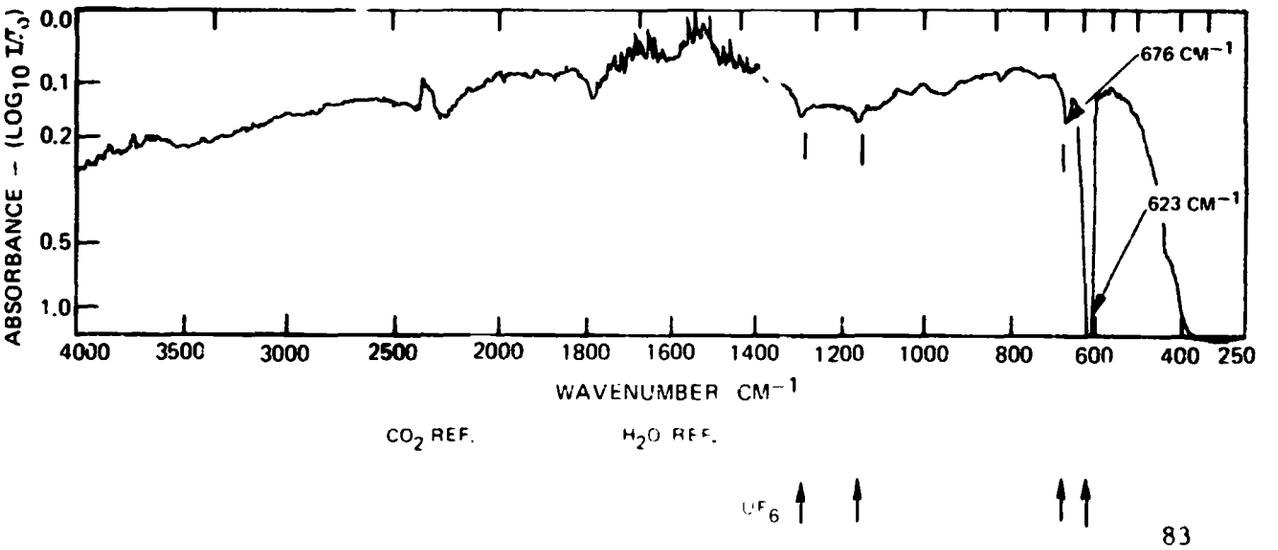

EXAMPLE OF ON-LINE IR SPECTROPHOTOMETRIC ABSORPTION MEASUREMENTS

SEE FIG. 6 FOR SCHEMATIC OF SAMPLING SYSTEM
SEE FIG. 8 FOR PHOTOGRAPH OF TEST CONFIGURATION
PERKIN ELMER MODEL 457 – – PATH LENGTH 10 – CM
623 CM^{-1} WAVENUMBER USED
SEE TABLE III FOR SUMMARY OF TEST CONDITIONS

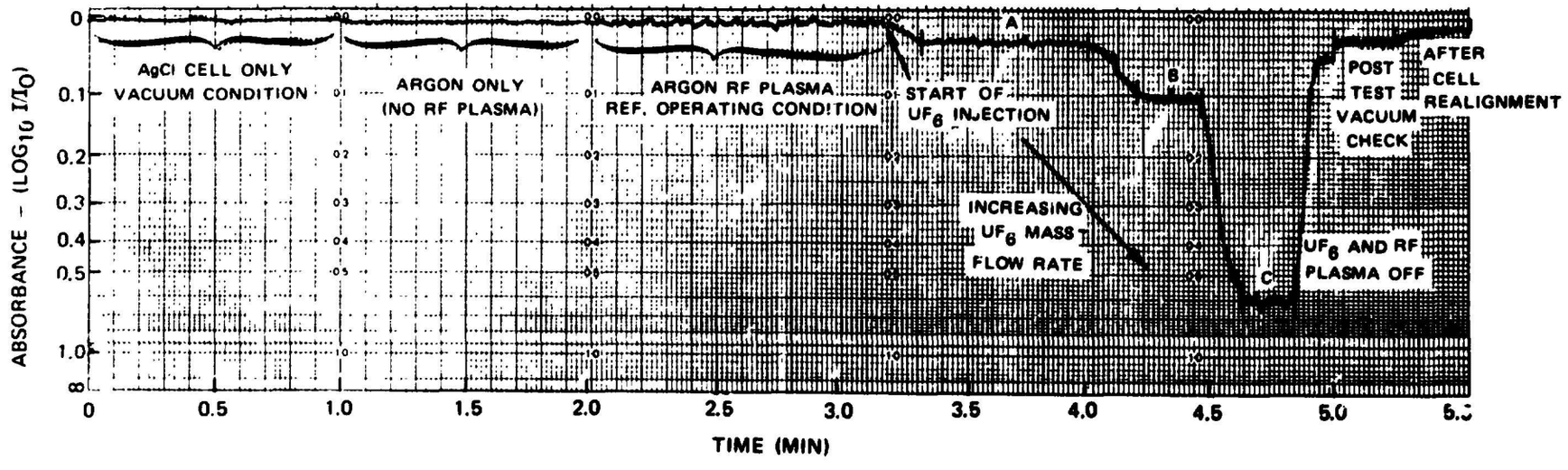

FIG. 26

MASS SPECTRAL RELATIVE INTENSITIES OF UF_6

MEASURED ON TOF MASS SPECTROMETER AT AN IONIZING [illegible] OF 70 ev. REF (12)

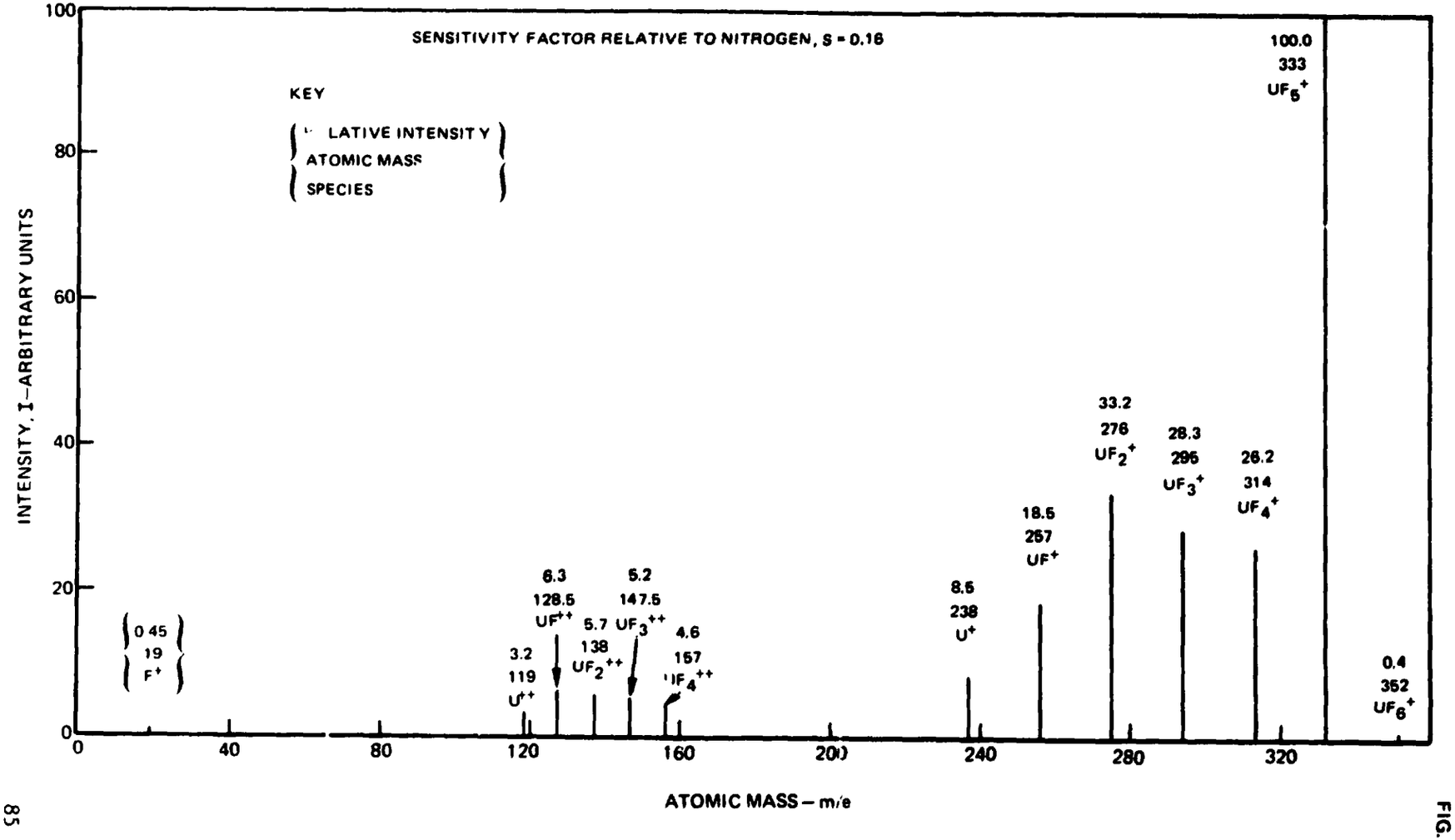

FIG. 27

EXAMPLE OF MASS SPECTRAL RELATIVE INTENSITIES OF UF_6/AR MIXTURE AS MEASURED WITH TOF MASS SPECTROMETER SYSTEM AND USED IN CALIBRATIONS OF UF_6 RF PLASMA TESTS

SEE FIG. 2 FOR SCHEMATIC OF EXHAUST GAS SAMPLING SYSTEM
SEE FIG. 10 FOR PHOTOGRAPH OF EQUIPMENT

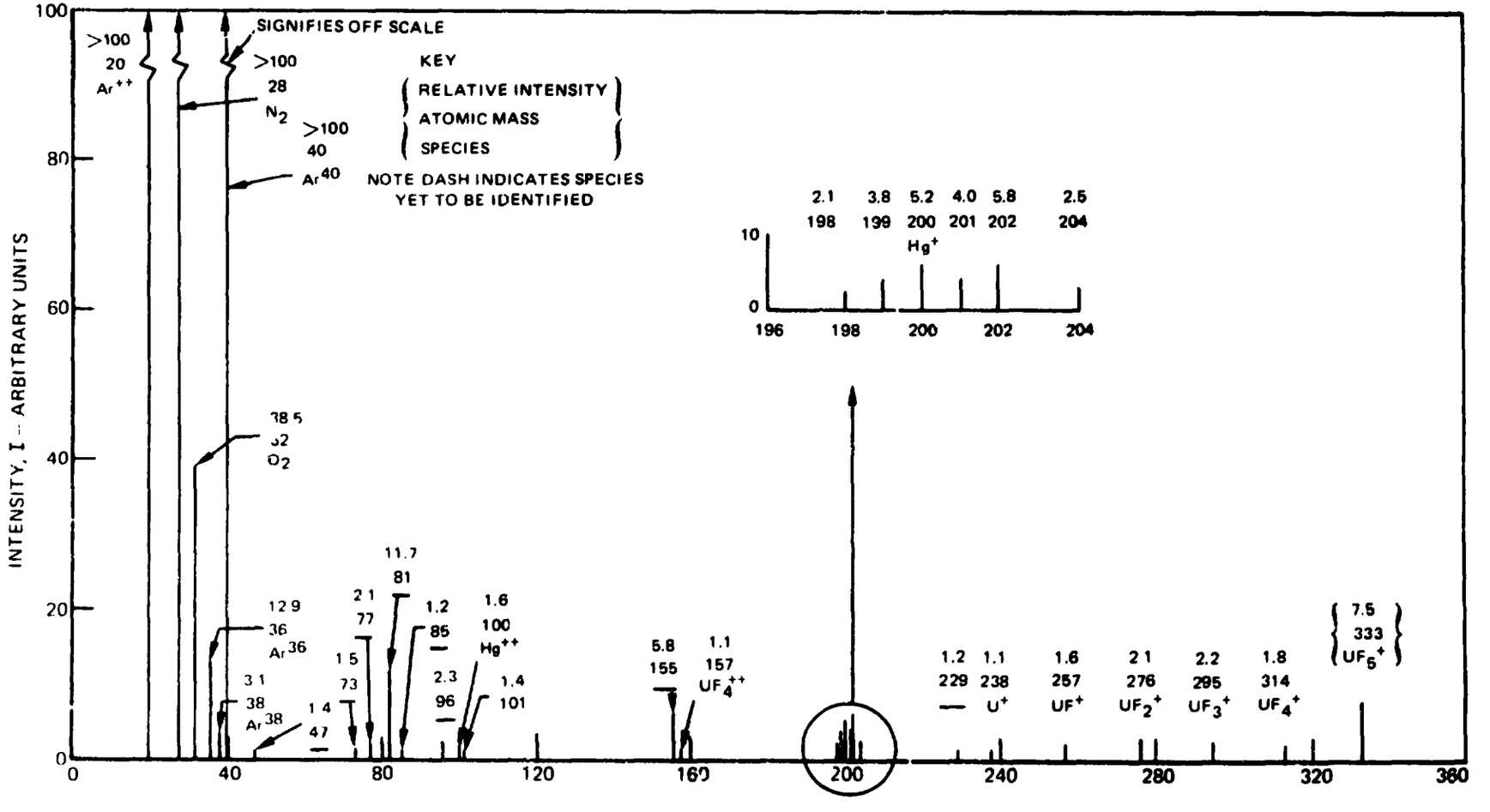

FIG. 28

EXAMPLE OF MASS SPECTRAL RELATIVE INTENSITIES OBTAINED IN UF_6 RF PLASMA TESTS USING ON-LINE TOF MASS SPECTROMETER SYSTEM

SAMPLING PROBE LOCATED IN ON-AXIS EXHAUST DUCT (DOWNSTREAM LOCATION B – SEE FIG. 6)
SEE TABLE IV FOR SUMMARY OF TEST CONDITIONS

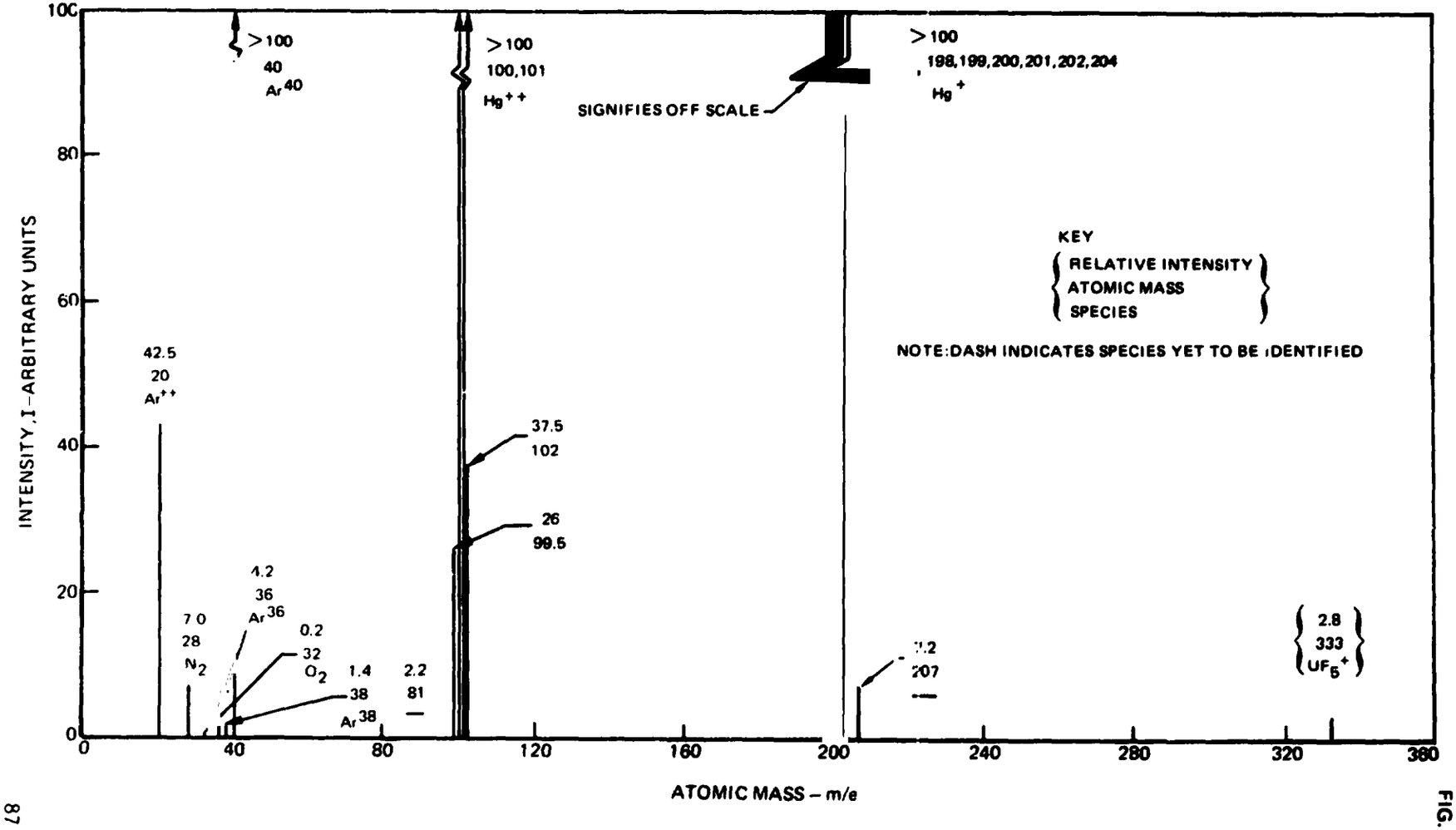

FIG. 29

EXAMPLE OF MASS SPECTRAL RELATIVE INTENSITIES OBTAINED IN UF_6 RF PLASMA TESTS USING ON–LINE TOF MASS SPECTROMETER SYSTEM

SAMPLING PROBE LOCATED IN AXIAL BYPASS EXHAUST DUCT (DOWNSTREAM LOCATION C – SEE FIG. 8)

SEE TABLE IX FOR SUMMARY OF TEST CONDITIONS

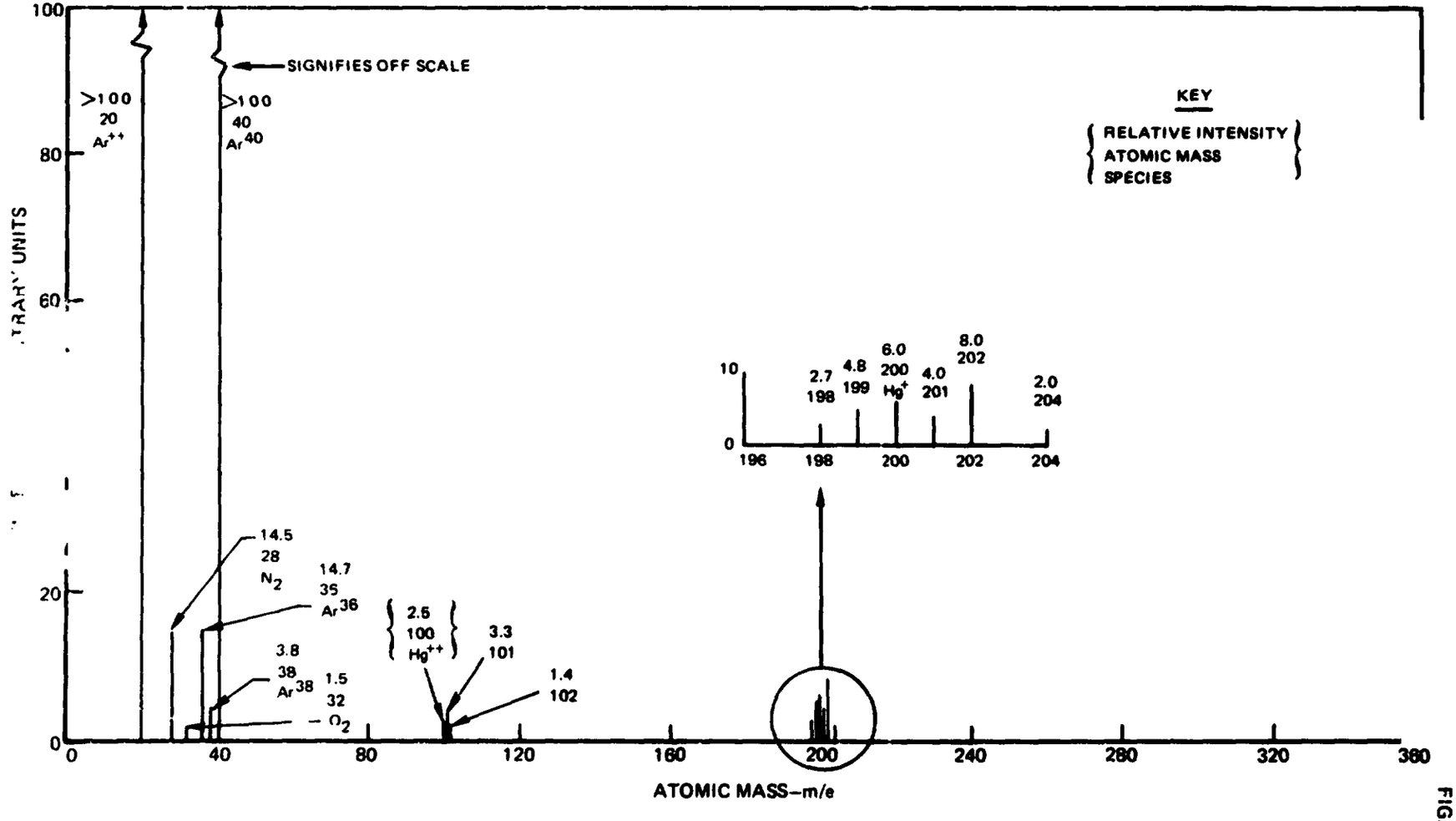

FIG. 30

FIG. 31

PHOTOGRAPHS OF TEST CHAMBER USED IN LONG RUN TIME TESTS WITH UF_6 RF PLASMA

a. BEFORE

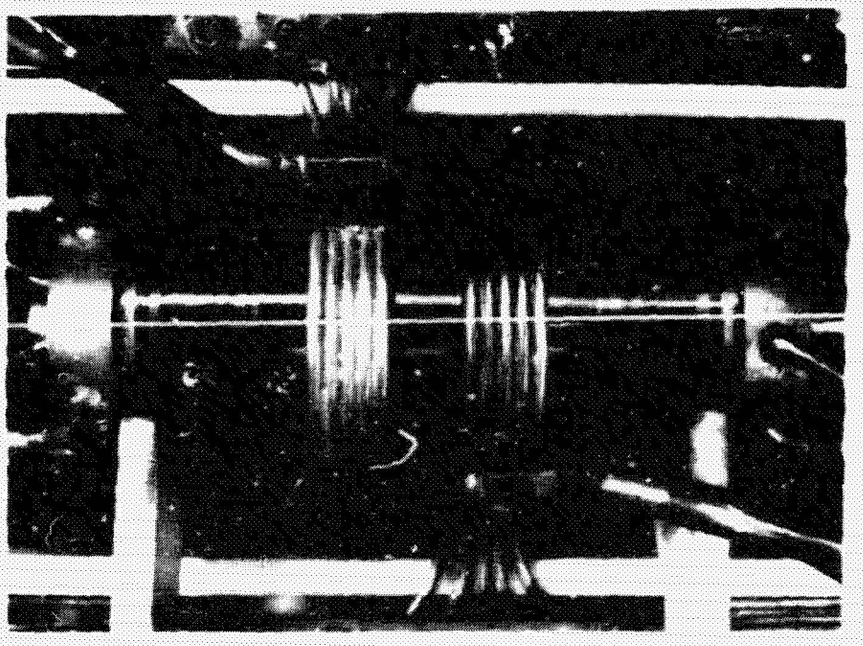

b. AFTER

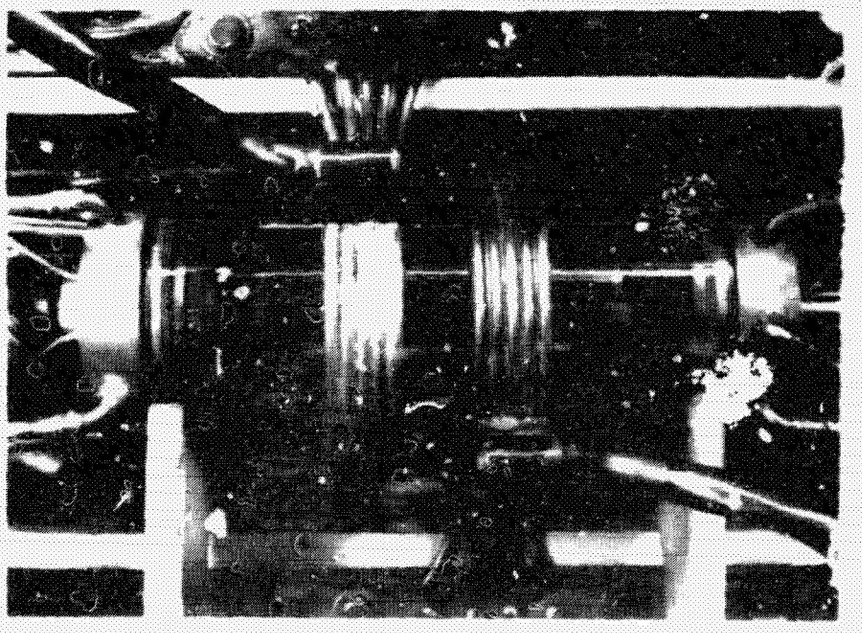

ELECTRON PHOTOMICROGRAPHS AND X-RAY MAPS OF A SAMPLE RESIDUE FROM SURFACE OF TEST CHAMBER AFTER LONG RUN TIME UF_6 RF PLASMA TEST

MAG 500 X

a.) UF_6 INJECTOR BACKSCATTERED ELECTRON MICROGRAPH

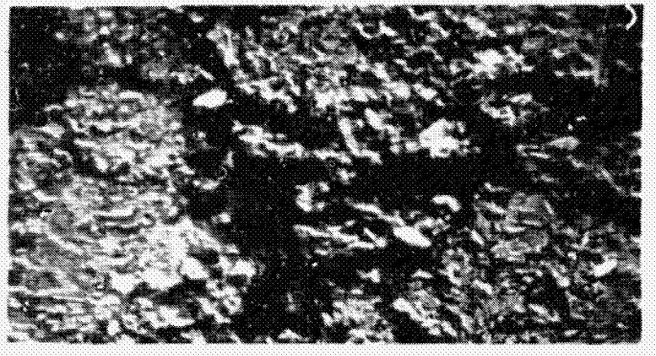

b.) UF_6 INJECTOR X - RAY SHOWING URANIUM - MAJOR MINOR F,O,Cu

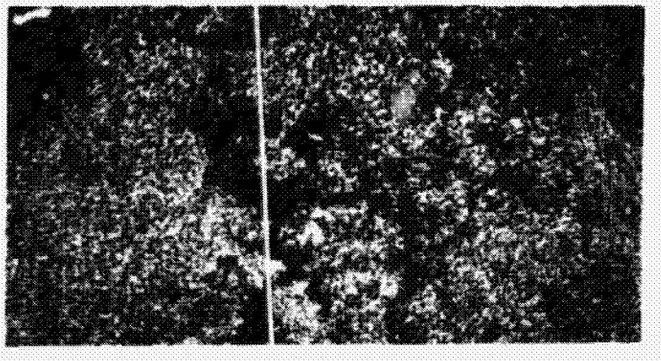

c.) LEFT ENDWALL BACKSCATTERED ELECTRON MICROGRAPH

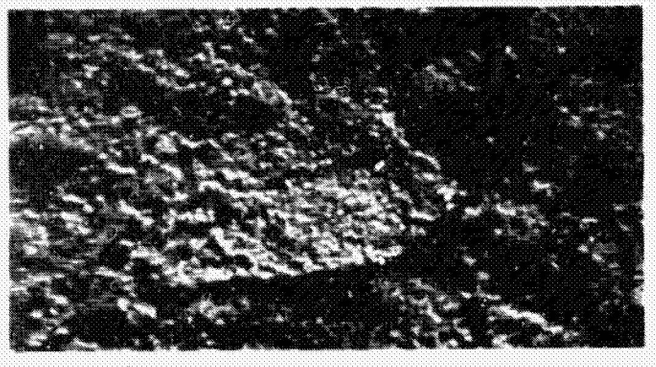

d.) LEFT ENDWALL X - RAY SHOWING URANIUM - MAJOR MINOR F,O

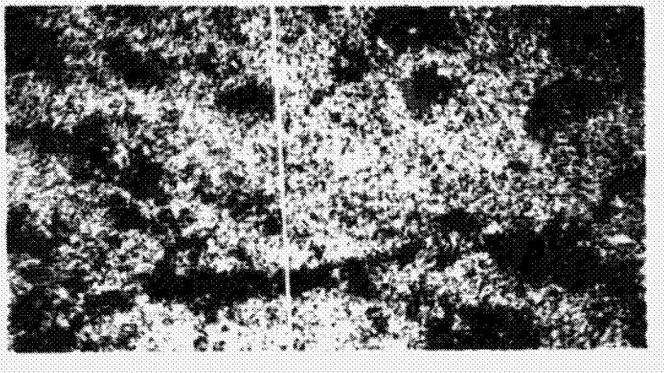

FIG 37

ELECTRON PHOTOMICROGRAPHS AND X-RAY MAPS OF A SAMPLE RESIDUE FROM SURFACE OF EXHAUST DUCT SYSTEM AFTER LONG RUN TIME UF_6 RF PLASMA TEST

MAG 500X

a.) AXIAL BYPASS EXHAUST DUCT ELECTRON MICROGRAPH

b.) AXIAL BYPASS EXHAUST DUCT X-RAY SHOWING
URANIUM-MINOR
MAJOR F,O

c.) INTERSTAGE EXHAUST DUCT ELECTRON MICROGRAPH

d.) INTERSTAGE EXHAUST DUCT X-RAY SHOWING
URANIUM-MAJOR
MINOR O,F,Fe TRACE Cu,Si

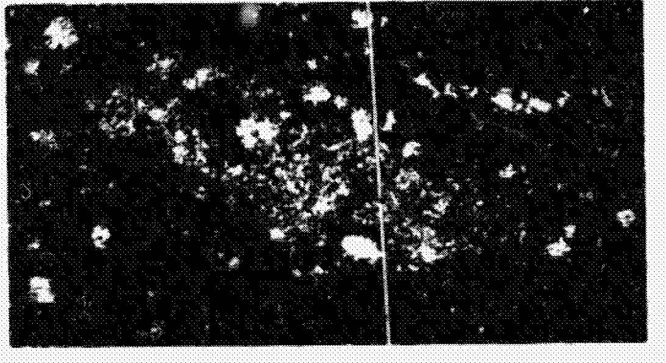

FIG 33

ELECTRON PHOTOMICROGRAPHS AND X-RAY MAPS OF A SAMPLE RESIDUE FROM SURFACE OF EXHAUST DUCT SYSTEM AFTER LONG RUN TIME UF_6 RF PLASMA TEST

MAG 500X

a.) POROUS MONEL EXHAUST DUCT BACKSCATTERED ELECTRON MICROGRAPH

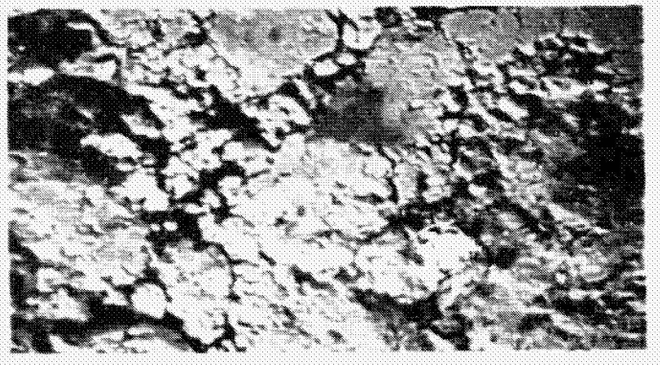

b.) POROUS MONEL EXHAUST DUCT X-RAY SHOWING URANIUM-MAJOR
MINOR F,O,Fe TRACE Cu,Zn

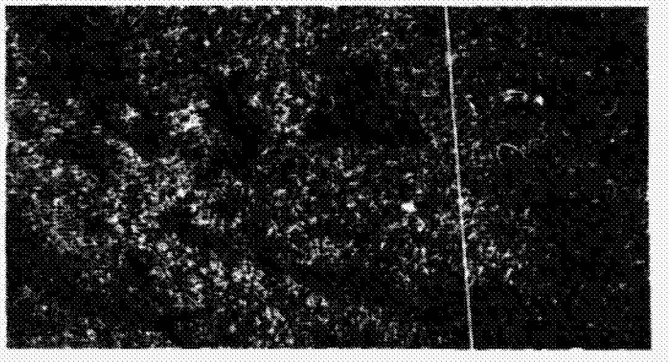

c.) HIGH - PRESSURE WATER COOLED EXHAUST DUCT BACKSCATTERED ELECTRON MICROGRAPH

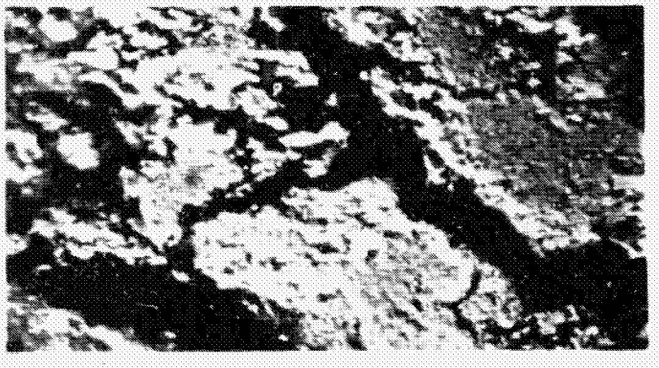

d.) HIGH-PRESSURE WATER COOLED EXHAUST DUCT X-RAY SHOWING URANIUM-MAJOR
MINOR F,O TRACE Cu

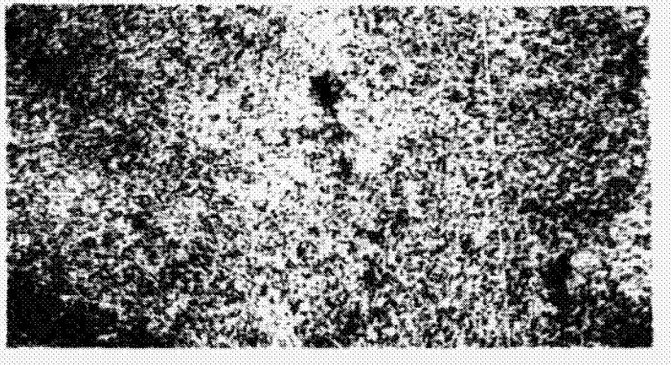

FIG. 34

FIG.35

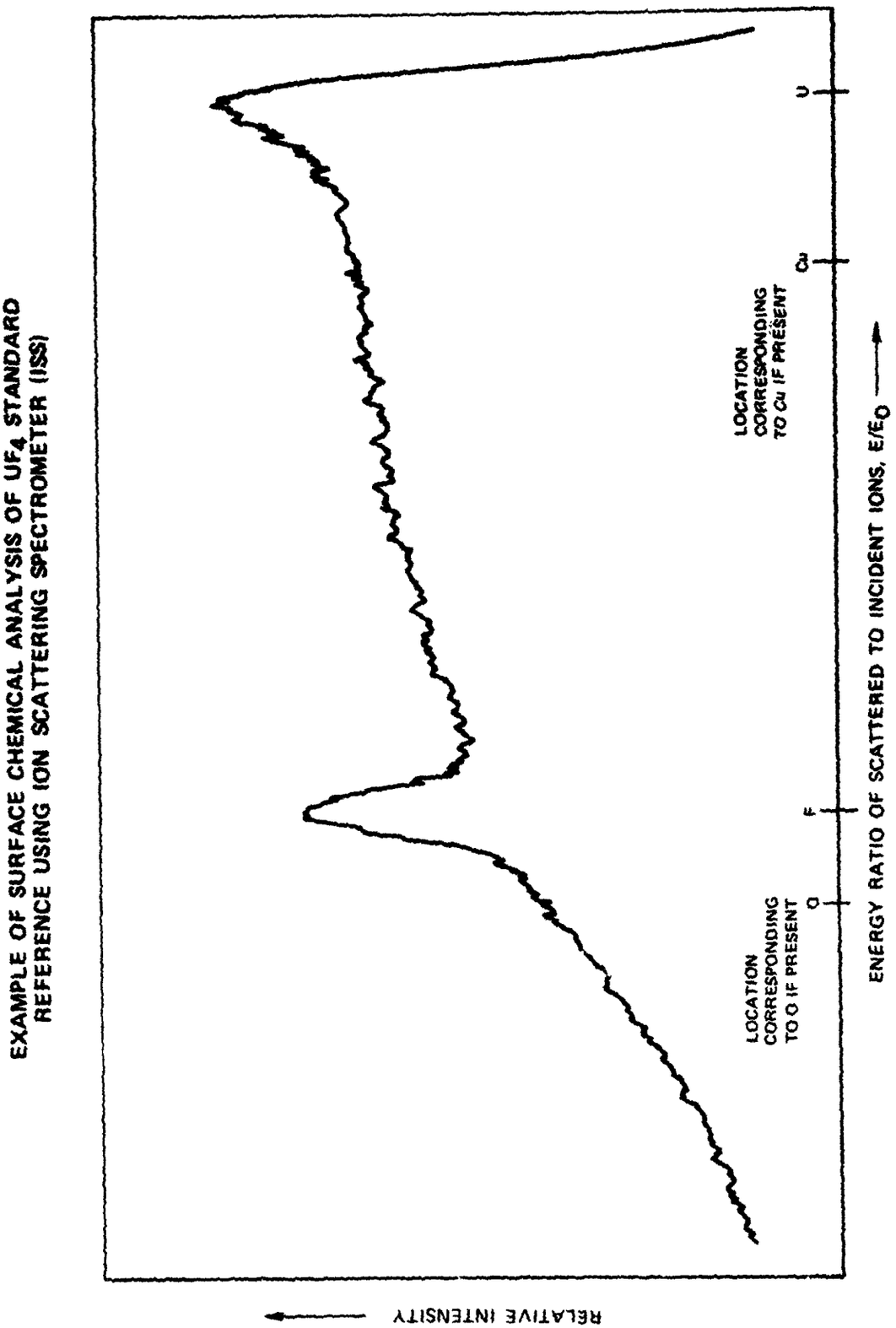

FIG.36

EXAMPLES OF SURFACE CHEMICAL ANALYSIS OF URANIUM COMPOUND RESIDUE USING SECONDARY ION MASS SPECTROMETER (SIMS)

238 U 254 UO 257 UF 276 UO_2 273 UOF
276 UF_2 286 UO_3 289 UO_2F 292 UOF_2 295 UF_3

a) RESIDUE SAMPLE FROM WALL OF EXHAUST DUCT (HIGH TEMPERATURE OPERATION) AFTER TEST WITH PURE UF_6 INJECTION

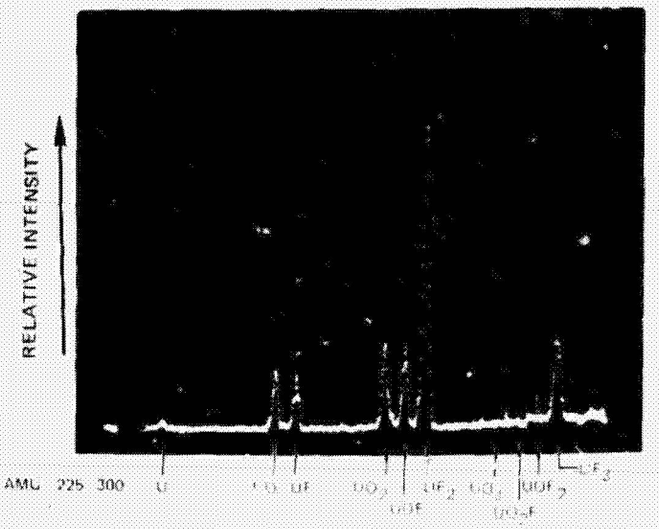

b) RESIDUE SAMPLE FROM WALL OF EXHAUST DUCT (LOW TEMPERATURE OPERATION) AFTER TEST WITH PURE UF_6 INJECTION (NO ARGON INLET FILTER TRAP USED)

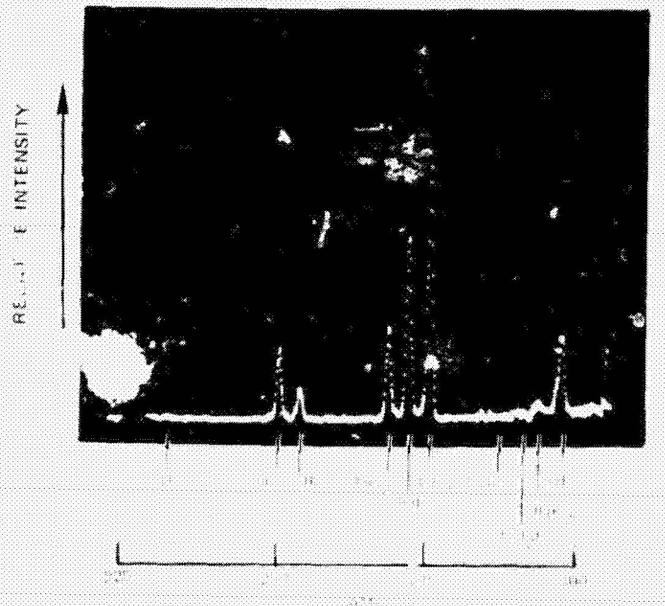

PHOTOGRAPHS OF LEFT ENDWALL ASSEMBLY THRU-FLOW DUCT ILLUSTRATING EROSION/ CORROSION EFFECTS

a.) NEW

b.) PARTIAL CORROSION

c.) EXHAUST DUCT FAILURE

FIG.38

COMPOSITION OF UF_6/ARGON MIXTURE AS A FUNCTION OF TEMPERATURE

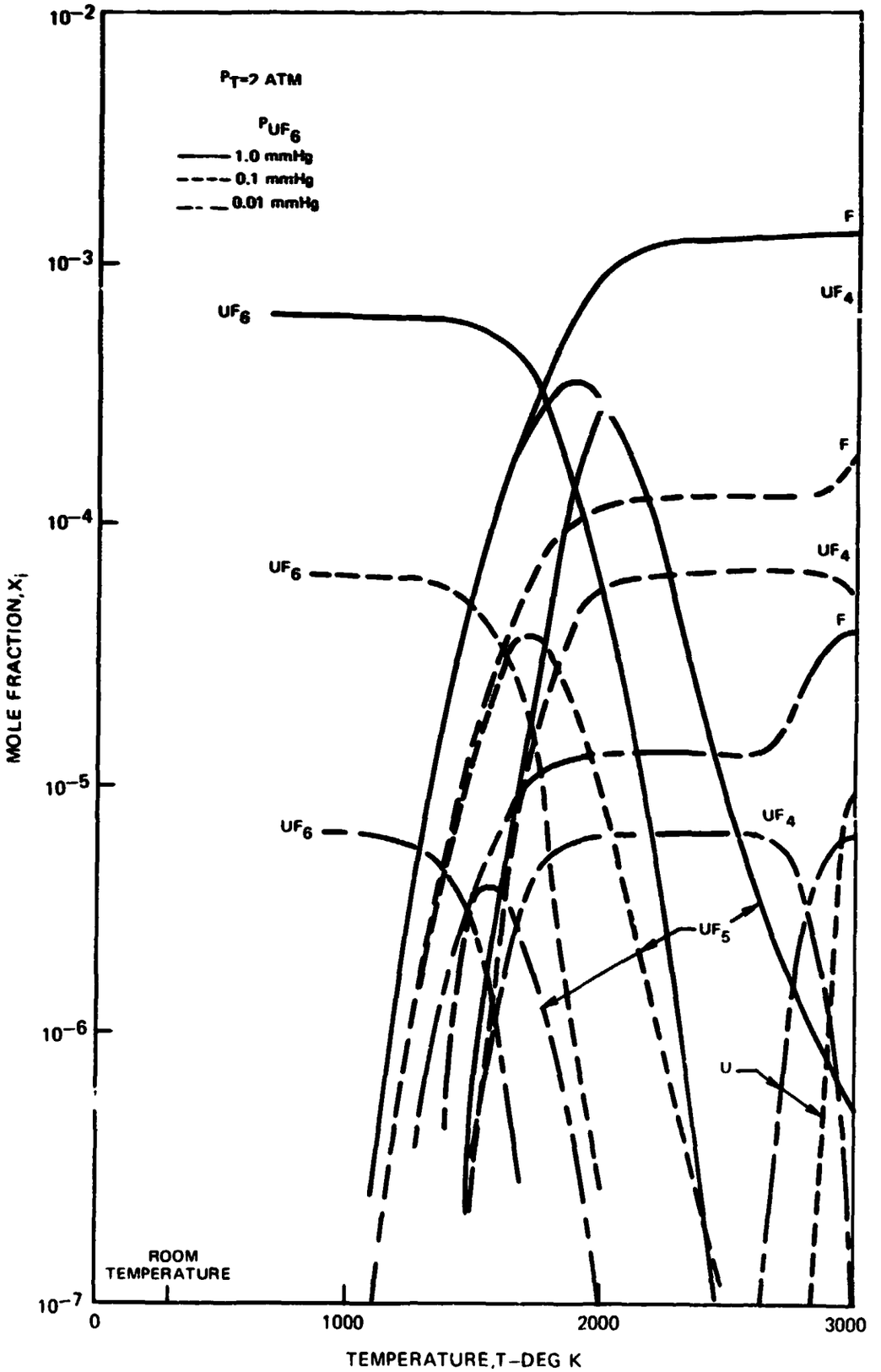

C-2

FIG. 39

EFFECT OF TEMPERATURE AND FLUORINE ON NICKEL MATERIAL PROPERTIES

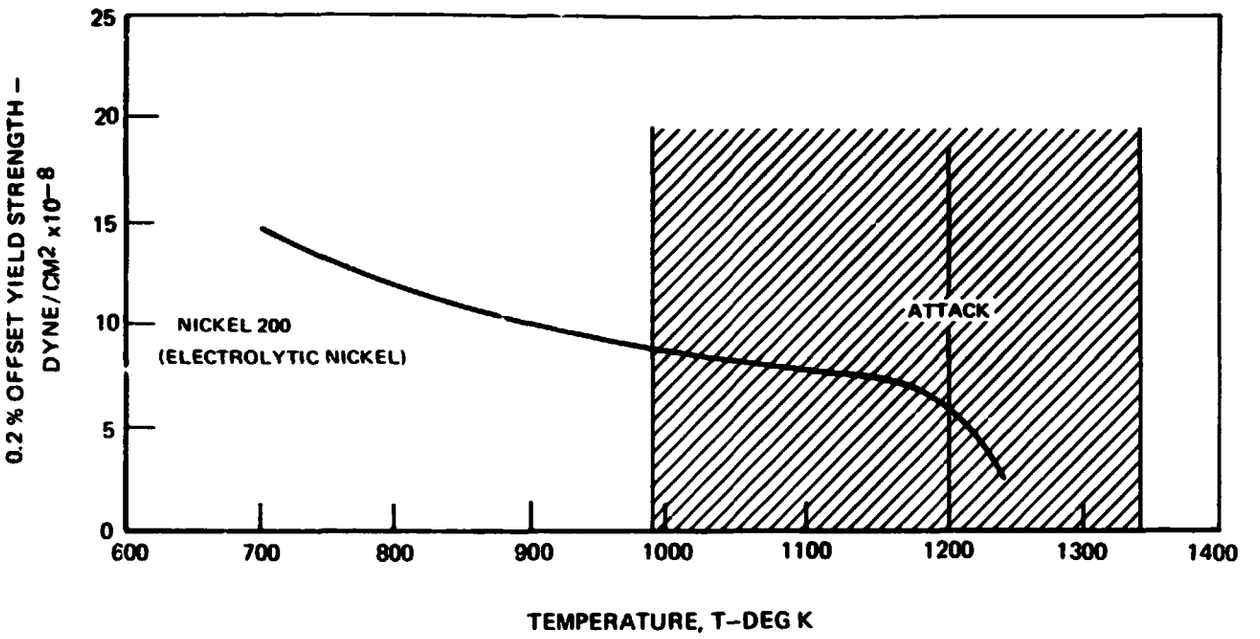

FIG. 40

EXAMPLE OF SEVERAL BASIC CONFIGURATIONS USED IN INTERSTAGE EXHAUST DUCT ANALYSIS

a) COOLED SOLID WALL EXHAUST DUCT WITH SWIRL – NO TRANSPIRATION INJECTION

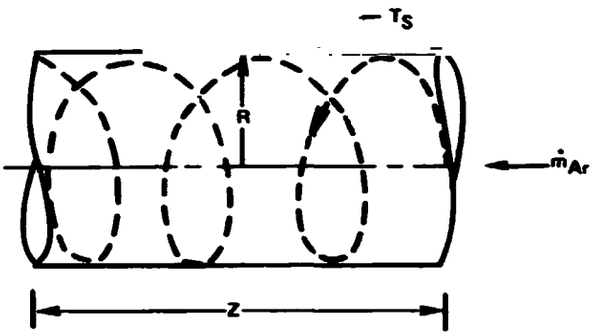

b) POROUS DUCT – WITH SWIRL AND TRANSPIRATION INJECTION

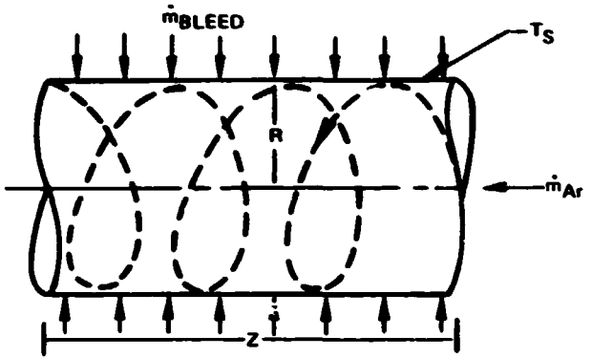

c) COMBINATION OF THE ABOVE; SOLID WALL EXHAUST DUCT FOLLOWED BY POROUS DUCT – WITH SWIRL AND TRANSPIRATION INJECTION

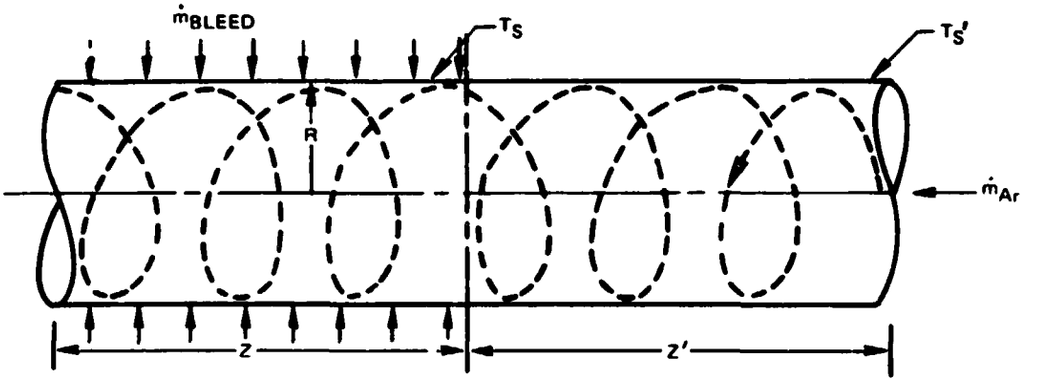

FIG. 41

COMPOSITE PLOTS SHOWING EFFECT OF INCREASING BLEED FLOW RATE THROUGH POROUS MONEL DUCT ON EXIT AXIAL AND SWIRL VELOCITY AND EXIT TEMPERATURE DISTRIBUTIONS